THE PHOTODISSOCIATION OF WATER VAPOR, EVOLUTION OF OXYGEN AND ESCAPE OF HYDROGEN IN THE EARTH'S ATMOSPHERE

Thesis by

Robert Terry Brinkmann

In Partial Fulfillment of the Requirements

For the Degree of

Doctor of Philosophy

California Institute of Technology

Pasadena, California

1969

(Submitted June 3, 1969)

ACKNOWLEDGMENTS

I thank Dr. G. Münch of the Astronomy Department for serving as advisor for this project. The working arrangement has been eminently satisfactory. Dr. A. Ingersoll in my own division, the Division of Geological Sciences, has kindly served as liaison advisor within that division and caught several important errors in early phases of this work. This study began as a term paper for a course taught by Dr. H. Brown and unassumingly titled "The Chemistry of the Solar System". I thank Dr. Brown for his encouragement and advice. Discussions with Dr. L. Kaplan at the Jet Propulsion Laboratory were both encouraging and useful. Similar discussions with Dr. W. B. DeMore of the Jet Propulsion Laboratory and V. L. Carter of the Aerospace Corporation are also gratefully acknowledged. D. G. Truhlar of the Chemistry Department was an indispensable source of information and advice regarding the cross-sections for the escape calculation. Part of the computer calculations was done through the regular channels at the Jet Propulsion Laboratory and part was bootlegged through various obscure channels. The assistance of the responsible individuals is gratefully acknowledged.

ABSTRACT

Previous theoretical studies of the photodissociation of water vapor and the resulting evolution of oxygen in the earth's atmosphere have led to the conclusion that over most of geologic time the atmospheric oxygen abundance has been quite low ($\lesssim 10^{-3}$ times the present atmospheric level). These studies have played a prominent role in subsequent investigations concerning biological evolution, interpretation of the geologic record and the evolution of planetary atmospheres. However, these early studies contain several objectionable features which cast serious doubt on the validity of the results. In particular, the path length dependence of the "effective absorption coefficient" in the Schumann-Runge bands of oxygen has not been properly handled and the calculations have been based on the incorrect assumption that dissociation of H_2O can be neglected when its rate is appreciably less than the rate of absorption by O_2. When these deficiencies are rectified it appears that, contrary to the previous findings, the O_2 level could have reached an appreciable fraction of the present amount in the absence of biological activity. Thus, if the earth's early atmosphere were indeed highly reducing, some other explanation for this fact must be found. One possibility which has been suggested is that very early in the earth's history sufficient quantities of hydrogen were outgassed to raise the thermal conductivity of the upper atmosphere, reduce its temperature and consequently retard the escape of hydrogen atoms. It has been suggested that such a "metastable"

atmosphere could have existed for perhaps a billion years. This estimate, however, depends on the efficiency of the gravitational escape of light atoms from a planetary atmosphere, i.e., on the importance of the deviations from Jean's classical escape equation due to the escape-induced departure of the atmospheric atoms' velocity distribution from a Maxwell-Boltzmann law. This problem is too complex to be handled entirely analytically, but the statistical approach seems promising. Indeed, three independent Monte Carlo calculations have been recently conducted. Unfortunately, 1) there are potentially serious errors or unjustified simplifications inherent in all three studies and 2) the results from the three studies are so discordant that even a qualitative idea of the validity of the Jeans escape rate cannot be obtained. In view of the importance of ascertaining the magnitude of the correction to Jeans' equation yet another Monte Carlo study has been conducted. This study differs from previous efforts in many respects, two of which are that accurate angular and velocity dependences have been calculated for the cross-section for the elastic scattering of an H (or He) atom by an O atom in the WKB approximation, and that rather than following the particles of the real atmosphere (as did all previous workers), here those particles missing from the real atmosphere by virtue of the escape process have been considered. It is found that only moderate corrections to Jeans' escape rate are needed. No firm picture can be sketched of the condition of the earth's early atmosphere from these considerations. Thus the nature of the evolution of the earth's atmosphere is less well known today than understood.

TABLE OF CONTENTS

I. Introduction: Dissociation of H_2O and Evolution of O_2

The question of the evolution of the earth's atmosphere throughout the 4.5 billion years or so of its existence is one of the most basic confronting planetary science today. The interrelationships among the atmospheric composition, the evolution of life forms and the geologic record make it a complicated question to attempt to answer but also add to its importance. A good deal of effort has been expended on this matter, upon which we do not intend to dwell. The interested reader can easily track down the necessary references from any of a number of papers [Rubey, 1955; Cloud, 1968; Berkner and Marshall, 1964, 1965, 1966]. We state here simply that the terrestrial near absence of the rare gases (considering their cosmic abundances) suggests that the earth was not left with an appreciable atmosphere at the conclusion of its formation. Our atmosphere today is the result of volcanic effluence. Volcanic gases consist mainly of water vapor with lesser amounts of such species as N_2, H_2, CH_4, SO_2 and probably CO_2, but no oxygen. If oxygen was not present initially and did not result from outgassing, where then did it come from? There are only two important oxygen-producing mechanisms known. Oxygen can result from the photodissociation of water vapor by the solar ultraviolet (if the hydrogen escapes the planet and the oxygen atoms combine with each other) or it can result from photosynthesis, which requires extensive and highly developed life forms. On the present-day earth the oxygen level is controlled by the balance between photosynthesis on the one hand and respiration, decay and inorganic oxidation (fires)

on the other. The question to which the present effort is addressed is this: Before life forms evolved to their present dominant role in the oxygen balance what was the oxygen level apt to be? Could it have been an appreciable fraction of the present amount? Or is photodissociation an ineffective means of producing oxygen-rich atmospheres? This investigation was prompted by an apparent Soviet measurement of an appreciable amount of molecular oxygen in Venus' atmosphere. (This measurement is now widely disbelieved. Earth-based spectroscopic searches for oxygen on Venus have produced upper limits on its abundance several orders of magnitude lower than the Soviet result of $\frac{1}{2}\%$. See the recent paper by Belton and Hunten [1968].) If verified, this measurement seems to require either that 1) photodissociation is a much more effective means of oxygenating an atmosphere than the results of Berkner and Marshall [1964, 1965, 1966] allow or 2) unlikely as it seems, and as suggested by Libby [1968], areas exist on the surface (or in the atmosphere) of Venus where life forms can survive. As will be shown, the first alternative now seems quite possible. Previous studies of the photodissociation of water vapor and the resulting evolution of oxygen in the earth's atmosphere have led to the conclusion that over most of geologic time the atmospheric oxygen abundance has been $\lesssim 10^{-3}$ times the present atmospheric level [Berkner and Marshall, 1964, 1965, 1966]. However, the basic calculational method used seems of doubtful validity and proper interpretation has not been made of the available laboratory absorption data for the Schumann-Runge band system of O_2. The calculations presented here suggest that the O_2 level could have reached an

appreciable fraction of the present amount in the absence of biological activity. We now consider in some detail the process of photodissociation of water vapor in the earth's atmosphere.

II. Mixing Ratio and Absorption Data

Molecular oxygen is uniformly mixed in the earth's atmosphere up to heights of about 90 km. Throughout this range about one molecule in five is an O_2 molecule [U. S. Air Force Geophysics Research Directorate, 1960, pp. 8-1 through 8-4]. Water vapor is now known to be uniformly mixed in the high troposphere and up to at least 30 km in the stratosphere (the altitude limit of the balloon-borne instruments) at about 3 parts per million by weight [Mastenbrook, 1968; Williamson and Houghton, 1965; Calfee and Gates, 1966], or about 5 molecules per million. (A recent paper by Sissenwine et al. [1968] reports balloon measurements of the mixing ratio at 32 kilometers which are a factor of 5 larger than the value adopted here. At the 1969 American Geophysical Union spring meeting Scholz et al. [1969] presented mixing ratios obtained by rocket between 43.6 and 62.3 km. which are a factor of 10 higher than the value used here. It seems unlikely that we are appreciably overestimating the H_2O mixing ratio.) Although few measurements have been conducted above 30 km the assumption has been made that the mixing ratio remains constant up to 70 km. or so [Hunt, 1966]. This assumption seems safe and is adopted here. Carbon dioxide is also probably uniformly mixed in this region at about 1 molecule in 3000 [U. S. Air Force Geophysics

Research Directorate, 1960; Goody, 1964, p. 10]. The final constituent to be considered in this calculation is ozone. Ozone is distributed approximately exponentially above 30 km but with a scale height of about 5 km (as opposed to about 8 km for the other species). We assume here that there are 0.03 atm-cm of O_3 above 30 km [Griggs, 1966].

Water molecules can be dissociated,

$$H_2O + h\nu \rightarrow OH + H$$

by photons of wavelength less than about 2390Å. However, the absorption coefficient of this dissociation continuum attains its maximum value at about 1650Å. Absorption coefficients have been measured [Thompson et al., 1963; Watanabe and Zelikoff, 1953] and are represented in Figure 1. The absorption spectrum of CO_2 has not been adequately investigated in this wavelength region. The nature of the transitions involved is not known. Nevertheless the available data [Thompson et al., 1963; Inn et al., 1953] is pictured in Figure 1. Absorption by O_3 in this wavelength region is due to a continuum with a few weak overlying bands [Thompson et al., 1963; Tanaka et al., 1953]. Figure 1 also includes the ozone absorption coefficients.

This leaves molecular oxygen to be considered. There are three absorption systems to be taken into account. At wavelengths shorter than about 1750Å the very intense Schumann-Runge continuum provides a virtually impenetrable barrier to solar photons seeking to make their way below about the 80 km level. Between 1750Å and about 2030Å

the Schumann-Runge band system absorbs. Finally there is the Herzberg absorption system underlying the Schumann-Runge bands and extending up to about 2600Å. This system consists of a very weak series of bands due to the forbidden transition $X\ ^3\Sigma_g^- \rightarrow A\ ^3\Sigma_u^+$ and a continuum, stronger than the Herzberg bands but about a million times weaker than the Schumann-Runge continuum, resulting from the dissociation $O_2\ ^3\Sigma_g^- \rightarrow O(^3P) + O(^3P)$. These systems have been investigated experimentally [Watanabe et al., 1953; Blake et al., 1966; Metzger and Cook, 1964; Hudson et al., 1966; Ditchburn and Young, 1962] and representative results are given in Figure 1. Some of these investigations have revealed pressure (possibly due to the formation of the complexes O_4, O_6, etc.) and temperature dependences. In this thesis we take data suitable for the middle atmosphere (low pressure and about 300°K). A more serious correction which must be applied, however, and one which apparently has been overlooked by Berkner and Marshall is the dependence of the "effective absorption coefficient" on the path length. This correction is important for the Schumann-Runge bands, the individual rotational lines of which are much narrower than the instrumental resolution attained by early investigators. These lines have natural (Lorentz) widths [Herzberg, 1961] in energy units of

$$w = \frac{h}{\tau} \qquad [1]$$

where h is Planck's constant and τ is the natural lifetime of the state. Taking $\tau \approx 1.1 \times 10^{-11}$ sec (the bands predissociate [Hudson

and Carter, 1968]) we obtain a natural line width of 1.0×10^{-16} erg, or about 1.6×10^{-2}Å at 1800Å. The Doppler widths at 300°K are given by

$$\frac{v}{c} \times 1800\text{Å} = \frac{\sqrt{2kT/\mu}}{c} \times 1800\text{Å} \approx 2 \times 10^{-3}\text{Å} \qquad [2]$$

These lines can be considered as purely Lorentzian when investigated with an instrumental resolution of about 2Å, as was the case for the data used by Berkner and Marshall. It is known [Goody, chapter 4] that under such conditions the "effective absorption coefficient", $k_{ef}(\lambda_0)$, for a single line, defined by

$$e^{-k_{ef}(\lambda_0)x} = \frac{\int f(\lambda - \lambda_0)\, e^{-k_\lambda x}\, d\lambda}{\int f(\lambda - \lambda_0)\, d\lambda} \qquad [3]$$

where k_λ is the monochromatic absorption coefficient, the integration extends over all wavelength, λ, and $f(\lambda)$ is the instrumental slit function, varies very nearly as the inverse square root of the path length, x. Thus absorption data obtained for a narrow line with a thickness of absorber x cannot be applied directly to calculate absorption through a thickness y, but rather the measured absorption coefficient, k_m, should be replaced by $k_m \times \sqrt{x/y}$. If in addition to the "spikes" in k_λ there is a component more or less constant over the instrumental resolution (due, for example, to dissociation continua), k_c, then the measured absorption coefficient, k_m, should be replaced by $k_c + (k_m - k_c) \times \sqrt{x/y}$. The values for k_c are plotted

in Figure 1. Accurate measurements have not yet been made of the Herzberg continuum absorption coefficient in the vicinity of the strong Schumann-Runge bands but measurements at longer wavelengths have been combined with theoretical calculations to produce reliable values. Blake et al. [1966] have shown that for optical thicknesses $\lesssim 3.2$ (the limit of their measurements) in the vicinity of 1800Å the absorption coefficient within the Schumann-Runge bands obeys the simple inverse square root scaling for a single line. This range of optical thickness includes all of the wavelength and altitude ranges in the present calculation with a few exceptions in the 1760 ± 5Å and 1770 ± 5Å wavelength ranges and the lowest three altitude ranges, none of which contributes very much to the total absorption rate. Since the continuum contribution to the absorption coefficient is negligible in the wavelength and path length ranges studied by Blake et al. we will take for our effective absorption coefficient the continuum value plus an inverse square root scaling on the Schumann-Runge band contribution. This should give more realistic values at longer wavelengths, where the continuum component may be appreciable.

For purposes of calculation we divide the earth's atmosphere into 12 layers. The first contains the uppermost 5 atm-cm, the second the next 10 atm-cm, the third the following 20 atm-cm and so on. Tables 1 and 2 list the amount and effective absorption coefficient for a number of wavelength regions of each of the four important species in each layer. For O_2 the effective absorption coefficient for the nth layer, k_n, is derived from

$$e^{-k_n(x_n - x_{n-1})} = e^{-(k_n' x_n - k_{n-1}' x_{n-1})} \qquad [4]$$

where x_n is the total thickness of oxygen above the base of the nth layer and k_n' is the effective absorption coefficient for the thickness of oxygen above the base of the nth layer, determined in the manner described above (continuum coefficient plus inverse square root scaling on the "spikes"). In order to apply the inverse square root scaling it is necessary to know the path length used in the measurement of the absorption coefficients. This information is contained in the "1/e absorption cross-sections" of Blake et al. [1966] from 1750Å to 1930Å and their measurements with 150 atm-cm path length for longer wavelengths. Since the vibrational structure of the bands is comparable to the wavelength differences between the entries in Table 2 calculations were carried out at 2Å intervals. These effective absorption coefficients were then combined to produce values at the appropriate wavelengths by averaging transmissions in the 2Å bands:

$$e^{-\bar{k}x} = \frac{\sum_{i=1}^{j} e^{-k_i x} \Delta_i}{\sum_{i=1}^{j} \Delta_i} \qquad [5]$$

Here $\bar{k}$ is the effective absorption coefficient for the wavelength interval defined by the summation, the k_i are the calculated 2Å coefficients, Δ_i is 1 or 2 depending on whether the entire 2Å interval or only half of it is included in the interval, and x is the path

length of absorber through the particular layer. The results are given in Table 2.

III. Calculated Dissociation Rate

Values for the solar flux incident on the atmosphere (assuming the sun to be directly overhead) are given in Table 3 [Detwiler et al., 1961; Brinkmann et al., 1966]. Since the earth's albedo in the far ultraviolet is extremely small (<1%), the atmosphere above the base of the 12th layer (26.5 km) is optically thick over almost the entire wavelength range considered and absorption by aerosols is unimportant it is safe to assume that all incident photons will be absorbed by one of the four important absorbers considered and that the rate at which photons are absorbed in the wavelength interval designated by λ_ℓ by the ith species in the jth layer is given to a good approximation by

$$n(i,j,\lambda_\ell) = F_{\lambda_\ell} e^{-\sum_{m=1}^{j-1}\sum_{n=1}^{4} k(n,m,\lambda_\ell)\, t(n,m)} \times \left[1 - e^{-\sum_{n=1}^{4} k(n,j,\lambda_\ell)\, t(n,j)}\right] \frac{k(i,j,\lambda_\ell)\, t(i,j)}{\sum_{n=1}^{4} k(n,j,\lambda_\ell)\, t(n,j)} \qquad [6]$$

Here F_{λ_ℓ} is the appropriate incident solar flux; m and n denote the various layers and species, respectively, absorbing above the jth

layer (note: if $j = 1$ the summation $\sum_{m=1}^{j-1}$ is defined to be zero); $t(n,m)$ is the integrated normal thickness of the nth species in the mth layer; and $k(n, m, \lambda_\ell)$ is the effective absorption coefficient for the nth species in the mth layer in the wavelength interval λ_ℓ.

These calculations have been carried out and the results summed to produce Figures 2 and 3. Figure 2 shows the total absorption rate for each of the four species as a function of wavelength. Since nearly every absorption by H_2O below 2000Å results in dissociation the curve for H_2O can also be taken to be the photodissociation rate. Figure 3 illustrates the corresponding quantities but as functions of layer, integrated over wavelength.

From Figures 2 and 3 we see that appreciable water vapor dissociation occurs over a wide altitude range and that about half is produced by photons in the narrow wavelength range 1775-1830Å. CO_2 absorption occurs somewhat lower in the atmosphere and to longer wavelengths. Ozone absorbs most strongly at the longest wavelengths considered and quite low in the atmosphere. O_2 is by far the dominant absorber everywhere. The total absorption rates by H_2O, CO_2, O_3 and O_2 are 6.42×10^9, 4.04×10^9, 7.88×10^{11} and 1.10×10^{13} photons cm^{-2} sec^{-1}, respectively.

We have considered only incident radiation in the wavelength range 1750-2000Å. Longer wavelength radiation does not dissociate water molecules appreciably. Strong absorption by atomic and molecular oxygen and nitrogen prevent shorter wavelength radiation from reaching significant amounts of H_2O. This is true even of the rather intense Ly α radiation at 1216Å; it is absorbed appreciably by oxygen

above 80 km, where the water vapor mixing ratio may be smaller. The Ly α flux seems to vary by an appreciable amount (available measurements, some of which are probably in error, vary within a factor of 50) with the solar cycle but the H_2O dissociation rate computed for a mean Ly α flux is a small but not altogether negligible fraction of the total dissociation rate. In earlier times when there was presumably less O_2 in the atmosphere the Ly α dissociation contribution could have been comparable to the long wavelength contribution. Our neglect of Ly α radiation then will slightly underestimate the O_2 levels if anything.

So far we have considered only the case in which the sun is directly overhead (0° zenith angle). Since ozone is not an important absorber in the wavelength range where H_2O absorbs most strongly, the dependence of the O_3 mixing ratio on height can be neglected in the succeeding calculation. Then, with the composition fixed, the previous results can be applied directly to the case of a zenith angle $\theta \neq 0°$ by dividing the former layer thicknesses by the secant of θ, to account for the longer optical path lengths, and reducing the solar flux by the same factor, since the incidence is now non-normal. For calculating total absorption/dissociation rates as a function of wavelength (integrated over altitude), the change in layer thickness is unimportant and only the "effective solar flux reduction factor" need be considered. Averaging over the course of a day and over latitude reduces the absorption rates by a factor of 4 (the ratio of the surface area of a sphere to its cross-section). This gives a mean total H_2O photodissociation rate for the earth's

present atmosphere of 1.60×10^{9} molecules cm^{-2} sec^{-1}. The earth is believed to be about 4.5×10^{9} years $\approx 1.5 \times 10^{17}$ seconds old. If we make the reasonable assumptions that over most of the earth's history 1) there has been about as much H_2O in the atmosphere (30 to 90 km) as we assumed to be present today (5 parts per million), 2) there have been no significant quantities of additional constituents which strongly absorb in the 1750-2000Å region and 3) the solar ultraviolet flux has been roughly that of Table 3, then we can draw the conclusion that $1.5 \times 10^{17} \times 1.60 \times 10^{9}$ molecules cm^{-2} = 7200 gm cm^{-2} or more of H_2O has been dissociated in the earth's atmosphere. This is about 2% of the total amount of water on the surface of the planet and is equivalent to about 100 meters of our present oceans. It is enough to provide for all our present atmospheric O_2 and 6200 gm cm^{-2} of oxygen in surface oxides. The absorption rates as a function of altitude averaged over the surface of the earth will not be calculated here. The effect would be to emphasize the higher altitudes at the expense of the lower ones.

IV. Dissociation Histories

Let us now consider a dynamical situation in which the composition of the atmosphere is allowed to change. We designate the column density of O_2 by σ_{O_2} (molecules cm^{-2}). Then

$$\frac{d\sigma_{O_2}}{dt} = P - L \qquad [7]$$

where P = column production rate of O_2 (molecules cm^{-2} sec^{-1})

$= \frac{f}{2} \times$ dissociation rate of H_2O

if we neglect other oxygen-producing mechanisms. Here f, the "escape efficiency", is the ratio of the number of H atoms which do escape to the number which could possibly escape (i.e., twice the dissociation rate of H_2O). Calculations have been performed for $f = \frac{1}{2}$.

L = column loss rate of O_2 (due to surface oxidation).

We assume here that $L = C \times \sigma_{O_2}$ and that C has been constant over most of geologic time. Now we need to know the H_2O photodissociation rate for various values of σ_{O_2}. We need only repeat the above calculations with different O_2 fractions in the atmosphere. We also change the O_3 fraction so that it is always in constant proportion to the O_2 level. This has been done and the results are given in Figure 4, which depicts the total absorption rates (integrated over altitude and wavelength) for each of the four species for O_2 levels from 1/1024 to 5 P.A.L. (present atmospheric level). For the lower O_2 concentrations the sum of the absorption rates is less than the solar influx because appreciable numbers of photons penetrate to the base of the bottom layer (26.5 km). In these cases the present results will underestimate the absorption rates somewhat.

The water vapor dissociation data of Figure 4 were then fit to a series of 14 power law functions,

$$\frac{2P}{f} = a_i \sigma_{O_2}^{b_i} \qquad [8]$$

where a_i and b_i are parameters for the ith interval in the abscissa. Equation [7] then becomes

$$\frac{d\sigma_{O_2}}{dt} = \frac{f}{2} a_i \sigma_{O_2}^{b_i} - C \sigma_{O_2} \qquad [9]$$

within the ith interval. This can be integrated to give

$$t = \frac{-1}{C (b_i - 1)} \log \left[\frac{\sigma_{O_2}^{b_i - 1}}{\sigma_{O_2}^{b_i - 1} - \frac{2C}{a_i f}} \right] + K_i \qquad [10]$$

or

$$\sigma_{O_2} = \left[\frac{-\frac{2C}{a_i f}}{e^{-C(b_i - 1)(K_i - t)} - 1} \right]^{\frac{1}{b_i - 1}} \qquad [11]$$

We assume that the dissociation rate for $0 \leq \sigma_{O_2} \leq 1/1024$ P.A.L. is constant and equal to the value in Figure 4 for $\sigma_{O_2} = 1/1024$ P.A.L. We can now calculate the dissociation rate history for the earth for various assumed values of the oxidation parameter, C, by applying Equations [10] and [11] to successively greater σ_{O_2} intervals. As each new interval is encountered the value of K_i is evaluated from the results of the previous interval at their common σ_{O_2} value. Values of C were chosen which give e-folding oxidation-loss times (in the absence of production mechanisms) ranging from 1.41×10^{13} sec (about half a million years) to 1.15×10^{17} sec (about 4 billion years).

The results of these calculations are given in Figure 5. The entire amount of oxidation for each of these curves can be calculated from

$$Q = C \int_{t=0}^{t} \sigma_{O_2}(t)\, dt \qquad [12]$$

where Q is this amount. This expression has been evaluated numerically and the results included in Figure 5 as labels on the curves. We see that with the extremely wide range of oxidation-time constants chosen the resulting atmospheres have had from roughly 1/40 to 3 times the P.A.L. of molecular oxygen over most of their history. Our lowest value is a factor of 25 higher than the upper limit of Berkner and Marshall. We can, however, limit the range further by considering the amount of oxidized material present in the earth's crust. The figures used here are those given by Poldervaart [1963]. There are about 2.18×10^{25} gm of matter in the lithosphere, or 3.87×10^{6} gm cm^{-2}. Most atmospheric oxidation involves the formation of Fe_2O_3 from FeO. The weight of the added oxygen atom is just 10% of the weight of the Fe_2O_3 molecule. The lithosphere contains 2.8% Fe_2O_3 as compared to 5.8% FeO. If all this Fe_2O_3 were produced by atmospheric oxidation this would amount to

$$.028 \times .1 \times 3.87 \times 10^{6} \text{ gm cm}^{-2} = 1.1 \times 10^{4} \text{ gm cm}^{-2}$$

of oxygen lost in oxidation. Taking this figure as an upper limit controlling the O_2 concentration in the atmosphere we see from Figure

5 that the curve for 1.09×10^{4} gm cm^{-2} reaches an O_2 level of slightly greater than .27 P.A.L. after five billion years and that it is greater than .25 P.A.L. over 99% of geologic time. This represents a lower limit, as outlined above. It could, according to these calculations, be somewhat higher. This is a factor of 250 higher than the upper limit of Berkner and Marshall and implies that our atmosphere could have been highly oxidizing over a large fraction of geologic time in the absence of the widespread biological activity which operates today. The implications of these results are discussed later. We have of course assumed here that the mantle has suffered no appreciable amount of oxidation and that the crust contained no large amounts of free iron initially. Even relaxing these assumptions somewhat it is hard to see how enough oxidation could have occurred to allow the very low levels of O_2 called for by Berkner and Marshall to persist. This is the result of the tendency of production and loss changes to cancel one another.

V. H_2O Mixing Ratio

Now we must consider two related problems: first, the possibility that the H_2O mixing ratio could have been substantially less over most of geologic time than it is today and second, the matter of the efficiency of escape of hydrogen atoms liberated by photodissociation. The only effective way that the H_2O mixing ratio could have been less than at the present is if the "cold trap" temperature at the tropopause were lower. This could presumably be caused by a

decrease in the level of CO_2 or, more likely, O_3, both of which heat the atmosphere by their absorption of longer wavelength radiations. However, calculations by Manabe and Wetherald [1967] of radiative convective equilibrium temperatures as a function of altitude for the earth's atmosphere with a wide range of CO_2 and O_3 distributions make this seem unlikely. Virtually no difference could be induced on the tropopause temperature by varying the CO_2 content. Virtually the same (within one degree Kelvin) temperature minimum was obtained with a typical ozone distribution as with no ozone at all. For O_3 distributions which have their maximum concentration below the typical level (about 22 km), which could be expected for atmospheres containing less O_3 than the present terrestrial one, the minimum temperature actually increased slightly. For the case in which the ozone is concentrated almost exclusively above the tropopause the temperature minimum did decrease by about 8 degrees, but this situation is not to be expected in an early terrestrial atmosphere. We conclude that it is unlikely that lower tropopause temperatures prevailed in the past and that the mixing ratio for water vapor has always been essentially the same as it is today, except possibly for short intervals.

VI. Escape of H Atoms: Photochemistry

The second question is whether the liberated H atoms really do escape the earth's gravitational field or whether they undergo chemical reactions leading back to the formation of more H_2O before being

able to escape. This question cannot be answered definitely because of the great uncertainties in our knowledge of upper and middle atmospheric processes. We judge it sufficient at this time to establish the plausibility, within the limits of our observational knowledge, that the earth is presently losing some 1.6×10^9 H atoms cm^{-2} sec^{-1}. This is considerably higher than current estimates, but it is felt that this is due at least in part to the current belief that the production rate of H atoms cannot be as high as that which has been derived here. A thorough treatment would establish two points: 1) in the photochemical region (below 100 km) do the H atoms retain their identity or participate in reaction cycles which restore their identity rather than allowing them to become locked back up as H_2O; and 2) do considerations of the classical escape problem and our knowledge of upper atmospheric composition and temperature allow of an average escape flux as high as 1.6×10^9 H atoms cm^{-2} sec^{-1}? This is not going to be a thorough treatment.

Table 4 below lists the dissociative energies of the various likely repositories for liberated hydrogen atoms, as collected by Herzberg [1961, 1966]. While the energies required in practice to cause a dissociation may be somewhat greater than those listed (for H_2O we saw that the dissociation cross-section reached its maximum value at about 1650Å), nevertheless we should be able to tell something from Table 4 about the relative ease or difficulty of causing various dissociations. Molecular hydrogen and OH are very difficult to dissociate while H_2O_2 and HO_2 can be readily broken up. The direct formation of H_2,

$$H + H + M \rightarrow H_2 + M \qquad k = 2.6 \times 10^{-32}$$

a slow three-body reaction [Larkin and Thrush, 1964], seems to present no great threat to the existence of hydrogen atoms. It would seem that the only real danger is presented by OH, which forms by the reactions [Kaufman, 1964; Phillips and Schiff, 1962]

$$H + O_3 \rightarrow OH + O_2 \qquad k = 2.6 \times 10^{-11}$$

$$H + HO_2 \rightarrow OH + OH \qquad k = 10^{-11}$$

At moderate altitudes, however, the hydrogen should be freed by the reaction

$$OH + O \rightarrow H + O_2 \qquad k = 5 \times 10^{-11}$$

Unfortunately our knowledge of the atmospheric concentrations of such species as HO_2 and H_2O_2 is practically nonexistent. As a result of this and other factors (poorly known reaction rates and mechanisms, the complexity of the dissociation problem, etc.), though a number of photochemical studies have been conducted [Kaufman, 1964, 1968; Phillips and Schiff, 1962; Hesstvedt, 1968; Bates and Nicolet, 1950; Colegrove, 1965, 1966; Hunt, 1966; Schofield, 1967; Patterson, 1966; Kockarts and Nicolet, 1962] it seems impossible to state definitely that hydrogen atoms either will or will not "last" long enough to be transported out of the photochemically active region of the atmosphere. It seems that its lifetime may be on the order of a day below 90 km or so. Fortunately for the hydrogen atoms, they are much more likely to be liberated during mid-day, when heating and convection should be most effective (and escape should be easiest). We conclude that previous photochemical considerations cannot rule out the possibility that a large fraction of the liberated H atoms do indeed survive long

enough to avoid eventual recombination to H_2O.

VII. Escape of H Atoms: At the Exobase

Secondly we consider the upper atmosphere escape problem. Stoney [1898, 1900a, b] appears to have been the first to recognize the importance of the loss of the lighter constituents from planetary atmospheres. (Sidney Chapman has suggested that thermal escape - i.e., the ballistic escape of the high energy tail of the velocity distribution function - be renamed "Stoney escape" in recognition of this fact. This usage is not followed here because it is anticipated that most readers will not yet be familiar with this alternative designation.) Jeans' subsequent analysis [1916] established the basic physical principles and further, more detailed investigations have verified the essential correctness of his results, at least as a fair approximation [Milne, 1923; Jones, 1923; Spitzer, 1957; Chamberlain, 1963; Hayes and Liu, 1965]. We might wish to divide Jeans' escape rate by a factor of 2 or so to allow for the deviation of the velocity distribution from true Maxwell-Boltzmann caused by the fact that many of the fast molecules leave (escape) the assemblage. (We will see later that a factor of 2 is a rather liberal allowance for this effect.) Jeans' escape rate is given by the equation

$$L = \frac{v_{rms}}{\sqrt{6\pi}}\left(\frac{GmM}{kT_cR_c} + 1\right) \rho_c \, e^{-GmM/kT_cR_c} \qquad [13]$$

Here L is the escape rate in molecules (atoms in our case) cm^{-2} sec^{-1};

v_{rms} is the root mean square speed of the molecule at the "critical level", in cm sec^{-1}; k is Boltzmann's constant; T_c is the temperature of the gas at the critical level; R_c is the distance from the center of the earth to the critical level; G is the gravitational constant; m is the mass of a molecule (1 a.m.u.); M is the mass of the earth; and ρ_c is the number density of the escaping species per cubic centimeter. The equation can be applied to any species independently of the others provided only that the critical level and temperature be properly defined. The escape rate is proportional to the hydrogen density (atoms) at the critical level (the critical level in the earth's atmosphere occurs typically at about 500 km altitude). Taking $v_{rms} = \sqrt{3kT_c/m}$ and including the factor of $\frac{1}{2}$ discussed above we need specify only T_c in order to calculate the escape rate.

The temperature of the critical level changes appreciably during the day and with the solar cycle. In choosing a representative temperature we select something nearer the maximum daily temperature than the minimum for the following reasons: 1) atmospheric convection is more effective in allowing atoms to rise to the base of the heterosphere (from which they should be able to proceed by thermal diffusion to the critical level) during the day, when the temperature is higher; and 2) the density of hydrogen atoms will increase during the night, enhancing the daytime escape rate over what we would expect from consideration of the mean density. Although T_c varies between perhaps 600°K and 2500°K depending on conditions, we choose 1500°K for a representative value. This is consistent with information presented for several reference atmospheres [Committee on Extension to the

Standard Atmosphere, 1962; COSPAR Working Group IV, 1965]. The escape rate is then

$$L = 3.785 \times 10^3 \frac{cm}{sec} \times \rho_c$$

Our mean escape flux for the present-day earth of 1.6×10^9 cm^{-2} sec^{-1} requires a density of hydrogen atoms at the base of the exosphere of

$$\frac{1.6 \times 10^9}{3.785 \times 10^3} = 4.23 \times 10^5 \text{ H atoms } cm^{-3}$$

This is considerably higher than values adopted in prior work [Kockarts and Nicolet, 1962; Liwshitz, 1967; Kellogg, 1964; Bates and Patterson, 1961; Brandt, 1962; Ingham, 1968] but it will be our contention that mean hydrogen densities this high cannot be ruled out. Most early estimates of the hydrogen atom density at the base of the exosphere were derived from diffuse Ly α, Lyβ or H α airglow measurements and involve, in addition to a tricky radiative transfer problem, an arbitrary normalization, usually to the 100 km level or so, although some have been normalized at 500 km. Thomas [1962] has pointed out that "radiative transfer in models whose total hydrogen abundance is consistent with daytime absorption measurements is ...inadequate in accounting for the observed nightglow features," and suggests that a nighttime buildup may raise the density. Donahue [1967] has suggested that the Ly α calculations may be seriously underestimating the hydrogen content of the upper atmosphere and that this may explain the discrepancy between results for Ly α and

H α and Ly β.

Several more recent measurements by other means, not involving the inversion of the radiative transfer equation, have produced results suggestive of higher H atom concentrations in the upper atmosphere. Brace et al. [1967], from Explorer 22 measurements of electron temperature and concentration at 1000 km altitude, conclude that "a local electron cooling exists in the equatorial region that is inconsistent with present neutral atmospheric models but suggests the existence of about 5×10^5 cm^{-3} atoms of neutral hydrogen at 1000 km". Hoffman [1967] reports mass spectrometer measurements of ion densities obtained on a rocket flight and, assuming chemical equilibrium between H^+ and O^+, he finds a neutral hydrogen density at 350 km of 5×10^6 cm^{-3}. Reber et al. [1967] have obtained mass spectrometer measurements of atomic hydrogen itself, and report a typical value of 2×10^6 cm^{-3} at 300 km at 0900 local time. These values, being more direct than the Ly α measurements, constitute strong evidence that the hydrogen atom density at 500 km may indeed be as high as the 4.23×10^5 required to allow the escape of 1.6×10^9 atoms cm^{-2} sec^{-1}. (These measurements were probably conducted near solar minimum, so that the effective temperatures may have been somewhat lower than 1500°K. At 1100°K, a typical daily maximum temperature near solar minimum, the Jeans escape flux is reduced by a factor of 5; i.e., a density increase of a factor of 5 is required to produce the same flux.) We conclude that, within the limits of present observational knowledge of the upper atmosphere, an escape rate of 1.6×10^9 cm^{-2} sec^{-1} does not seem out of the question.

VIII. Results of Dissociation Calculation

The calculations of Berkner and Marshall are in error 1) because they assume that photodissociation of H_2O becomes an inefficient oxygen-producing mechanism when the fraction of photons absorbed by O_2 becomes larger than the fraction absorbed by H_2O and 2) they have not allowed for the path length dependence of the oxygen absorption coefficient. We have seen that the "Urey self-regulation mechanism" for the shielding of oxygen by water vapor from the dissociating solar ultraviolet is much less effective than the papers of Berkner and Marshall assert. As a result, appreciable oxygen concentrations might have evolved in the earth's atmosphere ($\frac{1}{4}$ P.A.L. or more) before the evolution of widespread photosynthesizing organisms. It does not seem that early evolution could have proceeded in such an atmosphere. Further the geologic record strongly suggests that earlier than two billion years ago reducing conditions existed over much of the earth's surface. The evidence along these two lines, while not yet conclusive, is nevertheless appreciable. Yet the assumptions made in the present calculations do not seem unreasonable.

Perhaps there is a logical explanation consistent with the present results. Berkner and Marshall, for example, explained the presence of oxidized "red beds" of sediments away in terms of "local oxidizing conditions" (they proposed that the ozone would concentrate near ground level). If this is possible then maybe "local reducing conditions" can also exist. Or perhaps a "metastable" reducing atmosphere, along the lines proposed by Rasool and McGovern [1966] could

have persisted throughout the first 2.5 billion years. During this time the mean dissociation rate of H_2O would be, at 10^{-3} P.A.L. of O_2, something over 1×10^{11} cm^{-2} sec^{-1} (from Figure 4). But from Figure 5 we see that surface oxidation could not have been an adequate sink for the liberated oxygen atoms. Therefore there had to be an atmospheric sink. Oxidation of methane presents one possibility but does not seem likely in view of the large amounts involved (hundreds of atmospheres). The reformation of water vapor by recombination with free hydrogen seems the least objectionable sink. However, it is not clear that such a situation could exist for long periods of time without the hydrogen escaping, even with a much lower (750°K) exosphere temperature. We shall investigate the hydrogen escape problem in the next section.

IX. Introduction to the Atmospheric Escape Calculation

In the preceding section we have seen that an understanding of the processes by which the lighter components of an atmosphere escape to space is likely to figure prominently in any consistent explanation of the evolution of the earth's atmosphere (as well as its present state). The theory of thermal, or gravitational, escape has not advanced significantly since Jeans wrote his Dynamical Theory of Gases [1916]. The Jeans escape rate is based on the assumption of a Maxwell-Boltzmann distribution function throughout the atmosphere, even at the escape level. In fact, however, escape is itself a phenomenon which must alter the distribution function from

Maxwell-Boltzmann (M-B), so that the Jeans rate cannot be strictly correct. The mathematical complexity of evaluating the degree of error in Jeans' formula due to this effect has prevented, until recently, an assault on this problem. With the development of computers capable of performing 10^5 or so multiplications per second, it has become feasible to attack the problem in a statistical (as opposed to analytical) way. And, indeed, within the past few years three independent Monte Carlo studies have been conducted in an attempt to answer just this question [Lew and Venkateswaran, 1965; Liwshitz and Singer, 1966; Chamberlain and Campbell, 1967; see also Liwshitz, 1966 and Lew and Venkateswaran, 1966]. Unfortunately, the results of the separate studies are not consistent. For example, at 1730°K Lew and Venkateswaran (LV) found a correction factor of only 16%. Chamberlain and Campbell's value (CC) (at 1500°K) is 28% and Liwshitz and Singer (LS) conclude (also at 1500°K) that a 73% correction is needed (i.e., that Jeans' equation overestimates the escape flux by almost a factor of 4). There are other serious sources of discrepancy, such as the dependence of the correction on temperature (LS find a tendency for larger corrections at lower temperatures, in disagreement with CC; LV did their calculations at only one temperature). The work of LV has been roundly criticized by both LS and CC (LV was the first paper of the three to appear) for numerous reasons, two of which are 1) that LV have incorporated an abstruse "absorption" of particles in their calculation, which is difficult to justify physically, and 2) that LV do not release their "source" particles deeply enough in the atmosphere. It is the feeling of the

present author that, while credit is due LV for pioneering in the application of the statistical approach to the escape problem, their numerical results are of little value. A more detailed critique of all three papers will follow as the various relevant points are encountered. While the three sets of calculations have numerous differences, they are all basically similar. The results of LS and CC, in particular, seem so discordant that a programming error, rather than a difference in physical approach, may be responsible for the disagreement.

Since factors of 4 in escape rate may be non-negligible in calculations of atmospheric evolution, it was decided to undertake yet another Monte Carlo study of hydrogen (and helium) escape in the earth's atmosphere. All previous studies have grossly misrepresented the physics of the situation by assuming that the scattering (of H atoms by O atoms) is isotropic (in the center-of-mass frame of reference) and by adopting unjustifiable velocity dependences of the total scattering cross-sections. It was decided in the present study to obtain meaningful differential and total cross-sections and to correct several other errors in previous studies (which will be discussed as they are encountered). We now review briefly classical atom-atom elastic scattering theory, show that - if applicable - the simplest theory (the small deflection approximation) would seriously alter the physical picture of the escape region, and then settle on a compromise approach between the classical and full-blown quantum mechanical treatments. The results are believed to be fairly accurate.

X. Scattering Mechanics

In this section we derive approximate expressions for the angular dependence and velocity dependence of the elastic scattering cross-section for a collision of an H atom (mass about 1 a.m.u.) with an O atom (mass about 16 a.m.u.). We will consider first the familiar small deflection approximation to the classical problem, then the classical problem for arbitrary scattering angle, then a semi-classical correction to the classical problem for small-angle scattering (to avoid an infinite total cross-section), then describe the WKB approximation to the quantum mechanical approach and indicate briefly what the rigorous quantum mechanical calculation would involve. We consider only conservative central forces.

The geometry of the scattering problem in the center-of-mass system is shown in Figure 6. A particle (either the H atom or the O atom) approaches a fixed center of force from a large distance away with an initial momentum

$$\vec{p}_i = \mu v_i \hat{i} \qquad [14]$$

The reduced mass, μ, is given by

$$\mu = \frac{m_H m_O}{m_H + m_O}$$

The impact parameter is b. The angle Ψ is defined by the equation

$$\sin \Psi = \frac{p_y}{p} \qquad [15]$$

and Ψ_f is the scattering angle. In the small deflection approximation we assume that

$$\Psi \approx \sin \Psi \qquad [16]$$

and that

$$p \approx p_i \qquad [17]$$

Thus we can evaluate $\Psi_f = \Psi_f(v_i, b)$ if we know p_y;

$$p_y = \int_{-\infty}^{\infty} \frac{dp_y}{dt}\, dt = \int_{-\infty}^{\infty} F_y\, dt \qquad [18]$$

where $t = 0$ at the time of closest approach. For central forces F_y is given by

$$F_y = \frac{y}{r} F(r) \qquad [19]$$

For small angle scattering $y \approx b$ until, after the scattering, the particle is sufficiently far away from the scattering center that F_y makes no further important contribution to $\int_{-\infty}^{\infty} F_y\, dt$. With these assumptions we have

$$\Psi_f = \lim_{t' \to \infty} \frac{1}{p_i} \int_{-\infty}^{t'} \frac{b}{\sqrt{b^2 + v_i^2 t^2}} F\left(\sqrt{b^2 + v_i^2 t^2}\right) dt \qquad [20]$$

where we have substituted

$$\sqrt{b^2 + v_i^2 t^2} \approx r \qquad [21]$$

For a potential of the form $V(r) = \frac{C}{r^n}$, for which $F(r) = -\frac{nC}{r^{n+1}}$, we have

$$\Psi_f \approx \frac{b}{p_i v_i} (-n\,C) \frac{1}{b^{n+1}} \int_{-\infty}^{\infty} \frac{dw}{(1+w^2)^{\frac{n+2}{2}}} \propto b^{-n} \qquad [22]$$

where we have let $w = \frac{v_i t}{b}$. Thus we have

$$b(v_i, \Psi_f) = v_i^{-2/n}\, \Psi_f^{-1/n} \left[\frac{\mu}{-nC \int_{-\infty}^{\infty} \frac{dw}{(1+w^2)^{\frac{n+2}{2}}}} \right]^{-1/n} \qquad [23]$$

We let $I(\Psi_f)$ denote the cross-section (per particle per radian of Ψ_f) for scattering through an angle Ψ_f:

$$I(\Psi_f) = 2\pi\, b(\Psi_f) \left| \frac{\partial b(v_i, \Psi_f)}{\partial \Psi_f} \right|$$

$$= \frac{2\pi}{n}\, \Psi_f^{-1-2/n} v_i^{-4/n} \left[\frac{\mu}{nC \int_{-\infty}^{\infty} \frac{dw}{(1+w^2)^{\frac{n+2}{2}}}} \right]^{-2/n} \qquad [24]$$

The differential cross-section, $d\sigma/d\Omega$ (per steradian) is then proportional to

$$\frac{\Psi_f^{-1-2/n}}{\sin \Psi_f} \approx \Psi_f^{-2-2/n}$$

In atom-atom elastic scattering the dominant long range force is the attractive Van der Waals induced dipole-induced dipole or London dispersion force, which has an r^{-6} potential. The dominant short range force is a repulsion due to the overlap of the electron clouds of the two atoms. This potential is usually taken as r^{-12}, although other exponents are frequently used. The above equations hold for both attractive and repulsive potentials, provided only that the scattering angle is small ($\ll$ 1 radian). Thus the differential cross-section, $d\sigma/d\Omega$, should vary at small angles as $\Psi_f^{-2\frac{1}{3}}$ or $\Psi_f^{-2\frac{1}{6}}$ depending on which part of the potential is dominant (the repulsive part of the potential can become important at small angles only for very high relative velocities). The angle with which we have been concerned, Ψ_f, is the scattering angle in the center-of-mass frame. The correction for the scattering angle of the hydrogen atom (we are not concerned with the scattering angle of the oxygen atom) as measured in the "laboratory" reference frame (in which the O atom is initially at rest) is given by

$$\Psi_f^L = \tan^{-1}\left[\frac{\sin\Psi_f}{\cos\Psi_f + \frac{m_H}{m_O}}\right] \qquad [25]$$

Equation [24] also contains the velocity dependence of the cross-section:

$$I(v_i) \propto v^{-4/n} \qquad [26]$$

For the r^{-6} and r^{-12} potentials, respectively, the dependence of the

cross-section on initial relative velocity is of the form $v_i^{-2/3}$ and $v_i^{-1/3}$ at any angle or in any angular range. This is thus also true in the limit of the total cross-section, although the classical total cross-section is infinite for potentials which are non-constant at arbitrarily large distances.

Suppose we include both the r^{-6} and r^{-12} terms in the potential (e.g., the Lennard-Jones (12,6) potential,

$$V(r) = \varepsilon \left[\left(\frac{r_m}{r} \right)^{12} - 2 \left(\frac{r_m}{r} \right)^{6} \right]$$

where ε and r_m are parameters; see Figure 7). From Equation [20] we see that the scattering angle will now be given by the sum of two terms, one for each part of the potential. If we evaluate the integral we obtain

$$\Psi_f = + \frac{\varepsilon \, r_m^{\,6}}{\mu \, v_i^{\,2} b^6} \, \frac{15\pi}{4} \left[\frac{231}{320} \frac{r_m^{\,6}}{b^6} - 1 \right] \qquad [27]$$

This can be solved for b in terms of Ψ_f and v_i:

$$b = r_m \left[\frac{\frac{231}{160} K}{K \pm \sqrt{K^2 + \frac{231}{80} K \Psi_f}} \right]^{1/6} \qquad [28]$$

where

$$K = \frac{15\pi \varepsilon}{4 \mu \, v_i^{\,2}} \qquad [29]$$

For $\Psi_f < 0$, we may take the negative square root, giving very large

impact parameters. The dominant potential in this case is, of course, the attractive r^{-6} potential. Or we may take the positive root, as we must if $\Psi_f > 0$, giving values of b near

$$b = \left(\frac{231}{320}\right)^{1/6} r_m \approx .947\ r_m \qquad [30]$$

In this case there is a very narrow range in the impact parameter over which small angle scattering can occur. Both parts of the potential are important. In view of the very small range of b over which the r^{-12} potential can exert itself (for small angle scattering) and the relatively much greater region over which the r^{-6} potential can be effective, we would expect the small angle scattering behavior to follow, very nearly, laws derived for the simple attractive r^{-6} potential. We also note, for potentials more complicated than $V(r) = C\ r^{-n}$, that $b(\Psi_f)$ is not necessarily a single-valued function of Ψ_f.

Another important point is the following: at $b = .947\ r_m$ (for the LJ potential) the scattering angle is zero. For greater values Ψ_f is always negative. But we know that as $b \to \infty$ the scattering angle must $\to 0$. Since there are no singularities in this region there must be some value of b - and thus of $\Psi_f(b)$ - at which $d\Psi_f(b)/db = 0$. From Equation [24] we see that the cross-section $I(\Psi_f)$ must be infinite at this angle, Ψ_f^r, which is known as the rainbow angle. In reality the rainbow angle is large enough that the small deflection approximation is often inadequate. We would, however, expect the basic features of rainbow scattering to exist in the arbitrary-angle classical treatment.

The expressions derived above are very useful to laboratory experimentalists, who generally are not able to observe, or are not interested in observing, at large angles. In our application, however, it is essential that we know the differential scattering cross-section for scattering into all angles. Therefore we now turn to the arbitrary-angle classical problem.

The Lagrangian for the system in Figure 6 is

$$\mathcal{L} = \frac{\mu}{2} (\dot{r}^2 + r^2\dot{\theta}^2) - V(r) \qquad [31]$$

Lagrange's equations give

$$\mu r^2\dot{\theta} = \mu r^2 v_i \frac{b}{r^2}\bigg|_{t=-\infty} = \mu v_i b \qquad [32]$$

and

$$\mu \ddot{r} - \mu r \dot{\theta}^2 + \frac{dV}{dr} = 0 \qquad [33]$$

These can be readily solved to give

$$\theta_f = \Psi_f = v_i b \int_{traj.} \frac{1}{r^2} \frac{dr}{\sqrt{v_i^2 - \frac{v_i b^2}{r^2} - \frac{2V(r)}{\mu}}} \qquad [34]$$

where the integration is over the entire trajectory. A potential of the form $V(r) = C r^{-n}$ has a symmetrical trajectory (as do all central forces) about the direction to its point of closest approach, r_0, and $r(t)$ is monotonic before and after the time of closest approach, so that in this case

$$\Psi_f = 2\, v_i b \int_{r_0}^{\infty} \frac{1}{r^2} \frac{dr}{\sqrt{v_i^2 - \frac{v_i^2 b^2}{r^2} - \frac{2C}{\mu r^n}}} \qquad [35]$$

The value of r_0 is found by setting the radicand equal to zero and solving for the largest positive real root. The above integral cannot be evaluated analytically for most potentials, including the inverse sixth and twelfth power cases, and we must resort to numerical methods. The Lennard-Jones potential must also be handled numerically.

Before presenting numerical results we must do something about the infinite value of the total cross-section. This is a problem common to all force fields which are non-zero at arbitrarily large distances in classical mechanics and those which do not fall off faster than r^{-2} in quantum mechanics. The easy way out of this dilemma is first to invoke the Heisenberg uncertainty principle as follows: we do not care what the particular value of x of the incident particle is at a long time before scattering. We require only that the particle be far away from the scattering center initially and consequently the x-component of the momentum can be known with any desired degree of accuracy. The initial y value, b, of the incident particle is very important, however, and if the particle is to have a well-defined classical trajectory then the uncertainty in the impact parameter, Δb, must be much less than b. Once we have determined b to within this uncertainty, however, we have introduced an uncertainty into the y-component of the momentum of the form

$$\Delta p = \mu \, \Delta v_{y_i} \approx \frac{\hbar}{\Delta b} \qquad [36]$$

the wave packet which is the particle will spread after the measurement of y with an angle $2 \, \Delta v_{y_i} / v_i$;

$$\frac{2 \, \Delta v_{y_i}}{v_i} = \frac{2 \, \hbar}{\mu \, v_i \Delta b} \gg \frac{2 \, \hbar}{\mu \, v_i b} \qquad [37]$$

For small angle scattering this angle of uncertainty of the incident particle manifests itself in an equal uncertainty in the scattering angle. The classical description is valid if this angle of uncertainty is significantly less than the classical scattering angle; i.e., at

$$\Psi_f^* \lesssim \frac{2 \, \hbar}{\mu \, v_i b} \qquad [38]$$

the predictions of classical mechanics cannot be trusted. This should not be interpreted as implying that at angles smaller than the "limiting angle", Ψ_f^*, one cannot distinguish scattered particles from unscattered particles and hence that it is meaningless to talk about the (unmeasurable) scattering cross-section at such angles. For in an actual scattering situation we do not measure the impact parameter, b, to within an uncertainty Δb before the scattering. Instead we bombard the target atom with atoms whose position is essentially unknown - plane waves for all practical purposes. And the scattered intensity can be measured at arbitrarily small angles

provided only that we observe at large enough distances to avoid the inevitable diffraction effects on the incident beam. The invocation of the uncertainty principle merely tells us the angle below which quantum mechanical calculational methods - the expansion of the wave function in a sufficiently large number of partial waves and the determination of the phase shifts for each partial wave - may be required. (For this purpose we may substitute $b = \sqrt{\sigma/\pi}$ into Equation [38], where σ is the total cross-section.) Since only small angle scattering is usually involved one can make a number of simplifying assumptions (e.g., that only the attractive Van der Waals force is important). Such calculations have been done (e.g., Pauly and Toennies, 1965, p. 227 and p. 306). Theory and experiment are in surprisingly good agreement on this matter. Typical results can be reasonably well approximated by assuming that at angles less than Ψ_f^* the differential cross-section is constant and equal to its classical value at Ψ_f^*. How does this affect the total cross-section? We have

$$\sigma \propto v^{-2/3} \left[\int_{\Psi_f=0}^{\Psi_f^*} \Psi_f^{*-2\frac{1}{3}} \sin \Psi_f \, d\Psi_f + \int_{\Psi_f=\Psi_f^*}^{\pi} \frac{\Psi_f^{-1\frac{1}{3}}}{\sin \Psi_f} \sin \Psi_f \, d\Psi_f \right]$$

$$\approx v^{-2/3} \left[\Psi_f^{*-\frac{1}{3}} - 3\pi^{-\frac{1}{3}} + 3\Psi_f^{*-\frac{1}{3}} \right]$$

$$\approx v^{-2/3} \times 4 \Psi_f^{*-\frac{1}{3}} \qquad [39]$$

where we have approximated $\cos \Psi_f^*$ by $(1 - \Psi_f^{*2})$ and neglected the

$-3\ \pi^{-\frac{1}{3}}$ term. Now if we substitute

$$\Psi_f^* = \frac{2\hbar}{\mu v}\sqrt{\frac{\pi}{\sigma}} \qquad [40]$$

we get

$$\sigma \propto v^{-2/3} \times 4\left(\frac{2\hbar}{\mu}\sqrt{\pi}\right)^{-1/3} v^{1/3} \sigma^{1/6}$$

$$\sigma^{5/6} \propto v^{-1/3}$$

or

$$\sigma \propto v^{-2/5} \qquad [41]$$

For heavy atoms this is the dependence that is indeed observed. For the scattering of lighter atoms, however, such as Li by Xe or Hg, undulations are observed about the predicted form, due to quantum mechanical interference effects. It is necessary, of course, to use velocity selected beams to observe these undulations because they are usually "smeared out" when either target or projectile particles have a thermal distribution. There is no experimental data, to the author's knowledge, on the angular or velocity dependences of the scattering cross-section of H or He by O atoms. However, it seems likely, with such small reduced masses, that the "wavelength" of the undulations will not be negligible with respect to a velocity differential of physical interest (i.e., $\ll\sqrt{2kT/m}$, $m = m_H$ or m_{He}) and that one cannot assume that the classical prediction will be adequate for an escape calculation. Thus it is necessary to calculate the appropriate cross-sections in a better approximation.

XI. Classical Prediction

Before doing so let us look briefly at the atmospheric consequences were the classical small deflection approximation valid. The upward flux of atoms across a stationary horizontal plane in a Maxwell-Boltzmann gas is given by

$$\text{flux} = \rho \times \int_{\text{all } \vec{v} \text{ with } v_z>0} v_z \, f(v) \, d\vec{v} \qquad [42]$$

where ρ is the density, $f(v)$ the distribution function and v_z the vertical component of velocity. The factor v_z weights higher speeds more heavily than slower speeds. Consequently, a higher fraction of atoms crossing a given level will have speeds greatly in excess of the mean speed than is true of the distribution function alone (see Figure 8). Consequently, if the collision cross-section varies as $v^{-0.4}$, collisions will pose less of a problem to fast, potential escape particles than to the gas as a whole. This will allow escape to occur from a deeper level than would be indicated by the mean free path of the gas as a whole. More dramatic than this effect, however, is the pronounced forward-directedness of the differential cross-section ($I(\Psi_f)$ is approximately $\propto \Psi_f^{-1\frac{1}{3}}$ for $\Psi_f > \Psi_f^*$). Since the limiting angle, Ψ_f^*, becomes smaller with increasing speed the scattering is most strongly forward peaked for fast particles. Thus not only do the fast particles suffer fewer collisions but the collisions are less effective in robbing them of their speed (the excess over escape speed is the important quantity) or directivity. Consequently, escape could be expected to occur from a much greater depth than

envisioned by Jeans. We can obtain a crude estimate of this depth as follows: We can assume, for numerical purposes, that a fast particle will suffer half as many collisions per centimeter traveled as an average particle (which is probably an O atom, which is bigger and slower than an H or He to start with). The median scattering angle, $\Psi_{f_{med}}$, for a $\Psi_f^{-1\frac{1}{3}}$ angular dependence and a limiting angle of 2° (appropriate foran H atom at a speed of 11.5 km/sec) is found from

$$\frac{\int_{\Psi_f=0°}^{2\Psi\frac{\pi}{180°}} \left(2° \frac{\pi}{180°}\right)^{-1\frac{1}{3}} d\Psi_f + \int_{\Psi_f=2°\frac{\pi}{180°}}^{\Psi_{f_{med}}} \Psi_f^{-1\frac{1}{3}} d\Psi_f}{\int_{\Psi_f=0°}^{2°\frac{\pi}{180°}} \left(2° \frac{\pi}{180°}\right)^{-1\frac{1}{3}} d\Psi_f + \int_{\Psi_f=2°\frac{\pi}{180°}}^{180°} \Psi_f^{-1\frac{1}{3}} d\Psi_f} = \frac{1}{2} \qquad [43]$$

which gives

$$\Psi_{f_{med}} \approx 4.4°$$

An H atom traveling at 12 km/sec and scattering through 5° off an O atom loses (from conservation of energy and momentum, the obvious details of which are not reproduced here) only 1/4000 of its speed during the encounter. The average H atom having $v_H \geq v_{esc}$ has, let us say, 10% excess speed over that required for escape ($v_H \approx 1.1\ v_{esc}$). With $v_{esc} \approx 10.8$ km/sec a typical potential escape H atom will be able to suffer about 10% of 4000 = 400 collisions at the mean scattering angle before its speed would drop below v_{esc}. If the particle started at some depth in the atmosphere with its velocity nearly straight upward, it would execute very nearly a random walk in direc-

tion and the number of collisions expected before the atom would be deflected through 90° and (for the flat earth geometry) again be unable to escape is something like $(90°/5°)^2 = 324$. If we assume that the mean angle with the vertical of the H atoms' velocities is 30° during this time, then an appreciable number of escaping particles would have acquired their excess speed from depths of 324 cos 30° ≈280 typical (for fast particles) mean free paths. This is the thickness of atmosphere which would then have to be considered in treating the escape problem properly. There is a factor of 2 in depth because of the larger mean free paths of fast H atoms so that this thickness is about 560 typical mean free paths. This corresponds to an altitude of about 190 km. This is a far cry from the concept of a sharply defined "transition level" or limited "transition region". Furthermore, since the atmosphere is not isothermal below about 350 km, the correction to Jeans' escape rate due to the lower effective temperature (averaged appropriately over the entire escape region) might outweigh in importance any correction due to the departure from an M-B distribution function caused by the escape. Additional large correction factors might also be needed to characterize the sluggishness of diffusion processes in replenishing the various parts of the escape region. Clearly, if this picture of the escape process is qualitatively correct, then all prior notions of how best to treat the problem become suspect. Indeed, it was this point of view which led the present author to investigate more carefully the nature of the O-H elastic interaction and its effect on thermal escape. The true picture, of course, must lie somewhere between the two extremes dis-

cussed above (since the small angle approximation neglects the repulsive part of the potential). We now turn to the problem of finding where in this range a more accurate treatment of the escape process will fall.

XII. WKB Calculation of Elastic Cross-Sections

We have seen that the small angle classical calculation of the atom-atom elastic differential and total scattering cross-sections may not be valid for the O-H interaction at temperatures representative of those prevailing in the earth's upper atmosphere. The Schrödinger equation for the interaction of two particles (again in the center-of-mass system) is

$$-\frac{\hbar^2}{2\mu}\nabla^2\Psi + V(r)\,\Psi = E\,\Psi \qquad [44]$$

Here $\hbar$, μ, $V(r)$ and E are, respectively, Planck's constant (divided by 2π), the reduced mass, the potential energy of the system as a function of interatomic distance r and the kinetic energy

$$E = \frac{\mu}{2}(\dot{r}^2 + r^2\dot{\theta}^2) = \frac{\mu}{2}v^2$$

The wave function for the system is denoted by Ψ (the scattering angle does not enter the development until Equation [54], so no confusion should result). We let $k = \frac{\mu v}{\hbar}$ and expand the wave function in spherical harmonics (separation of variables) to obtain the differential equation for the ℓth radial wave function

$$\frac{d^2(r\,\Psi_\ell)}{dr^2} + \left[k^2 - \frac{\ell(\ell+1)}{r^2} - \frac{2\mu\,V(r)}{\hbar^2}\right] r\,\Psi_\ell = 0 \qquad [45]$$

For two non-interacting particles we have

$$\frac{d^2(r\,\Psi^o_\ell)}{dr^2} + \left[k^2 - \frac{\ell(\ell+1)}{r^2}\right] r\,\Psi^o_\ell = 0 \qquad [46]$$

We can write the solution to Equation [45] as

$$r\,\Psi_\ell = \exp\left(\frac{i}{\hbar}\,u_\ell(r)\right) \qquad [47]$$

where

$$u_\ell(r) = {}^0u_\ell(r) + \left(\frac{\hbar}{i}\right){}^1u_\ell(r) + \left(\frac{\hbar}{i}\right)^2 {}^2u_\ell(r) + \cdots \qquad [48]$$

If we substitute Equations [47] and [48] into Equation [45] and equate terms of equal power in $\hbar$ (neglecting the $\hbar^2$ in the centrifugal potential) the ${}^ju_\ell$'s can be determined and the solution written

$$r\,\Psi_\ell = \left[\frac{\hbar^2}{2\mu}\left(k^2 - \frac{\ell(\ell+1)}{r^2} - \frac{2\mu\,V(r)}{\hbar^2}\right)\right]^{-\frac{1}{4}}$$

$$\times \exp \pm i\left(\int_{r_0}^{r}\left[k^2 - \frac{\ell(\ell+1)}{r^2} - \frac{2\mu\,V(r)}{\hbar^2}\right]^{\frac{1}{2}} dr\right.$$

$$\left. + \text{smaller terms}\right) \qquad [49]$$

Here r_0 is the point of closest approach. Equation [49] represents two solutions, one with the exponent positive and one with it nega-

tive. By taking linear combinations of these two solutions we can find two wave functions for the classical,

$$k^2 - \frac{\ell(\ell+1)}{r^2} - \frac{2\mu V(r)}{\hbar^2} > 0$$

and non-classical,

$$k^2 - \frac{\ell(\ell+1)}{r^2} - \frac{2\mu V(r)}{\hbar^2} < 0$$

regions. Using Kramer's connection formulae [Merzbacher, 1961] to join these solutions gives, for the first approximation in the classical region,

$$r\,\Psi_\ell = \left[\frac{\hbar^2}{2\mu}\left(k^2 - \frac{\ell(\ell+1)}{r^2}\right)\right]^{-\frac{1}{4}} \times \cos\left(-\frac{\pi}{4} + \int_{r_0}^{r}\sqrt{k^2 - \frac{\ell(\ell+1)}{r^2} - \frac{2\mu V(r)}{\hbar^2}}\,dr\right) \qquad [50]$$

At large r this becomes

$$r\,\Psi_\ell \sim \cos\left(kr - kr_0 - \frac{\pi}{4} + \int_{r_0}^{r}\left[\sqrt{k^2 - \frac{\ell(\ell+1)}{r^2} - \frac{2\mu V(r)}{\hbar^2}} - k\right]dr\right) \qquad [51]$$

The corresponding solution to Equation [46] is

$$r\,\Psi_\ell^o \sim \cos\left(kr - \frac{\pi}{4} - \frac{\pi}{2}\sqrt{\ell(\ell+1)}\right) \qquad [52]$$

The phase shift for a given ℓ value is the difference in the argument between Equations [51] and [52]; i.e., it is the phase difference between the two radial wave functions (solutions of Equations [45]

and [46] at large r). The phase shift, η_ℓ, is then

$$\eta_\ell(k) = \frac{\pi}{2}\sqrt{\ell(\ell+1)} - kr_0 + \int_{r_0}^{r}\left[\sqrt{k^2 - \frac{\ell(\ell+1)}{r^2} - \frac{2\mu V(r)}{\hbar^2}} - k\right] dr \qquad [53]$$

The scattering amplitude, $f(\Psi)$, where Ψ is now the scattering angle, is given by

$$f(\Psi) = \frac{1}{2ik}\sum_{\ell=0}^{\infty}(2\ell+1)[\exp(2i\eta_\ell) - 1]\,P_\ell(\cos\Psi) \qquad [54]$$

where P_ℓ is the ℓth Legendre polynomial. The differential cross-section is given by

$$\frac{d\sigma}{d\Omega} = |f(\Psi)|^2 \qquad [55]$$

and the total cross-section by

$$\sigma = \int_{\chi=0}^{2\pi}\int_{\Psi=0}^{\pi}|f(\Psi)|^2\,d\Psi\,d\chi = \frac{4\pi}{k^2}\sum_{\ell=0}^{\infty}\sin^2(\eta_\ell) \qquad [56]$$

These equations describe the elastic scattering for a central force in the (first) WKB approximation. The approximation that has been made is the joining of classical and non-classical region wave functions by the use of the Kramer's connection formulae. While the development above is sketchy, to say the least, further details are readily available (e.g., Hirschfelder et al., 1954, pp. 685 ff., which is followed in the above, or Dicke and Wittke, 1961, pp. 245 ff.). The approximation is valid for large scattering angles as well as small - in contrast to the Born approximation, for example, which is valid

only for small "perturbation" scattering - and is much easier to apply than the rigorous, straightforward integration of the Schrödinger equation. Marchi and Mueller [1962] have compared WKB phase shifts to "exact" numerical results for an H_2-Hg system, which has a very low reduced mass ($\approx$ 2 a.m.u.) as do the systems of atmospheric interest. The relative speed is not stated but presumably it is on the order of 2 km/sec. The agreement is excellent and is well within the rather small experimental error in all available data. In a later paper [Marchi and Mueller, 1963] they made a more extensive comparison of the two methods. Again the agreement was excellent. One "criterion of validity" for the WKB method is [Bohm, 1951, chapter 12]

$$\frac{h\mu\left|\frac{\partial V(r)}{\partial r}\right|}{[2\mu(E - V(r))]^{3/2}} \ll 1 \qquad [57]$$

For an O-H interaction at a relative speed of 1 km/sec (this is a rather slow collision in the upper atmosphere; the most probable speed of an H atom at 1500°K is about five times this great) Equation [57] is not satisfied for r much smaller than about 5Å. Marchi and Mueller found, however, that the WKB approximation still predicted accurate cross-sections when the major portion of the contribution to the integrand in Equation [53] was from values of r smaller than this. In fact, except for unlikely energy resonances and cases of orbiting the WKB approximation gave good results in all cases tested. Consequently we adopt the method here for use on O-H (or O-He) elastic scattering in the upper atmosphere.

In order to calculate the total and differential cross-sections in this manner, we need to know the parameters of the (assumed) Lennard-Jones (12,6) potential function - $\mathcal{E}$ and r_m (see Figure 7). We do this for the systems O-H, O-He, He-He and Ar-Kr in order to have a wide range of cases to better assess the reasonableness of our results. We first use the Slater-Kirkwood formula for the Van der Waals constant in terms of the atomic polarizabilities.

$$C = -\frac{3}{2}\frac{e\hbar}{m^{\frac{1}{2}}}\frac{\alpha_1\alpha_2}{\left(\frac{\alpha_1}{N_1}\right)^{\frac{1}{2}}+\left(\frac{\alpha_2}{N_2}\right)^{\frac{1}{2}}} \qquad [58]$$

where C, e, $\hbar$, α_1, α_2, N_1 and N_2 are respectively the Van der Waals constant, electron charge, Planck's constant (divided by 2π), electron mass, polarizabilities of the two atoms and total number of electrons in the two atoms. This formula is believed to be more accurate than the earlier version in which N_1 and N_2 referred only to outer shell electrons and the even earlier form due to London [Pauly and Toennies, 1965]. Polarizabilities are taken from a paper by Dalgarno [1962] and Allen's Astrophysical Quantities [1963], Dalgarno's value being preferred for O. The values of α and N are as follows:

	α	N
H	0.67×10^{-24} cm^3	1
He	0.21 " "	2
O	0.73 " "	8
Ar	1.64 " "	18
Kr	2.48 " "	36

The values for the Van der Waals constant, C, are

	C
O-H	10.98×10^{-60} erg cm^6
O-He	6.16 " "
He-He	1.71 " "
Ar-Kr	181.44 " "

Next we collect the values for the covalent radii of each of the atomic species, add 0.8Å to each to give a reasonable approximation to the Van der Waals radii [Gould, 1962, p. 149] and add these latter quantities to obtain the values of r_m for the appropriate systems:

	covalent radius	Van der Waals radius
H	.28Å	1.08Å
He	~.2 Å	1.0 Å
O	.74Å	1.54Å
Ar	1.91Å	2.71Å
Kr	2.2 Å	3.0 Å

	r_m
O-H	2.62Å
O-He	2.54Å
He-He	2.0 Å
Ar-Kr	5.71Å

The Van der Waals constant is related to ε and r_m by

$$C = 2 \varepsilon r_m^6 \qquad [59]$$

Thus we can obtain the values of ε also:

	ε
O-H	1.70×10^{-14} erg
O-He	1.15 "
He-He	1.34 "
Ar-Kr	0.26 "

These values for ε and r_m seem very reasonable and were adopted for the WKB calculations. Results of the calculations are shown in Figures 9-35. Figures 9 and 10 depict the phase shifts for the O-H and O-He systems, respectively. Figures 11-34 show the differential cross-sections for O-H (13 different relative velocities from 600 m/sec to 60 km/sec) and O-He (11 relative velocities from 600 m/sec to 25 km/sec). Also plotted for comparison are the classical calculations for both small and arbitrary angle (hence the rainbow effects) extending to the low-angle cutoff specified by the uncertainty principle. Figure 35 is a plot of the total cross-section for the two systems as a function of relative speed. Also shown is the curve used by LS in their paper for the velocity dependence of the O-H cross-section (more will be said about this shortly). This completes the section describing the calculation of the appropriate differential and total cross-sections in the WKB approximation.

In the next section we discuss the actual Monte Carlo calculation of the escape flux in the earth's atmosphere using these cross-sections and describe the computer program which was written to perform the calculation.

XIII. Monte Carlo Escape Calculation

A Monte Carlo calculation may be useful in describing the behavior of the aggregate of a large number of mutually independent events. In the present application the procedure is as follows: We neglect the barometric density dependence of the upper atmosphere on altitude and instead (as did CC and in analogy with plane-parallel atmosphere radiative transfer calculations) consider a uniform plane-parallel infinite slab of background gas (O atoms at the arbitrary density of 10^8 cm^{-3}) of finite thickness. The slab is considered to be composed of 10 layers, each 10% of the total slab thickness. Since hydrogen is a minor component in the upper atmosphere, it is the oxygen atoms, with their much smaller diffusive equilibrium scale height, which determine the position of the "escape level". The temperature of the oxygen atom background gas is specified and it is assumed that this temperature is constant and that the O atoms have an M-B distribution appropriate to this temperature. The H (or He) atoms are assumed not to interact with each other, but only with the (M-B) background gas. An H (or He) atom is released into the background gas. There were two different procedures adopted in the present calculations: in one the particles are injected at the bottom of the slab (as was done by LV, LS, and CC) with a speed and direction appropriate for an M-B distribution (this requires that the slab be made thick enough that departures from M-B due to escape at the top are small at the bottom of the slab). The particle's parameters must not be chosen directly from an M-B distribution, however, but from

the appropriate flux:

$$F = \rho_0 \left(\frac{m_H}{2\pi kT}\right)^{3/2} \int_{v=v'}^{\infty} \int_{\theta=0}^{\pi/2} \int_{\varphi=0}^{\pi} v^2 \, e^{-\frac{m_H v^2}{2kT}} \, (v \cos\theta) \sin\theta \, d\theta \, d\varphi \, dv \qquad [60]$$

This is the integral of the M-B distribution function multiplied by the vertical component of the velocity. We disagree on this point with LV, who drew their parameters simply from an M-B distribution. If we integrate Equation [60] over the angular coordinates we obtain

$$F = \rho_0 \left(\frac{m_H}{2\pi kT}\right)^{3/2} \pi \int_{v=v'}^{\infty} v^3 \, e^{-\frac{m_H v^2}{2kT}} \, dv \qquad [61]$$

A pseudo-random number, i_R, is generated (by the method of congruences) between 0 and 1 and this is set equal to

$$i_R = \frac{\int_{v=v'}^{v} v^3 \, e^{-\frac{m_H v^2}{2kT}} \, dv}{\int_{v=v'}^{\infty} v^3 \, e^{-\frac{m_H v^2}{2kT}} \, dv} \qquad [62]$$

This determines the speed, v, of the incident atom. The lower limit on the integration, v′, is zero when particles are being injected from the bottom of the slab. In the second procedure, in which particles representative of the "missing" particles in a real atmosphere (i.e., reflected escape particles) are injected from the top, the value of v′ is $v' = v_{esc}$. The integrals in Equation [62] can be solved in terms of the error function. Prior to the running of the main Monte Carlo program, this equation is solved for v for i_R =

0.00, 0.02, 0.04, ..., 1.00 for the appropriate values of m_H (for H or He) and T and these values are read into the computer as a table from which v can be obtained for arbitrary i_R by interpolation. The value of v for $i_R = 1.00$ is strictly infinite, which would cause serious error in the calculation so instead an "effective" value of v was obtained by extrapolating from the v values for $i_R = 0.94$, 0.96 and 0.98. A slight error remains in the procedure here but it is of no important consequence. Once the speed of the incident particle has been chosen the angle which its trajectory makes with the vertical is obtained, from Equation [60], as follows:

$$i_R = 1 - \frac{\int_{\theta=0}^{\theta} \cos\theta \sin\theta \, d\theta}{\int_{\theta=0}^{\pi/2} \cos\theta \sin\theta \, d\theta} = \cos^2\theta \qquad [63]$$

where i_R is another random number between 0 and 1. The positive root is taken for the first case (injection at the bottom) and the negative root for the second (injection at the top). Thus 45° is the median angle. For the M-B distribution as a whole, as used by LV, the value is $\cos^{-1}(.5) = 60°$. We need not specify the azimuthal angle.

The particle now has a speed and a direction. We fix its position by specifying that it be initially at the bottom of the slab in the first case or at the top in the second. At this point its mean free path is needed and here a slight digression is necessary. The mean free path of a hydrogen atom moving with a finite speed through a M-B distribution of O atoms is a function of the speed of the hydro-

gen atom in the rest (or atmospheric) frame, v_H, even for hard sphere model atoms. The dependence is obtained by integrating over the O atom velocity distribution the product of density, cross-section, distribution function and relative speed (again the flux factor) to obtain the collision frequency, P:

$$P(v_H) = \int_{v_O=0}^{\infty} \int_{\beta=0}^{\pi} \int_{\gamma=0}^{2\pi} \rho_O \sigma v_r f(\vec{v}_O) d\vec{v}_O \qquad [64]$$

where

$$v_r = \sqrt{v_H^2 + v_O^2 - 2 v_H v_O \cos \beta} \qquad [65]$$

For hard sphere atoms the cross-section is constant and the integration can be performed in terms of the error function. This is the velocity dependence used by CC. We have seen, however, that the cross-section is strongly velocity dependent. The results of Figure 35 were fit to the parametric form

$$\sigma(v_r) = \frac{A}{v_r} + \frac{B}{v_r^2} + C, \qquad v_r \geq 1400 \text{ m/sec}$$

$$\sigma(v_r) = D, \qquad v_r \leq 1400 \text{ m/sec} \qquad [66]$$

The values of A, B and C were (in c.g.s. units) 94.2×10^{-11}, 185.0×10^{-6} and 22.8×10^{-16} for O-H and 51.7×10^{-11}, 93.0×10^{-6} and 22.0×10^{-16} for O-He. This can be substituted into Equation [64] and the integration performed piecewise in terms of the error function:

$$P(v_H) = \rho_0\left(\frac{m_0}{2\pi kT}\right)^{3/2} \frac{2\pi}{v_H} \int_{v_0=0}^{\infty} v_0 \, e^{-\frac{m_0 v_0^2}{2kT}} \int_{v_r=|v_H-v_0|}^{v_H+v_0} v_r^2 \sigma(v_r) \, dv_r \, dv_0 \qquad [67]$$

where we have used the relationship

$$v_r \, dv_r = v_H v_0 \sin\beta \, d\beta \qquad [68]$$

The integrations are straightforward and the integrated forms, which are fairly complicated, are not reproduced here. The mean free path is related to the collision frequency by

$$\ell(v_H) = \frac{v_H}{P(v_H)} \qquad [69]$$

Values of $\ell(v_H)$ are calculated, again in a preliminary program, for 51 values of v_H ranging from 0 to 5 times the most probable speed

$$\sqrt{\frac{2kT}{m_H}}$$

in equal steps and are read into the computer as a table by the main program. The mean free path for arbitrary v_H is obtained by interpolation. Figure 36 depicts typical results.

Once the mean free path is known the distance which the particle will travel before its next collision with an O atom is obtained from another random number between 0 and 1 as follows:

$$d = -\log_e(i_R) \times \ell \qquad [70]$$

It should be pointed out that, whereas CC assumed that the cross-section was velocity independent, LS adopted a velocity dependence

but failed to take into account the integration over background gas velocities. Furthermore, their velocity dependence, shown in Figure 35, was obtained from collision integrals [Krupenie et al., 1963] sensitive only to large angle scattering and hence is not really appropriate in the escape problem. LV also neglect the integration over background gas but do provide for a velocity dependent cross-section. Unfortunately they do not reveal the values of the parameters in their interatomic potential so it is difficult to assess the value of the procedure.

Having specified the location of the next collision we must now obtain the parameters (speed and two angles) for the O atom with which the H atom will collide. CC err in this matter by simply choosing the speed and direction from an isotropic M-B distribution. LV make the same mistake and LS do not state what method was used in deriving the target particle parameters other than they were drawn "at random". In fact, the parameters of the ultimate target particle are influenced by the speed of the incident particle. For "fast" H atoms the effect is not important but for "slow" H atoms it can be quite appreciable. To find the appropriate speed of the O atom we generate another random number between 0 and 1 and set it equal to the fraction of the total collision frequency of the H atom due to oxygen speeds less than v_0:

$$i_R = \frac{\int_{v_0=0}^{v_0} v_0 \, e^{-\frac{m_0 v_0^2}{2kT}} \int_{v_r=|v_H-v_0|}^{v_H+v_0} v_r^2 \, \sigma(v_r) \, dv_r \, dv_0}{\int_{v_0=0}^{\infty} v_0 \, e^{-\frac{m_0 v_0^2}{2kT}} \int_{v_r=|v_H-v_0|}^{v_H+v_0} v_r^2 \, \sigma(v_r) \, dv_r \, dv_0} \qquad [71]$$

Values of v_0 for the previously mentioned 51 values of v_H and values of i_R = 0.00, 0.02, 0.04, ..., 1.00 were calculated with a preliminary program and the resulting 51 x 51 matrix read into the computer as a table. Values of v_0 for arbitrary v_H and i_R are obtained by two dimensional interpolation. For i_R = 1.00, v_0 is strictly infinite, but here again the value of v_0 was obtained by extrapolating from the three previous values.

With the speed of the target particle properly chosen we must now generate two angles to describe its direction of approach. One is an azimuthal angle (about the vector $\vec{v}_H$) which is essential to the calculation but is not mentioned by LV, LS or CC. This angle, γ, is obtained simply by generating a random number between 0 and 2π. The second angle, β, the angle between the vectors $\vec{v}_0$ and $\vec{v}_H$, is obtained from Equation [67] with v_0 = constant:

$$i_R = \frac{\int_{|v_H-v_0|}^{v_r} \sigma(v_r) \, v_r^2 \, dv_r}{\int_{|v_H-v_0|}^{v_H+v_0} \sigma(v_r) \, v_r^2 \, dv_r} \qquad [72]$$

where i_R is yet another random number. The angle β is obtained from

$$\beta = \cos^{-1}\left(\frac{v_H^2 + v_O^2 - v_r^2}{2\, v_H v_O}\right) \qquad [73]$$

The integrations in Equation [72] are, as before, done piecewise and are straightforward but awkward (the solution of a cubic equation is generally required). This part of the calculation is done in the main program because a three dimensional matrix (v_H, v_O, i_R) would require too much core space.

Now we must specify the scattering angles (as before, two angles are required; no mention is made by LV, LS or CC of an azimuthal angle. Furthermore, all three have assumed isotropic scattering.). The appropriate differential cross-sections of Figures 11-34 were read into another preliminary program which generated tables of scattering angle, Ψ, versus probability, i_R, for the various given values of v_r,

$$i_R = \frac{\int_{\Psi=0}^{\Psi} I(\Psi)\, d\Psi}{\int_{\Psi=0}^{\pi} I(\Psi)\, d\Psi} \qquad [74]$$

which were read into the main program. Then, by generating another random number between 0 and 1 and knowing v_r, the scattering angle (in the center-of-mass reference system) can be obtained by two dimensional interpolation. The corresponding angle in the "laboratory" system (in which the O atom is initially at rest) is obtained by use of Equation [25]. The corresponding azimuthal angle, χ, is generated at random (between 0 and 2π) as was γ.

The four equations of conservation of energy and momentum for a two particle collision involve 14 quantities: two speeds, two masses, two angles each for the initial directions of the two particles, two speeds after collision and four more direction angles. Two can be eliminated by choosing the coordinate system in a convenient manner. We know all the precollisional quantities and two post-collisional quantities (the scattering angles). The three uninteresting remaining quantities (oxygen speed and direction angles) can be eliminated to give a single equation for the post-collisional hydrogen speed:

$$m_H v_H'^2 [m_O + m_H] - 2 m_H v_H' [m_O v_O \sin\beta \sin\Psi \cos(\chi - \gamma) + m_H v_H \cos\Psi + m_O v_O \cos\beta \cos\Psi] + m_H v_H [m_H v_H + 2 m_O v_O \cos\beta - m_O v_H] = 0 \qquad [75]$$

where v_H' is this speed. In the reference system in which the O atom is initially at rest ($v_O = 0$) Equation [75] takes on a slightly less cumbersome form and we can readily obtain the post-collisional hydrogen speed in that system (since Ψ and χ are defined in this system; β is defined in the atmospheric system but drops out when $v_O = 0$). We then must add the vector $\vec{v}_O$ to this vector to produce the vector appropriate to the atmospheric system. All the necessary quantities are known. To transform the two scattering angles Ψ and χ back into the atmospheric system, we first obtain the angles (in the laboratory coordinate system) to this new vector $\vec{v}_H'$ and then rotate the "laboratory" coordinate system in the plane containing

$\vec{v}_H$ and $\vec{v}_O$ (see Figure 37) counterclockwise through an angle ($\pi - \varepsilon - \beta$) where

$$\varepsilon = \cos^{-1}\left(\frac{v_r^2 + v_O^2 - v_H^2}{2\, v_r v_O}\right) \qquad [76]$$

and find the new angular coordinates of the vector $\vec{v}_H'$. The details of the transformation are omitted as they are straightforward.

The angle which the scattered H atom now makes with the vertical is given by

$$\cos\theta' = \cos\theta \cos\Psi' + \sin\theta \sin\Psi' \cos(\chi' - \gamma) \qquad [77]$$

Here θ is the prior value of θ' and Ψ' and χ' are the transformed scattering angles. We have now specified completely one leg of the H (or He) atom's trip throughout the slab of O atom background gas. The speed of the H atom has been constant in going from its injection point (or the site of its prior collision) to the site of the present collision. The time spent in traversing one complete layer of the atmosphere is then

$$t = \frac{d_\ell}{v_H \cos\theta} \qquad [78]$$

where d_ℓ is the layer thickness (one-tenth of the slab thickness). The time spent by the H atom in each layer is computed and added to an accumulation register for that layer. This will make it possible to obtain a density distribution function at the end of the calculation.

We now repeat the above process (except for the injection part)

repeatedly until one of two things happens: 1) the atom reaches the upper limit of the slab with a speed greater than v_{esc} in which case it has "escaped" or 2) the particle reaches the bottom of the slab in which case its path is also terminated. If it reaches the upper surface with less than escape speed (10.785 km/sec) it is specularly reflected and the calculation continues. Each time a particle escapes a "1" is added to an "escape register" and the appropriate increments made in the density registers; a similar accounting is made of particles which fall below the base of the slab. A program run consists of the program deck (written in Fortran IV and included as an Appendix), the appropriate tables and control cards specifying the temperature, slab thickness, number of particles whose histories are to be followed between printouts and whether the particles are to be injected at the top or at the bottom of the slab. The major portion of the execution time is spent in evaluating transcendental functions, most of which would be necessary regardless of the particular manner in which the cross-sections, etc. are handled. Execution time on the 7094 Model I (which is about 40% slower than the Model II) is considerably less than 10 milliseconds per collision. In view of the larger number of collisions per particle necessitated by the strong forward scattering, however, the time per particle (typically 1/3 second) is probably considerably greater than for previous investigators, who followed hundreds of thousands of particles in compiling their statistics. We will not be able to accumulate such large numbers but will achieve comparable statistical accuracy by injecting the particles at the top of the slab rather than at the bottom, which results

in a reduction in calculation time (for a given accuracy) of typically a factor of 100. The apparent statistical accuracy of the previous investigators may be, of course, misleading because of possible flaws in their procedures. LV, for example, state that they generated an average of 5.5 random numbers per particle followed. In the present study, however, slightly more than 6 random numbers were generated per collision, with many tens of collisions, in general, for each particle. It is theoretically possible to economize on the number of random numbers needed but the effort is awkward and would not improve the program efficiency since relatively few machine cycles are required to generate a random number. Thus we suspect that the previous investigators may have oversimplified the problem, perhaps by neglecting the importance of the third dimension, and certainly in their choice of models, which do, however, allow the use of a relatively thin slab of gas (a few mean free paths in thickness).

We shall shortly remark on some of the results of the Monte Carlo runs conducted with the above program and speculate on the effects on the evolution of the terrestrial atmosphere. We will first consider an intermediate temperature, 1500°K. Calculations were performed with particles incident at the top of the slab with total thicknesses of 10^7, 2×10^7 and 3×10^7 cm, corresponding to approximately 5, 10 and 15 typical mean free paths (for hydrogen). The philosophy here is that a real atmosphere (i.e., one with an escaping component) can be considered as being composed of two types

of H atoms: first, the atoms that are really there and second, the atoms which are "missing" because of escape. While neither component is itself M-B in character (except near the lower boundary of the slab), the two components taken together as one system do satisfy the M-B distribution. The "missing" atoms can be visualized as being "red" atoms and the real atoms as being "green". "Red" atoms are injected, as previously described, into the top of the slab in a fashion which is equivalent to placing a specular reflector on top of the slab (instead of the "semi-permeable membrane" in the real atmosphere which reflects slow particles while allowing fast ones to pass through). Their trajectories are followed until 1) they re-escape (that is, hit the lid with greater than escape speed) or 2) they pass below the lower boundary of the slab. The density distribution of these particles is established, as is the fraction ending its career in each fashion. Now if the bottom of the slab is placed deeply enough that the hydrogen distribution in its vicinity is nearly M-B then, as found by LS and as is intuitively expected, it makes little difference in what manner the particles - which in the real atmosphere are diffusing upwards - are injected. Consequently, when a "red" particle reaches the level of the lower boundary it can be considered to be specularly reflected from this boundary, being dyed green in the process. This is equivalent to simply injecting "green" particles into the real atmosphere from the bottom from the entire M-B distribution. These particles also have one of two fates: 1) they can diffuse upwards to the upper boundary and, if they have sufficient speed, escape or 2) they can, in their mean-

derings, return to the lower boundary of the slab. In either case they have left the slab. Since both the upper and lower boundaries are equivalent, for the sum of the two components, to specular reflectors (or contact with an isothermal M-B region at either end) the total hydrogen density (the real plus missing parts) must be constant throughout and the total distribution function M-B throughout. As a result, if we can characterize either one of the two components for a given temperature and total density we can easily find the other component. The density of the entire system is of course directly related to the total flux (or escape flux) at either boundary. In most cases it seems that it may be much easier to perform the calculation "from above" than "from below" and it is the former method which has been relied upon most heavily in the present work.

XIV. Results of Monte Carlo Calculation

Table 5 lists the calculated escape fluxes. The "number escaping" always refers to a computer run of 250 injected particles. Typically, a dozen or so such runs were conducted for each species-temperature-thickness combination. The rms deviation among these runs was taken as the probable uncertainty. For O-He fewer runs were made, in general, and in this case the error bars are meant to be indicative only. Particles were injected at the top for all such combinations and additionally at the bottom for O-H at 1500°K, in order to test the consistency of the two procedures. We can also get an idea of the relative efficiency of the two approaches from

Table 5. For injection at the top the mean uncertainty in the "number escaping" (the rms deviation among the various runs) for all thickness-temperature combinations (considering only the O-H data now) is 6.7 and the mean "number escaping" is 76.0. This refers to the "missing" component of the atmosphere. For the real atmosphere this representative escape flux is 250 - (76 ± 6.7) = 174 ± 6.7, or about 3.85% uncertainty. It is easily seen that (for the 1500°K case) injection at the bottom (for which approximately equal numbers of particles were involved and equal machine time spent) produced much worse accuracy, typically 32.6% (from a mean escape number of 10.63 ± 3.47). Since the accuracy improves only as the square root of the computing time the order of magnitude advantage in accuracy enjoyed by injecting the particles at the top represents two orders of magnitude advantage, if the calculations are to be performed to a given degree of accuracy. Thus we have been able to obtain statistical accuracy with only a couple of thousand source particles comparable to that obtained by other investigators with a couple hundred thousand source particles. For O-He, since the correction term is so much smaller, the advantage is even more spectacular. Since CC were investigating the real component of the atmosphere they were unable to calculate the O-He correction at temperatures much below 7000°K (their lowest point).

To transform the data of Table 5 into corrections to Jeans' escape rate we must know the fractional density at the "escape level" due to each component of the hydrogen distribution (i.e., the "real" particles and the "missing" particles). In all cases treated here,

it is not very important precisely how we define the "escape level"; we take it to be the mean free path (from the top of the slab) for a hydrogen atom with the most probable speed for the given temperature, $\sqrt{2kT/m_H}$. The density distributions for the cases calculated for Table 5 are shown in Figures 38-43. The densities have been normalized to correspond to a total hydrogen (or helium) density (real plus missing) of 1 cm^{-3}. The escape level is indicated. For O-He the density corrections are seen to be always very small and have been neglected. The density distribution for the 1500°K case (for O-H) with the particles injected at the bottom has been incremented by the corresponding density with injection at the top. The sum should, of course, be equal to 1. This serves as a check on the entire procedure. We see that the agreement is pretty good; the mean deviation from 1 is within the mean error bars in all three cases. It may appear suspicious that the calculated densities tend to fall below 1 in all cases, but it must be remembered that the ten density points comprising each curve are not independent. If a given set of calculations produces a low density at one altitude there will be a strong tendency to produce a low density at all altitudes. More machine time could reduce the error bars, but if an error exists in the program, we can see that it is likely to be a small one. Also shown in Figures 38-43 are least-square fits of straight lines to each species-temperature-depth combination (eyeball fits for O-H, machine-calculated fits for O-He). They extrapolate (as was found by CC) to some value below the base of the slab, but whereas CC found the convergent point about 2/3 of a typical mean

free path below the base, we find it to be somewhat lower, about 1.6, 1.5 and 1.35 typical mean free paths respectively for slab thicknesses of 1×10^7, 2×10^7 and 3×10^7 cm (for O-H).

The densities were read from these figures and Table 6 was compiled, giving the corrections to Jeans' escape rate for the various cases. The results are compared in Figure 44 to those of previous workers. The present results are in excellent agreement with those of CC. We disagree strongly with those of LS and LV. For the first time, a Monte Carlo calculation of hydrogen escape agrees with a previous such calculation. Furthermore, these two calculations are the two most recent and their authors have thus been able to profit by their predecessors' mistakes. We conclude that the escape of hydrogen in terrestrial-type atmospheres is about 70% as fast as indicated by the Jeans equation. The rate of escape of helium is predicted even more accurately by Jeans' equation, the error being only some 1 to 3%. A straight line could be drawn, if Figure 44 were extended to include high enough temperatures, through the three present O-He points and CC's O-He points at 7000°K and 11000°K. This provides further reassurance that the agreement is more than coincidental. Although the uncertainty limits in prior work (see Figure 44) prohibited a clear prediction of the temperature dependence of the correction factor it is seen from the present work that the correction term becomes larger with increasing temperature. In Figures 45-49 we present the calculational results indicating the angle at which the various particles which were followed escaped or,

in the case of injection at the top of "escape" particles, re-escaped. For hydrogen at 1000°K we see a marked tendency for particles escaping from the "missing" component of the atmosphere to emerge at angles more nearly horizontal than is true for a M-B flux. Therefore the particles escaping from the "real" atmosphere will tend to emerge more nearly vertical than for a M-B distribution. This is intuitively reasonable. At 1500°K the effect is not as pronounced as at 1000°K and at 2000°K it is less pronounced yet. Figure 48 shows results for 1500°K with the atoms injected at the bottom of the slab. It is difficult to see the slight favoring of angles nearer the vertical, again demonstrating the statistical advantage of following the "missing" component of the atmosphere. Figure 49 depicts results for O-He analogous to those of Figures 45-47. Because of the smaller number of escapes, results for all three temperatures have been added together. The proclivity of the "missing" helium atoms to escape near the horizontal is dramatic indeed. The corresponding effect in the escaping "real" atmosphere might be very difficult to demonstrate by straightforward calculation because of the smallness of the re-escaping ("missing") component.

XV. Summary and Conclusions

We have shown that previous calculations of the dissociation of water vapor and evolution of oxygen in the early terrestrial atmosphere are seriously in error. The widely accepted conclusion that in the absence of life forms no more than about 10^{-3} P.A.L. of O_2

could evolve has been shown not to be justified; indeed, amounts comparable to the P.A.L. could conceivably have built up in the available time. The calculated equilibrium oxygen level, furthermore, is only weakly sensitive to postulated environmental differences, due to the tendency of production and loss changes to cancel one another. If indeed the earth's early atmosphere was highly reducing, then some other explanation for this must be found. The most promising possibility seemed to be a Rasool-McGovern type "metastable" atmosphere resulting from an early outgassing of vast quantities of hydrogen. Rasool and McGovern claimed that such a reducing state could exist for up to a billion years before the hydrogen would escape. If the escape of hydrogen were much slower than indicated by Jeans' escape equation (due to the departure from an M-B distribution near the escape level), this time interval could conceivably be extended to the 3 billion or so years suggested by the geologic and fossil records. But we have seen that Jeans' equation is likely to be in error, for hydrogen escape in the earth's atmosphere, by no more than about 30%. Thus the question regarding the early state of the earth's atmosphere remains open. An obvious next step would be to examine the photochemistry of O-H complexes throughout the photochemically active region of the atmosphere (including a better treatment of eddy diffusion than is presently available) to see if the hydrogen atoms are indeed provided safe passage to the heterosphere with a reasonable efficiency. It is not clear, however, whether the available laboratory and theoretical data (e.g., the eddy diffusion coefficient) are good enough to make such an effort worthwhile.

We achieved excellent agreement with the results of CC and disagreement with those of LV and LS. Several questions present themselves. First, could this agreement be a result of the cross-sections used and thus be only an apparent agreement? It seems unlikely that this could be the case; it seems more probable that in retrospect the escape fluxes are not very sensitive to the particular form of the cross-section. The only way to provide a definite answer to this question, of course, is to repeat the calculations using an isotropic differential cross-section and simplifying the velocity dependence of the total cross-section, so as to simulate CC's model. By far the more important of the two changes is the angular dependence of the cross-section. It was possible, by modifying a single card in the computer program, to make the change to an isotropic cross-section. The previous velocity dependence of the total cross-section was retained, but this should be only of secondary importance. Three sets of 250 H atoms ("missing" atoms) were released at the top of the slab (about 5 typical mean free paths thick, typical of the work of CC or LS. The resulting escape flux for the "real" atmosphere was 0.678 times the Jeans rate, within the error bar for the corresponding (15 typical mean free path slab thickness) WKB differential cross-section calculation even without its own (rms) uncertainty of about 0.027. This confirms that the agreement with the results of CC is more than just accidental.

Another question which might be raised is whether the cause for the discrepancy between the present results and those of CC, on the one hand, and those of LS, on the other, might lie in the use of a

uniform slab of background gas by the former and a diffusive-equilibrium background density distribution by the latter. Perhaps the different treatment accorded the role of gravity might account for the difference. One can clearly see, however, if one consults the appropriate literature, that the sole difference between the treatments presented here and by CC, on the one hand, and by LS, on the other, regarding the role of gravity is that LS proposed an exponential height distribution for the background oxygen gas. The role of gravity in influencing the trajectories of individual H atoms (which don't really move in straight lines nor at constant speed) is neglected in all these investigations, except for the specular reflection of slow particles (having less than escape speed) off the "top" of the atmosphere. Now an exponentially distributed atmosphere can be approximated arbitrarily closely by a series of thin uniformly dense layers of background gas with gaps, or voids, of varying thickness between these layers. The gaps are simply regions where there is no background gas. Such a situation could not arise in the real world but for calculational purposes this is a valid construct. If the layers are made thin enough then on a macroscopic level the two atmospheres would be equivalent. Now if we inject hydrogen (or helium) atoms at either the top or bottom of the construct atmosphere we have the following situation. Since collisions can't occur in the gaps the density must be constant there and equal to the common density of the constituent at the base of the overlying slab of background gas and at the top of the corresponding underlying slab. It is easily seen that the gaps play a completely passive role in the escape pro-

cess except for the resulting influence on the density distribution of the escaping component. This density as a function of "optical depth" of the background gas is the same in the "construct" atmosphere and in a single uniform slab. Consequently, since the density was presumably correctly calculated by LS and the density correction (which is small anyway) correctly derived it is clear that the two approaches should give the same answer. The above considerations would not be strictly correct if LS had taken fully into account the effect of the gravity field on the individual trajectories (though it would undoubtedly still be a very good approximation) but this was not done.

There are two final points which should be mentioned. First, although for most practical purposes they are probably qualitatively correct, the "relaxation time" calculations of LS should be redone. This would serve as reassurance that no important diurnal or other time dependent effects are being overlooked. The other comment concerns the helium escape problem. The production rates of He^3 and He^4 for the various mechanisms suggested are highly uncertain. Nevertheless if the currently favored values are roughly correct then, as has been pointed out many times, there is some difficulty in explaining the present atmospheric He^3:He^4 ratio (about 10^{-6}); there is simply too much He^3. This has led to a search for non-thermal escape mechanisms (e.g., the "polar wind") which will not favor the loss of He^3 so greatly over that of He^4 as in thermal, or gravitational, escape. If large corrections to Jeans' equation had been corroborated (factors as high as 15 are consistent with the

error bars of LS for hydrogen) then the possibility would have been open that the correction factor for He^3 would be significantly larger than for He^4 and that this could be at least a contributing factor explaining the high He^3 atmospheric abundance. Alas, it has been shown that the correction factors for He^3 and He^4 are both very small and hence that no justification can be advanced from these calculations for a high He^3:He^4 ratio.

REFERENCES

Allen, C. w., Astrophysical Quantities, Athlone Press, London, 1963, p. 87.

Bates, D. R., and M. Nicolet, "The photochemistry of atmospheric water vapor", J. Geophys. Res., 55, 301-327, 1950.

Bates, D. R., and T. N. L. Patterson, "Hydrogen atoms and ions in the thermosphere and exosphere", Planet. Space Sci., 5, 257-273, 1961.

Bohm, D., Quantum Theory, Prentice-Hall, Englewood Cliffs, New Jersey, 1951, chap. 12.

Belton, M. J. S., and D. M. Hunten, "A search for O_2 on Mars and Venus: a possible detection of oxygen in the atmosphere of Mars", Ap. J., 153, 963-974, 1968.

Berkner, L. V., and L. C. Marshall, "The history of oxygenic concentration in the earth's atmosphere", Disc. Faraday Soc., 37, 122-141, 1964.

Berkner, L. V., and L. C. Marshall, "On the origin and rise of oxygen concentration in the earth's atmosphere", J. Atmos. Sciences, 22, 225-261, 1965.

Berkner, L. V., and L. C. Marshall, "Limitation on oxygen concentration in a primitive planetary atmosphere", J. Atmos. Sciences, 23, 133-143, 1966.

Blake, A. J., J. H. Carver and G. N. Haddad, "Photo-absorption cross-sections of molecular oxygen between 1250Å and 2350Å",

J. Quant. Spectrosc. Radiat. Transfer, 6, 451-459, 1966.

Brace, L. H., B. M. Reddy and H. G. Mayr, "Global behavior of the ionosphere at 1000-kilometer altitude", J. Geophys. Res., 72, 265-283, 1967.

Brandt, J. C., "On the role of secondary scattering in the Lyman-α problem", Planet. Space Sci., 9, 67-68, 1962.

Brinkmann, R. T., A. E. S. Green and C. A. Barth, "A digitalized solar ultraviolet spectrum", Jet Propulsion Laboratory Technical Report No. 32-951, 1966.

Calfee, R. F., and D. M. Gates, "Calculated slant-path absorption and distribution of atmospheric water vapor", Applied Optics, 5, 287-292, 1966.

Chamberlain, J. W., "Planetary coronae and atmospheric evaporation", Planet. Space Sci., 11, 901-960, 1963.

Chamberlain, J. W., and F. J. Campbell, "Rate of evaporation of a non-Maxwellian atmosphere", Ap. J., 149, 687-705, 1967.

Cloud, P. E., Jr., "Atmospheric and hydrospheric evolution on the primitive earth", Science, 160, 729-736, 1968.

Colegrove, F. D., W. B. Hanson and F. S. Johnson, "Eddy diffusion and oxygen transport in the lower thermosphere", J. Geophys. Res., 70, 4931-4941, 1965.

Colegrove, F. D., F. S. Johnson and W. B. Hanson, "Atmospheric composition in the lower thermosphere", J. Geophys. Res., 71, 2227-2236, 1966.

Committee on Extension to the Standard Atmosphere, U. S. Standard Atmosphere, 1962, U. S. Govt. Printing Office, Washington, D. C.,

1962.

COSPAR Working Group IV, CIRA 1965, COSPAR International Reference Atmosphere, 1965, North Holland Pub. Co., Amsterdam, Holland, 1965.

Dalgarno, A., "Atomic polarizabilities and shielding factors", Adv. in Physics, 11, 281-315, 1962.

Detwiler, C. R., D. L. Garrett, J. D. Purcell and R. Tousey, "The intensity distribution in the ultraviolet solar spectrum", Ann. de Geophys., 17, 9-18, 1961.

Dicke, R. H., and J. P. Wittke, Introduction to Quantum Mechanics, Addison-Wesley, Reading, Massachsetts, 1961.

Ditchburn, R. W., and P. A. Young, "The absorption of molecular oxygen between 1850 and 2500Å", J. Atmos. Terr. Phys., 24, 127-139, 1962.

Donahue, T. M., "Comments on "Observation of the airglow H_α emission" by E. B. Armstrong", Planet. Space Sci., 15, 1223, 1967.

Goody, R. M., Atmospheric Radiation I. Theoretical Basis, Oxford Univ. Press, London, 1964.

Gould, E. S., Inorganic Reactions and Structure, Holt, Rinehart and Winston, New York, 1962, p. 149.

Griggs, M., "Atmospheric Ozone", in The Middle Ultraviolet: Its Science and Technology, edited by A. E. S. Green, pp. 83-117, Wiley, New York, 1966.

Hayes, P. B., and V. C. Liu, "On the loss of gases from a planetary atmosphere", Planet. Space Sci., 13, 1185-1212, 1965.

Herzberg, G., Spectra of Diatomic Molecules, Van Nostrand, Princeton, New Jersey, 1950.

Hesstvedt, E., "On the effect of vertical eddy transport on atmospheric composition in the mesosphere and lower thermosphere", Geofys. Publikasjoner, 27, 1-35, 1968.

Hirschfelder, J. O., C. F. Curtiss and R. B. Bird, Molecular Theory of Gases and Solids, Wiley, New York, 1954.

Hoffman, J. H., "A mass spectrometer determination of the composition of the nighttime topside ionosphere", J. Geophys. Res., 72, 1883-1888, 1967.

Hudson, R. D., V. L. Carter and J. A. Stein, "An investigation of the effect of temperature on the Schumann-Runge absorption continuum of oxygen, 1580-1950Å", J. Geophys. Res., 71, 2295-2298, 1966.

Hudson, R. D., and V. L. Carter, "Absorption of oxygen at elevated temperatures (300 to 900 K) in the Schumann-Runge system", J. O. S. A., 58, 1621-1629, 1968; also private communication.

Hunt, B. G., "Photochemistry of ozone in a moist atmosphere", J. Geophys. Res., 71, 1385-1398, 1966.

Ingham, M. F., "Observations of the night sky $H\alpha$ emission line", Mon. Not. R. Astr. Soc., 140, 155-172, 1968.

Inn, E. C. Y., K. Watanabe and M. Zelikoff, "Absorption coefficients of gases in the vacuum ultraviolet. Part III. CO_2", J. Chem. Phys., 21, 1648-1650, 1953.

Jeans, J. H., Dynamical Theory of Gases, Cambridge Univ. Press, London, 1916.

Jones, J. E., "Free paths in a non-uniform rarefied gas with an application to the escape of molecules from isothermal atmos-

pheres", Trans. Cambridge Phil. Soc., 22, 535-556, 1923.

Kaufman, F., "Aeronomic reactions involving hydrogen, a review of recent laboratory studies", Ann. de Geophys., 20, 106-114, 1964.

Kaufman, F., "Neutral reactions involving hydrogen and other minor constituents", in Symposium on Laboratory Measurements of Aeronomic Interest (Proceedings), International Association of Geomagnetism and Aeronomy, September, 1968.

Kellogg, W. W., "Pollution of the upper atmosphere by rockets", Space Science Reviews, 3, 275-316, 1964.

Kockarts, G., and M. Nicolet, "Le probleme aeronomique de l'helium et de l'hydrogen neutres", Ann. de Geophys., 18, 269-290, 1962.

Krupenie, P. H., E. A. Mason and J. T. Vanderslice, "Interaction energies and transport coefficients of Li + H and O + H gas mixtures at high temperatures", J. Chem. Phys., 39, 2399-2408, 1963.

Larkin, F. S., and B. A. Thrush, "Recombination of hydrogen atoms in the presence of atmospheric gases", Disc. Faraday Soc., 37, 112-117, 1964.

Lew, S. K., and S. V. Venkateswaran, "A study of hydrogen diffusion in the earth's upper atmosphere near the critical level", J. Atmos. Sciences, 22, 623-635, 1965.

Lew, S. K., and S. V. Venkateswaran, "Reply", J. Atmos. Sciences, 23, 817-819, 1966.

Libby, W. F., "Ice caps on Venus?", Science, 159, 1097-1098, 1968.

Liwshitz, M., "The effect of thermal escape on neutral hydrogen density above 120 kilometers", J. Geophys. Res., 72, 285-293, 1967.

Liwshitz, M., "Comments on 'A study of hydrogen diffusion in the earth's upper atmosphere near the critical level' ", J. Atmos. Sciences, 23, 816-817, 1966.

Liwshitz, M., and S. F. Singer, "Thermal escape of neutral hydrogen its distribution in the earth's thermosphere", Planet. Space Sci., 14, 541-561, 1966.

Manabe, S., and R. T. Wetherald, "Thermal equilibrium of the atmosphere with a given distribution of relative humidity", J. Atmos. Sciences, 24, 241-259, 1967.

Marchi, R. P., and C. R. Mueller, "WKB approximation and molecular beam scattering", J. Chem. Phys., 36, 1100, 1962.

Marchi, R. P., and C. R. Mueller, "Validity of the WKB approximation in the interpretation of molecular beam scattering data", J. Chem. Phys., 38, 740-744, 1963.

Mastenbrook, H. J., "Water vapor distribution in the stratosphere and high troposphere", J. Atmos. Sciences, 25, 299-311, 1968.

Merzbacher, E., Quantum Mechanics, Wiley, New York, 1961.

Metzger, P. H., and G. R. Cook, "A reinvestigation of the absorption cross-sections of molecular oxygen in the 1050-1800Å region", J. Quant. Spectrosc. Radiat. Transfer, 4, 107-116, 1964.

Milne, E. A., "The escape of molecules from an atmosphere with special reference to the boundary of a gaseous star", Trans. Cambridge Phil. Soc., 22, 483-517, 1923.

Patterson, T. N. L., "Atomic and molecular hydrogen in the thermosphere", Planet. Space Sci., 14, 417-423, 1966.

Pauly, H., and J. P. Toennies, in Advances in Atomic and Molecular

Physics, D. R. Bates and I. Estermann, eds., Academic Press, New York, 1965.

Phillips, L. F., and H. I. Schiff, "mass spectrometric studies of atomic reactions. III. Reactions of hydrogen atoms with nitrogen dioxide and with ozone", J. Chem. Phys., 37, 1233-1238, 1962.

Poldervaart, A., "Chemistry of the earth's crust", in Geol. Soc. America Special Paper 62, Crust of the Earth, edited by A. Poldervaart, pp. 119-144, Geol. Soc. America, New York, 1963.

Rasool, S. I., and W. E. McGovern, "Primitive atmosphere of the earth", Nature, 212, 1225-1226, 1966.

Reber, C. A., J. E. Cooley and D. N. Harpold, "Preliminary atmospheric composition data from the Explorer 32 mass spectrometers" (abstract), Trans. Am. Geophys. Union, 48, 75, 1967.

Rubey, W. W., "Development of the hydrosphere and atmosphere, with special reference to probable composition of the early atmosphere", in Geol. Soc. America Special Paper 62, Crust of the Earth, edited by A. Poldervaart, pp. 631-650, Geol. Soc. America, New York, 1963.

Schofield, K., "An evaluation of kinetic rate data for reactions of neutrals of atmospheric interest", Planet. Space Sci., 15, 643-670, 1967.

Scholz, T. G., L. E. Heidt, E. A. Martell and D. H. Ehhalt, "Water vapor and trace gases near the stratopause" (abstract), Trans. Am. Geophys. Union, 50, 176, 1969.

Sissenwine, N., D. D. Grantham and H. A. Salmeda, "Mid-latitude humidity to 32 km", J. Atmos. Sciences, 25, 1129-1140, 1968.

Spitzer, L., Jr., "The terrestrial atmosphere above 300 km", in The Atmospheres of the Earth and Planets, edited by G. P. Kuiper, pp. 211-247, Univ. of Chicago Press, Chicago, Illinois, 1957.

Stoney, G. J., "Of atmospheres upon planets and satellites", Ap. J., 7, 25-55, 1898.

Stoney, G. J., "On the escape of gases from planetary atmospheres according to the kinetic theory. Part I.", Ap. J., 11, 251-258, 1900.

Stoney, G. J., "On the escape of gases from planetary atmospheres according to the kinetic theory. Part II.", Ap. J., 11, 357-372, 1900.

Tanaka, Y., E. C. Y. Inn and K. Watanabe, "Absorption coefficients of gases in the vacuum ultraviolet. Part IV. Ozone", J. Chem. Phys., 21, 1651-1653, 1953.

Thomas, G. E., "Lyman α scattering in the earth's hydrogen geocorona, 1", J. Geophys. Res., 68, 2639-2660, 1963.

Thompson, B. A., P. Harteck and R. R. Reeves, Jr., "Ultraviolet absorption coefficients of CO_2, CO, O_2, H_2O, N_2O, NH_3, NO, SO_2 and CH_4 between 1850 and 4000 Å", J. Geophys. Res., 68, 6431-6436, 1963.

U. S. Air Force Geophysics Research Directorate, Handbook of Geophysics, Rev. Ed., MacMillan, New York, 1960.

Watanabe, K., E. C. Y. Inn, and M. Zelikoff, "Absorption coefficients of oxygen in the vacuum ultraviolet", J. Chem. Phys., 21, 1026-1030, 1953.

Watanabe, K., and M. Zelikoff, "Absorption coefficients of water vapor in the vacuum ultraviolet", J. O. S. A., 43, 753-755, 1953.

Williamson, E. J., and J. T. Houghton, "Radiometric measurements of emission from stratospheric water vapor", Quart. J. Roy. Meteor. Soc., 91, 330-338, 1965.

Table 1

layer	atm-cm in layer	atm-cm in and above layer	height of base (km)	atm-cm in layer			
				H_2O	CO_2	O_3	O_2
1	5	5	85	.00025	.0017	.0000005	1.0
2	10	15	79	.00050	.0033	.00000116	2.0
3	20	35	73.5	.000100	.0067	.0000034	4.0
4	40	75	68	.00020	.0133	.000010	8.0
5	80	155	62	.00040	.027	.000034	16.
6	160	315	56.5	.00080	.053	.00010	32.
7	320	635	51	.00160	.107	.00030	64.
8	640	1275	45	.0032	.21	.00106	128.
9	1280	2555	40	.0064	.43	.0025	256.
10	2560	5115	35.5	.0128	.85	.0060	512.
11	5120	10235	31	.026	1.71	.0146	1024.
12	10240	20475	26.5	.051	3.41	.036	2048.

Table 2 (Part 1)

$\Delta\lambda$(Å)	k_{H_2O}	k_{CO_2}	k_{O_3}	$k_{ef}(cm^{-1})$ in layer (O_2)			
				1	2	3	4
1760±5	57.	.16	23.	1.66	.62	.39	.27
1770±5	46.	.12	22.	1.13	.42	.26	.177
1780±5	37.	.09	22.	.66	.24	.152	.102
1790±5	27.5	.07	22.	.63	.23	.144	.096
1800$\pm^{10}_{5}$	19.3	.05	21.	.66	.25	.153	.102
1820±10	8.0	.035	20.	.41	.152	.095	.063
1840±10	2.55	.020	19.	.36	.133	.083	.055
1860±10	.90	.010	17.	.25	.092	.058	.039
1880±10	.35	.005	16.	.154	.057	.036	.024
1900±10	.135	.0035	15.	.100	.037	.023	.0156
1920±10	.053	.0017	13.	.084	.031	.0195	.0132
1940±10	.022	.00055	11.	.046	.0170	.0108	.0074
1960±10	.0093	.00010	9.3	.024	.0092	.0059	.0041
1980±10	.0040	.00001	8.6	.0186	.0070	.0045	.0032
2000±10	.0016	.000001	8.0	.0081	.0032	.0021	.00156

Table 2 (Part 2)

$k_{ef}(cm^{-1})$ in layer (O_2)							
5	6	7	8	9	10	11	12
.191	.138	.10	.073	.054	.041	.031	.025
.122	.086	.060	.043	.030	.022	.0161	.012
.070	.049	.035	.024	.0173	.0123	.0089	.0064
.066	.046	.032	.022	.0152	.0106	.0074	.0052
.069	.048	.033	.023	.0158	.0109	.0076	.0054
.043	.030	.020	.0140	.0096	.0066	.0046	.0032
.037	.026	.0175	.0119	.0081	.0055	.0038	.0026
.026	.0184	.0128	.0090	.0063	.0044	.0031	.0023
.0165	.0116	.0082	.0058	.0041	.0030	.0022	.00160
.0109	.0077	.0055	.0039	.0028	.0021	.00157	.00120
.0092	.0065	.0046	.0034	.0025	.00182	.00137	.00107
.0052	.0037	.0027	.0021	.0016	.00121	.00097	.00080
.0029	.0022	.00164	.00127	.0010	.00083	.00071	.00061
.0023	.0017	.00133	.00105	.00085	.00071	.00061	.00055
.0012	.00094	.00077	.00065	.00057	.00051	.00047	.00044

Table 3 : Solar Spectral Irradiance at 1 a.u.

$\Delta\lambda$	Flux (photons/cm^2 sec)
1760 ± 5	10.0×10^{10}
1770 ± 5	12.8 "
1780 ± 5	14.0 "
1790 ± 5	15.6 "
$1800 \pm \frac{10}{5}$	26.9 "
1820 ± 10	46.3 "
1840 ± 10	46.5 "
1860 ± 10	55.0 "
1880 ± 10	63.6 "
1900 ± 10	88.4 "
1920 ± 10	108.9 "
1940 ± 10	129.2 "
1960 ± 10	176.1 "
1980 ± 10	192.3 "
2000 ± 10	229.0 "

Table 4 : Dissociation Energies of Hydrogen-Containing Species

Species	Products	Energy Required (eV)	(Å)
H_2O	H + OH	5.113	2424
H_2	H + H	4.476	2769
OH	O + H	4.35	2849
H_2O_2	HOO + H	3.88	3194
HO_2	OH + O	2.7	4590
H_2O_2	OH + OH	2.12	5846
HO_2	H + O_2	1.99	6228

Table 5

"Number Escaping"

O-H

slab thickness=		1×10^7 cm	2×10^7 cm	3×10^7 cm
	1000°K	52.0 ± 5.3	60.4 ± 6.2	62.8 ± 6.5
(top)	1500°K	62.4 ± 5.8	81.7 ± 7.4	87.6 ± 7.4
(bottom)	1500°K	10.9 ± 3.2	11.0 ± 2.9	10.0 ± 4.3
	2000°K	78.5 ± 6.5	90.3 ± 6.1	108.0 ± 8.7

O-He

	1000°K	2.33 ± .88	3.00 ± 1.41	1.33 ± 1.25
	1500°K	4.43 ± 1.29	4.00 ± 2.19	3.75 ± 2.49
	2000°K	4.50 ± 1.50	5.33 ± 1.25	8.33 ± 2.36

Table 6 (Part 1)

	T(°K)	typical mean free path (km)	real (H or He) atmosphere fractional density slab thickness = 1×10^7 cm	2×10^7 cm	3×10^7 cm
O-H					
	1000	17.2	.996	.992	.988
	1500	20.0	.972	.940	.915
	2000	22.0	.924	.869	.822
O-He					
	1000	8.77	} density correction negligible		
	1500	9.74			
	2000	10.77			

Table 6 (Part 2)

		fraction of Jeans' escape rate slab thickness =			
	T(°K)	1×10^7 cm	2×10^7 cm	3×10^7 cm	adopted
O-H					
	1000	.795 ± .021	.765 ± .025	.758 ± .026	.758
	1500	.772 ± .024	.716 ± .031	.710 ± .032	.710
	2000	.742 ± .028	.735 ± .028	.691 ± .042	.691
O-He					
	1000	.991 ± .004	.988 ± .006	.995 ± .005	.991
	1500	.982 ± .005	.984 ± .009	.985 ± .010	.984
	2000	.982 ± .006	.979 ± .005	.967 ± .009	.967

FIGURE CAPTIONS

Fig. 1 Absorption coefficient data. "THR" refers to the work of Thompson, Harteck and Reeves [1963].

Fig. 2 Absorption rates for the various species at 0° zenith angle as functions of wavelength.

Fig. 3 Absorption rates for the various species at 0° zenith angle as functions of altitude.

Fig. 4 Mean absorption rates for the various species as functions of the oxygen level.

Fig. 5 Oxygen level histories for the earth. The quantity C is the oxidation loss rate; Q is the amount of oxygen lost by the atmosphere to the crust.

Fig. 6 Scattering geometry.

Fig. 7 Lennard-Jones potential function. "r_m" is the internuclear distance corresponding to minimum potential energy and "ε" is the depth of this well.

Fig. 8 Ratio, R, of the number of particles having a given speed in a Maxwell-Boltzmann flux to the corresponding number in a Maxwell-Boltzmann distribution function. Speed is given in units of the most probable speed, $\sqrt{2kT/m}$. Speeds sufficient for escape from the earth for hydrogen atoms (at 1000, 1500 and 2000°K) and helium (at 1000°K) are shown.

Fig. 9 Phase shifts for O-H elastic scattering for various relative speeds ranging from 6×10^4 cm/sec to 6×10^6 cm/sec. Hori-

zontal axis gives the ℓ-value, vertical axis the phase shift. Insert shows the upper-left-hand corner in greater detail.

Fig. 10 Phase shifts for O-He elastic scattering for various relative speeds ranging from 6×10^4 cm/sec to 2.5×10^6 cm/sec. Horizontal axis gives the ℓ-value, vertical axis the phase shift. Insert shows the upper-left-hand corner in greater detail.

Fig. 11 Differential elastic scattering cross-section for O-H calculated in several approximations. Relative speed is 600 m/sec. Shown are the small-deflection classical approximation, the arbitrary angle classical calculation, the WKB approximation and the cumulative WKB calculation. Horizontal axis gives the (center-of-mass) scattering angle in degrees, vertical axis the differential cross-section in Å^2/radian except for the cumulative curve which is simply in Å^2. Note in succeeding figures that as the relative speed becomes larger the agreement between the arbitrary angle classical calculation and the WKB calculation becomes progressively better, first at the very large scattering angles and then to successively smaller angles.

Fig. 12 Same as Fig. 11 except v_r = 1000 m/sec.

Fig. 13 Same as Fig. 11 except v_r = 1400 m/sec.

Fig. 14 Same as Fig. 11 except v_r = 2000 m/sec.

Fig. 15 Same as Fig. 11 except v_r = 2700 m/sec.

Fig. 16 Same as Fig. 11 except v_r = 3700 m/sec.

Fig. 17 Same as Fig. 11 except v_r = 5000 m/sec.

Fig. 18 Same as Fig. 11 except v_r = 7200 m/sec.

Fig. 19 Same as Fig. 11 except v_r = 11000 m/sec.

Fig. 20 Same as Fig. 11 except v_r = 15000 m/sec.

Fig. 21 Same as Fig. 11 except v_r = 25000 m/sec.

Fig. 22 Same as Fig. 11 except v_r = 40000 m/sec.

Fig. 23 Same as Fig. 11 except v_r = 60000 m/sec.

Fig. 24 Same as Fig. 11 except v_r = 600 m/sec and the system is O-He.

Fig. 25 Same as Fig. 24 except v_r = 1000 m/sec.

Fig. 26 Same as Fig. 24 except v_r = 1400 m/sec.

Fig. 27 Same as Fig. 24 except v_r = 2000 m/sec.

Fig. 28 Same as Fig. 24 except v_r = 2700 m/sec.

Fig. 29 Same as Fig. 24 except v_r = 3700 m/sec.

Fig. 30 Same as Fig. 24 except v_r = 5000 m/sec.

Fig. 31 Same as Fig. 24 except v_r = 7200 m/sec.

Fig. 32 Same as Fig. 24 except v_r = 11000 m/sec.

Fig. 33 Same as Fig. 24 except v_r = 15000 m/sec.

Fig. 34 Same as Fig. 24 except v_r = 25000 m/sec.

Fig. 35 Velocity dependences of the total elastic scattering cross-sections. The various curves and points include the calculated WKB values, the curve fits to these points, the corresponding small-deflection approximations and the curve used by LS for O-H.

Fig. 36 Typical dependence of the mean free path on particle speed, at the arbitrary background density of 10^8 cm^{-3}. Speed is

plotted in units of the most probable speed, $\sqrt{2kT/m}$. A "fast" particle can travel about twice as far between collisions as a particle having the most probable speed.

Fig. 37 Geometric quantities involved in transforming between the "laboratory" system (in which the O atom is initially at rest) and the "atmospheric" system (in which the O atom has initial velocity $\vec{v}_0$). Primes denote quantities subsequent to scattering. Subscripts "L" and "A" refer to the "laboratory" and "atmospheric" systems respectively.

Fig. 38 Calculated density profile of the "missing" hydrogen component at 1000, 1500 and 2000°K for a slab thickness of 1 x 10^7 cm. Straight lines through the error bars are (eyeball) least-square fits. The "escape level" is indicated in each case. Series of error bars with no straight line drawn through them is the sum of the "real" and "missing" density profiles (at 1500°K) and should add to 1.0 (0.2 on this scale).

Fig. 39 Same as Fig. 38 except slab thickness is 2 x 10^7 cm.

Fig. 40 Same as Fig. 38 except slab thickness is 3 x 10^7 cm.

Fig. 41 Same as Fig. 38 except that 1) the system treated is O-He, 2) the least-square fits were calculated precisely and 3) calculations were not performed for the "real" component of the helium distribution at 1500°K.

Fig. 42 Same as Fig. 41 except the slab thickness is 2 x 10^7 cm.

Fig. 43 Same as Fig. 41 except the slab thickness is 3 x 10^7 cm.

Fig. 44 Escape rate in units of the Jeans rate (vertical axis) versus temperature (horizontal axis) in °K. Present results

are labelled "B" (the values above 0.9 on the vertical scale are for O-He, those below 0.9 for O-H), previous results LV (Lew and Venkateswaran), LS (Liwshitz and Singer) and CC (Chamberlain and Campbell). Present results compare favorably with CC, disagree with LV and LS.

Fig. 45 Zenith angle distribution of the escape flux for a temperature of 1000°K and slab thicknesses of 1×10^7, 2×10^7 and 3×10^7 cm. The particles were injected from the top of the atmosphere and hence are the "missing" component. Vertical axis is the percent of the escape flux emerging in 5° intervals of zenith angle; horizontal axis is the zenith angle. Also shown is the appropriate distribution for a Maxwell-Boltzmann flux. The departure shows up clearly; particles from the "missing" component tend to escape with greater zenith angles (i.e., more nearly horizontally) than for the sum of the two components.

Fig. 46 Same as Fig. 45 except that the temperature is 1500°K. The departure from the M-B curve is somewhat less pronounced.

Fig. 47 Same as Fig. 45 except that the temperature is 2000°K. The departure from the M-B curve is much less pronounced.

Fig. 48 Same as Fig. 45 except 1) the temperature is 1500°K and 2) the particles were released at the bottom of the atmosphere ("real" particles). Departures from the M-B curve are ambiguous.

Fig. 49 Same as Fig. 45 except 1) the system treated is O-He and 2) because of the paucity of statistics all temperatures

were grouped together. The departure from the M-B curve is striking.

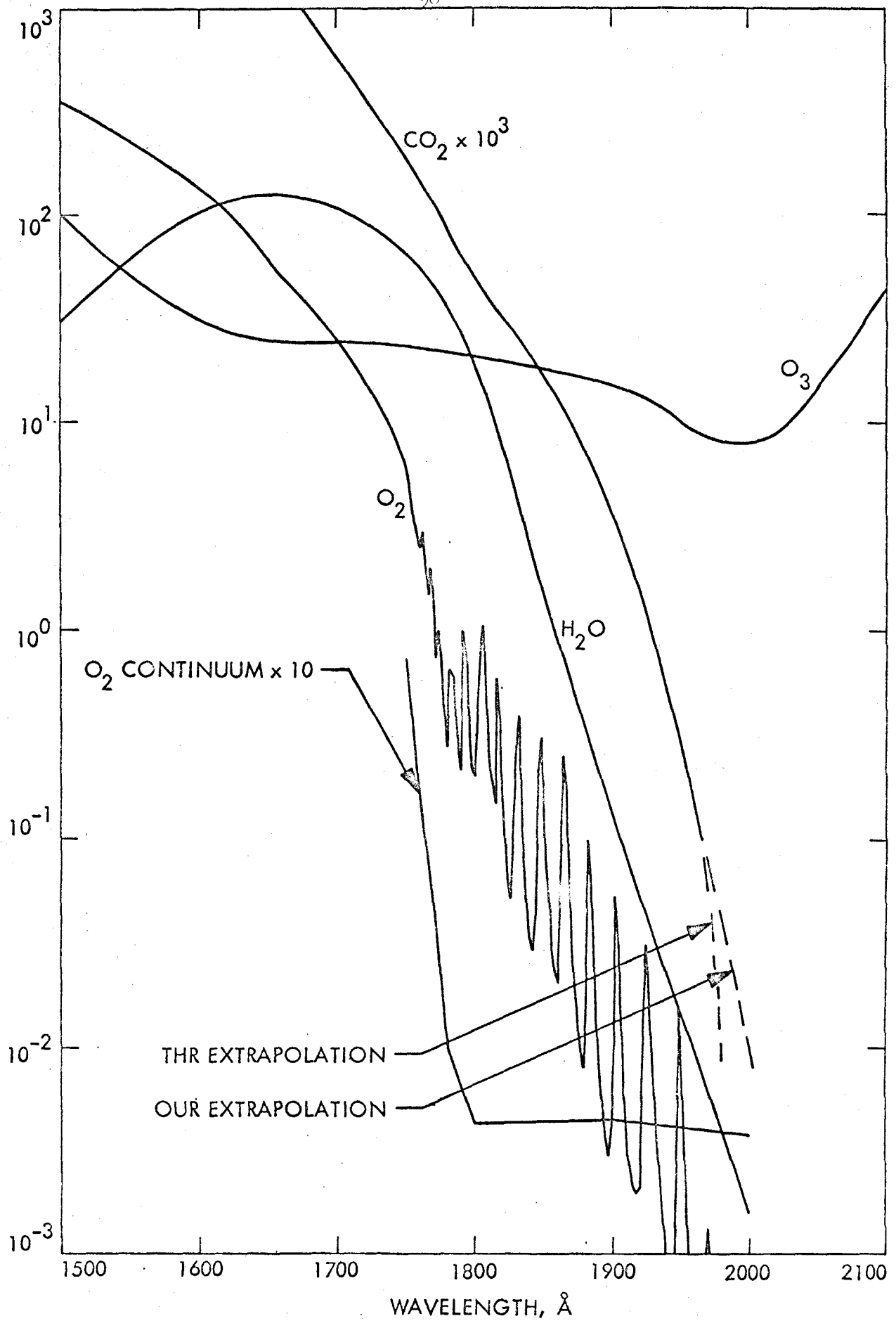
10^3
10^2
10^1
10^0
10^{-1}
10^{-2}
10^{-3}
$CO_2 \times 10^3$
O_3
O_2
H_2O
O_2 CONTINUUM x 10
THR EXTRAPOLATION
OUR EXTRAPOLATION
1500
1600
1700
1800
1900
2000
2100
WAVELENGTH, Å

Figure 1

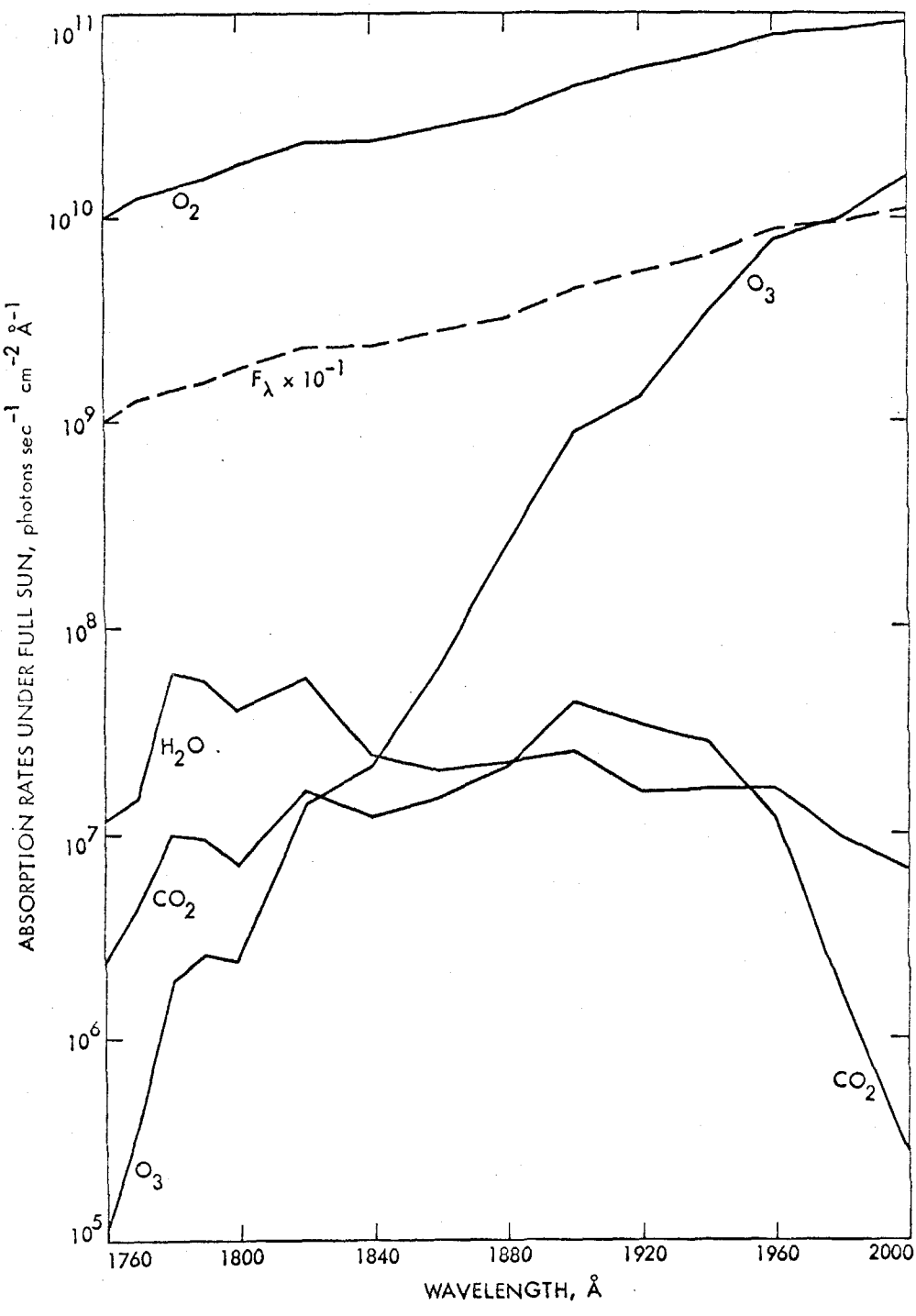
10^{11}
10^{10}
10^{9}
10^{8}
10^{7}
10^{6}
10^{5}
O_2
$F_\lambda \times 10^{-1}$
O_3
H_2O
CO_2
O_3
CO_2
ABSORPTION RATES UNDER FULL SUN, photons sec^{-1} cm^{-2} $Å^{-1}$
1760
1800
1840
1880
1920
1960
2000
WAVELENGTH, Å

Figure 2

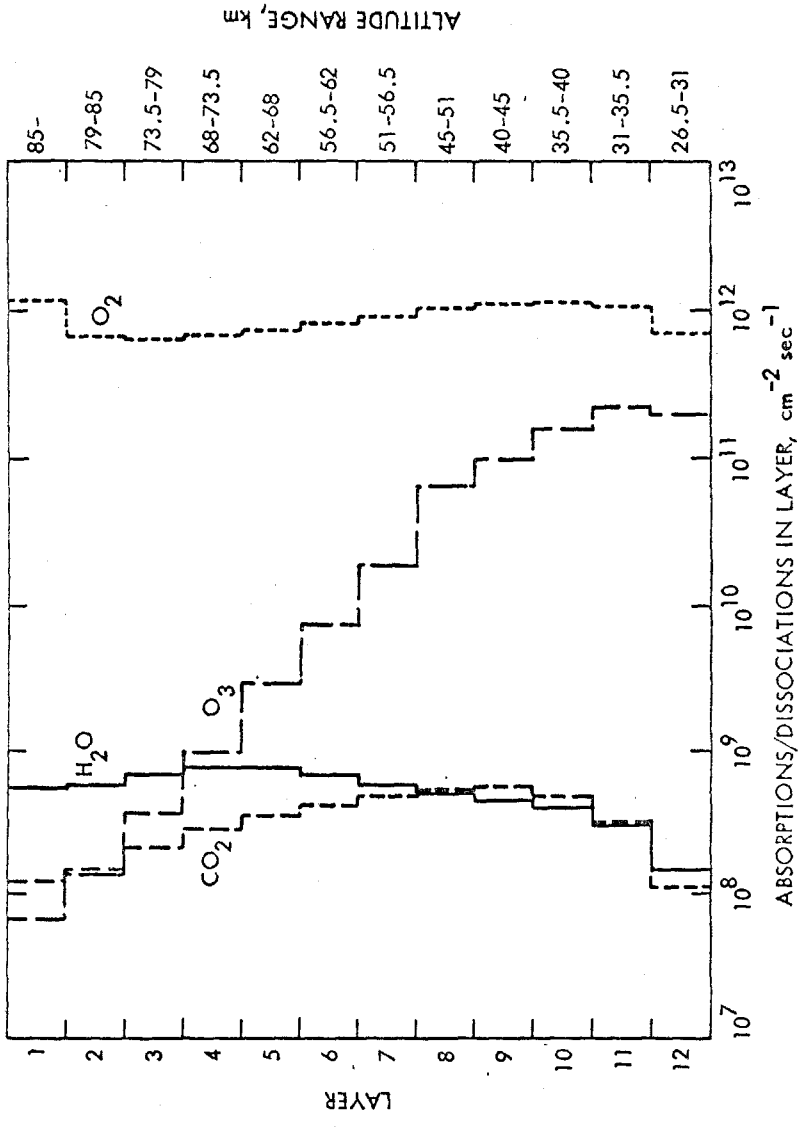
ALTITUDE RANGE, km
85-
79-85
73.5-79
68-73.5
62-68
56.5-62
51-56.5
45-51
40-45
35.5-40
31-35.5
26.5-31
O_2
O_3
H_2O
CO_2
LAYER
1
2
3
4
5
6
7
8
9
10
11
12
10^7
10^8
10^9
10^{10}
10^{11}
10^{12}
10^{13}
ABSORPTIONS/DISSOCIATIONS IN LAYER, cm^{-2} sec^{-1}

Figure 3

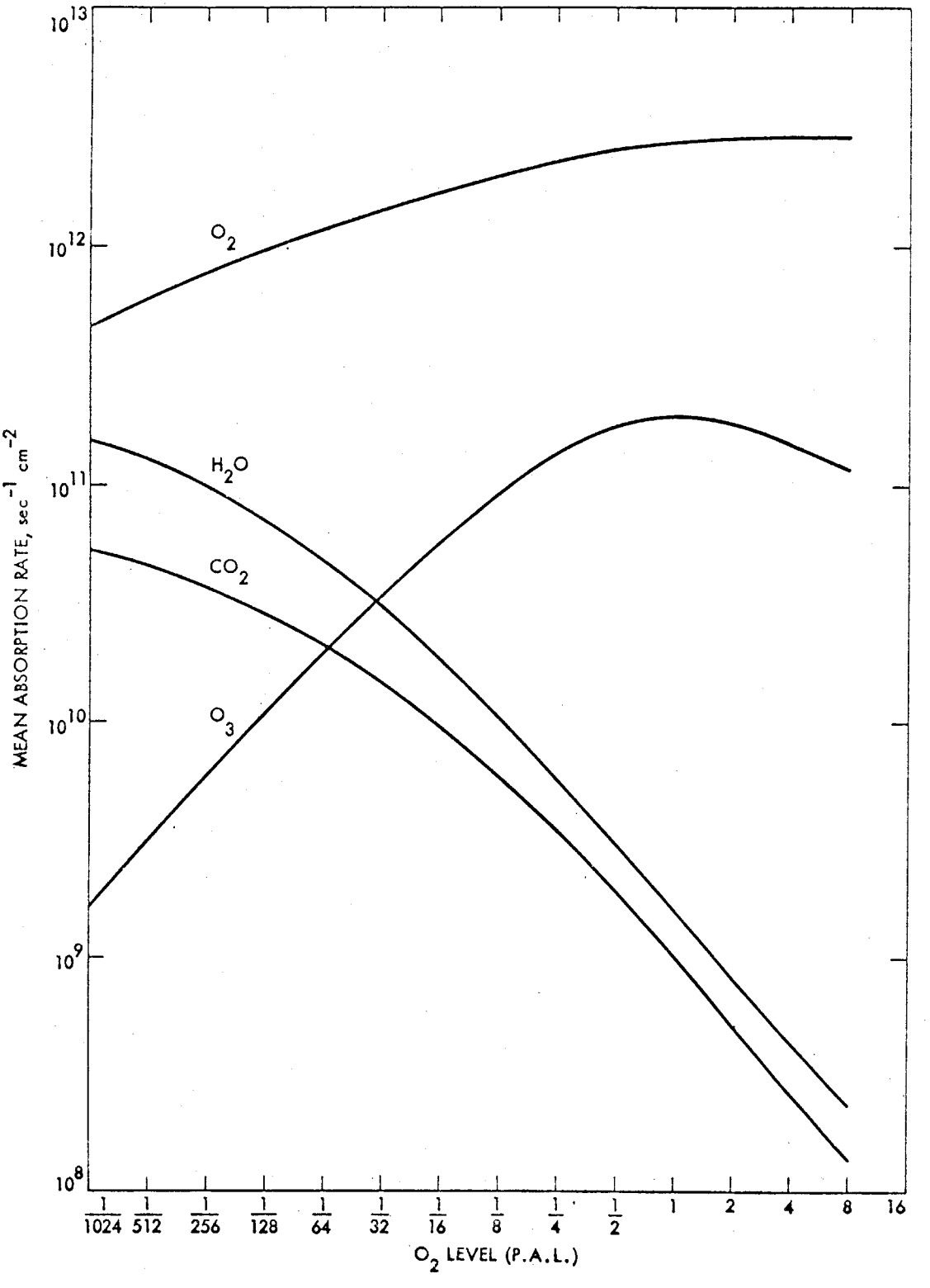
MEAN ABSORPTION RATE, sec^{-1} cm^{-2}
10^{13}
10^{12}
10^{11}
10^{10}
10^{9}
10^{8}
O_2
H_2O
CO_2
O_3
1/1024 1/512 1/256 1/128 1/64 1/32 1/16 1/8 1/4 1/2 1 2 4 8 16
O_2 LEVEL (P.A.L.)

Figure 4

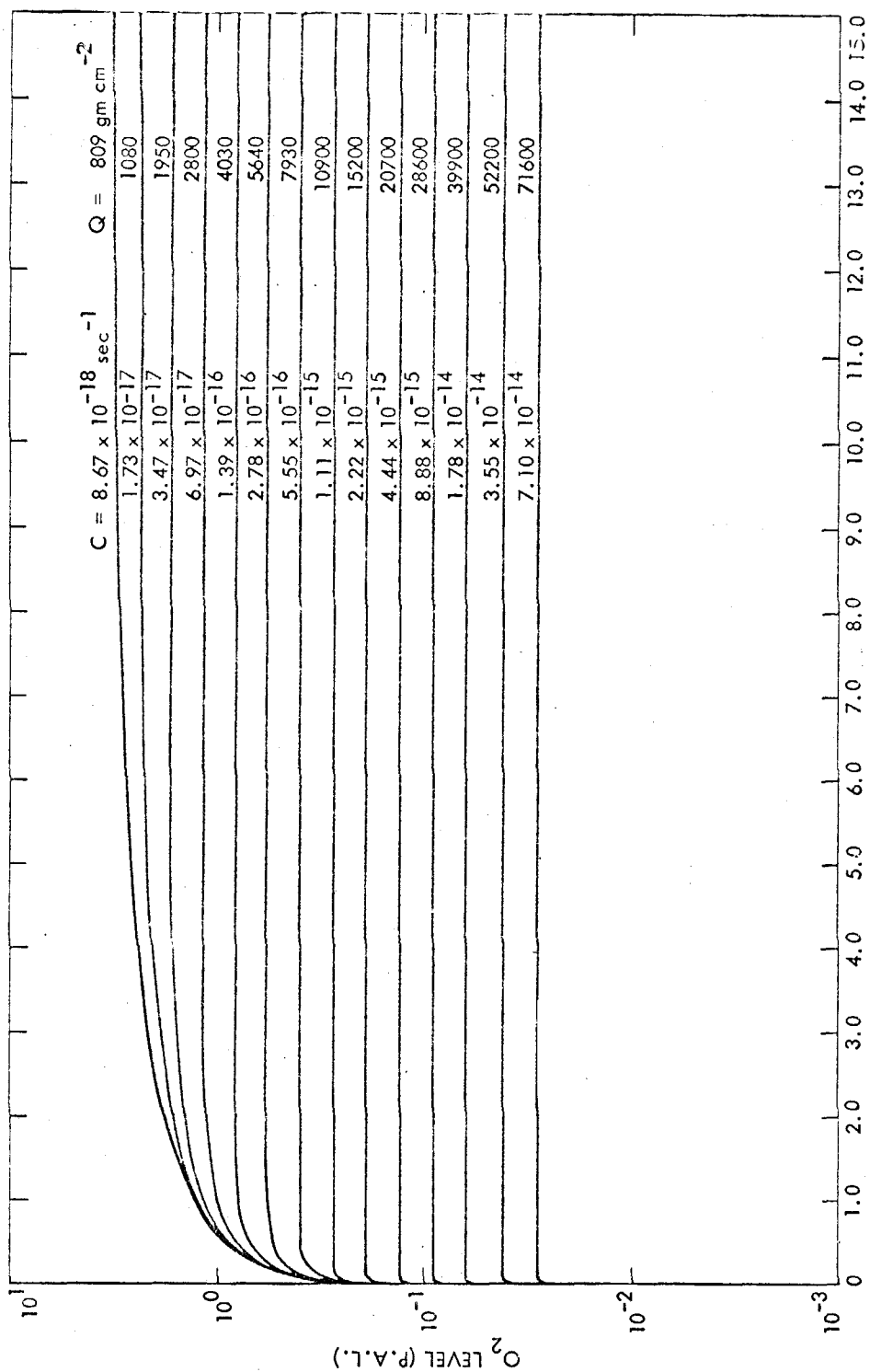
C = 8.67 x 10^-18 sec^-1
Q = 809 gm cm^-2
1.73 x 10-17 1080
3.47 x 10^-17 1950
6.97 x 10^-17 2800
1.39 x 10^-16 4030
2.78 x 10^-16 5640
5.55 x 10^-16 7930
1.11 x 10^-15 10900
2.22 x 10^-15 15200
4.44 x 10^-15 20700
8.88 x 10^-15 28600
1.78 x 10^-14 39900
3.55 x 10^-14 52200
7.10 x 10^-14 71600
O2 LEVEL (P.A.L.)
TIME, sec x 10^16
10^1
10^0
10^-1
10^-2
10^-3
0
1.0
2.0
3.0
4.0
5.0
6.0
7.0
8.0
9.0
10.0
11.0
12.0
13.0
14.0
15.0

Figure 5

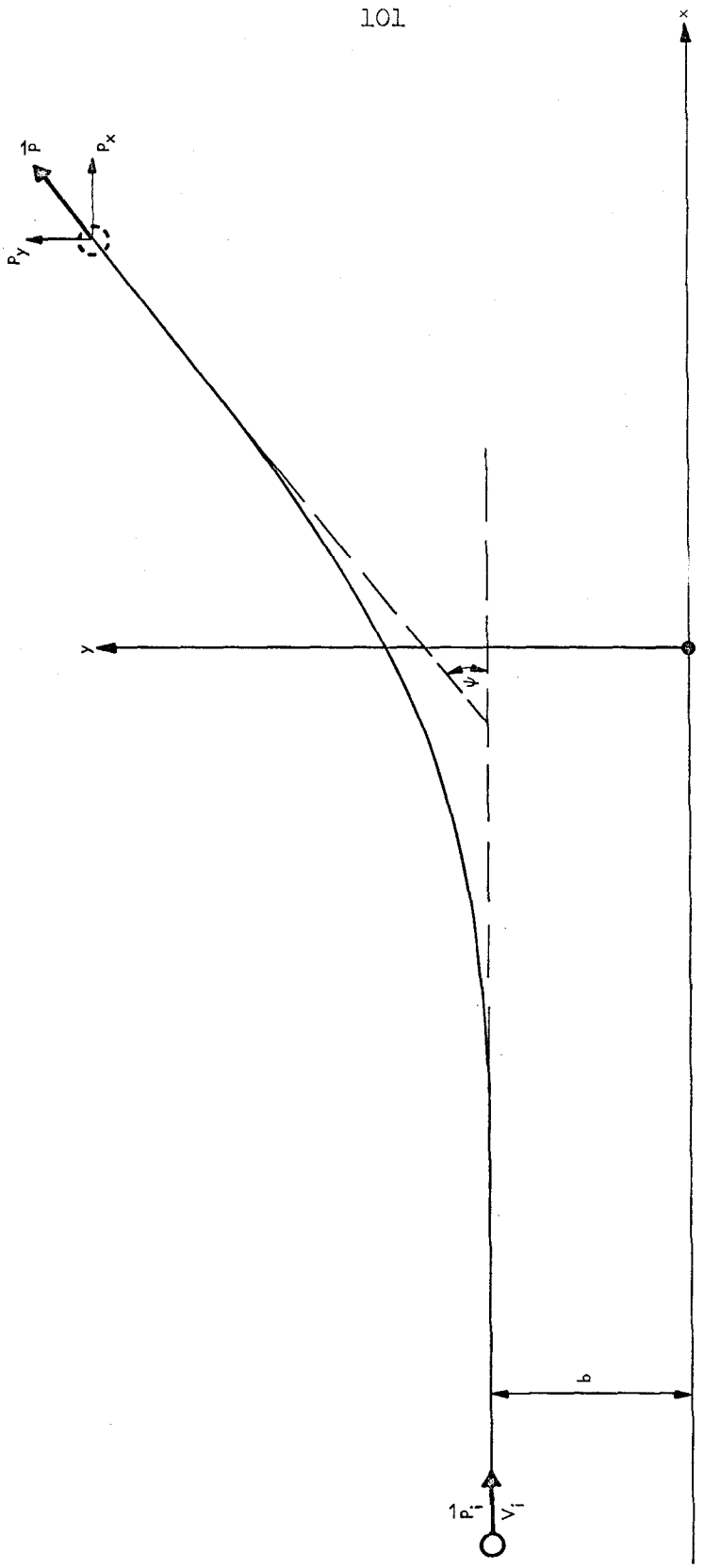

Figure 6

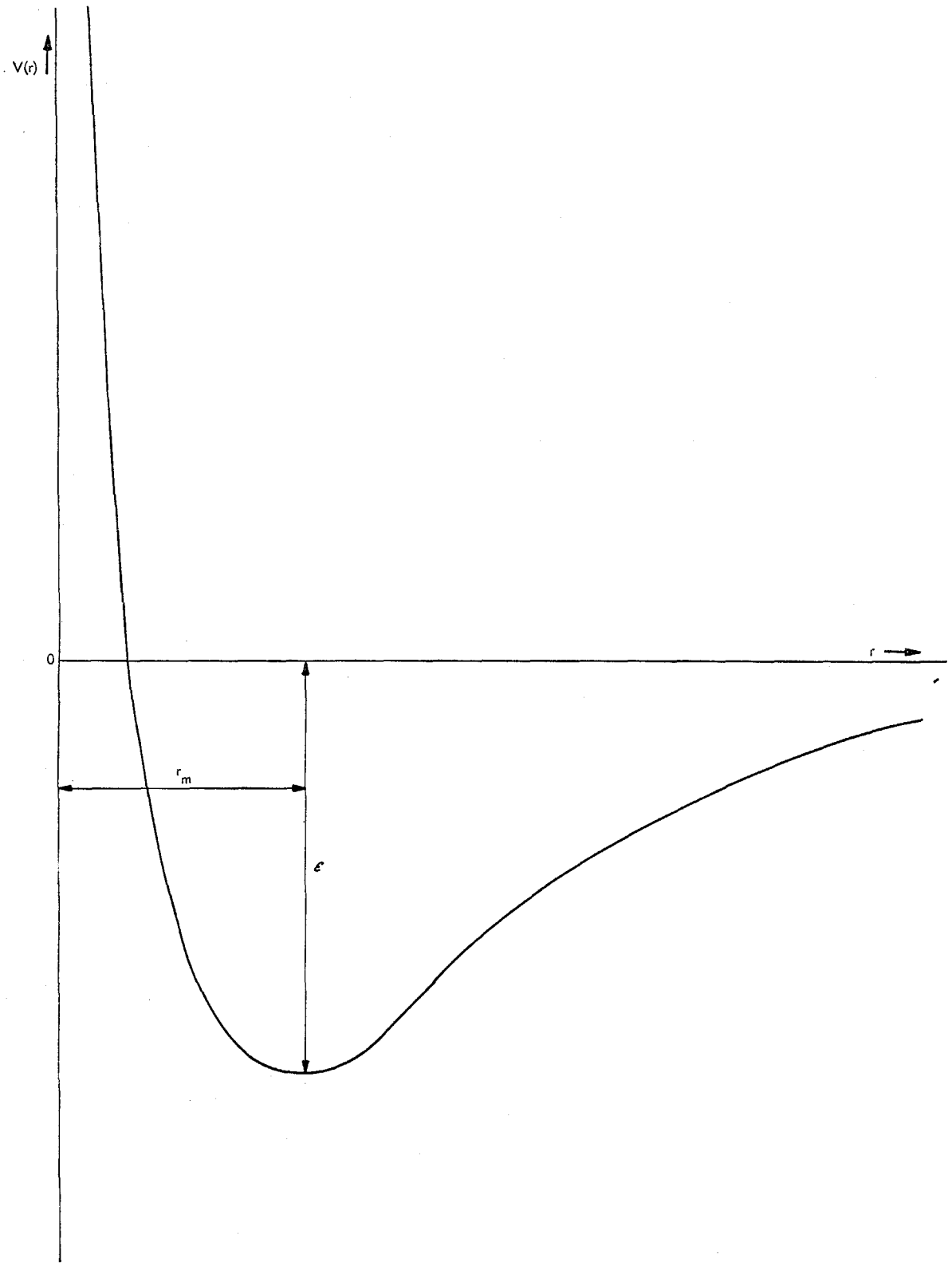

Figure 7

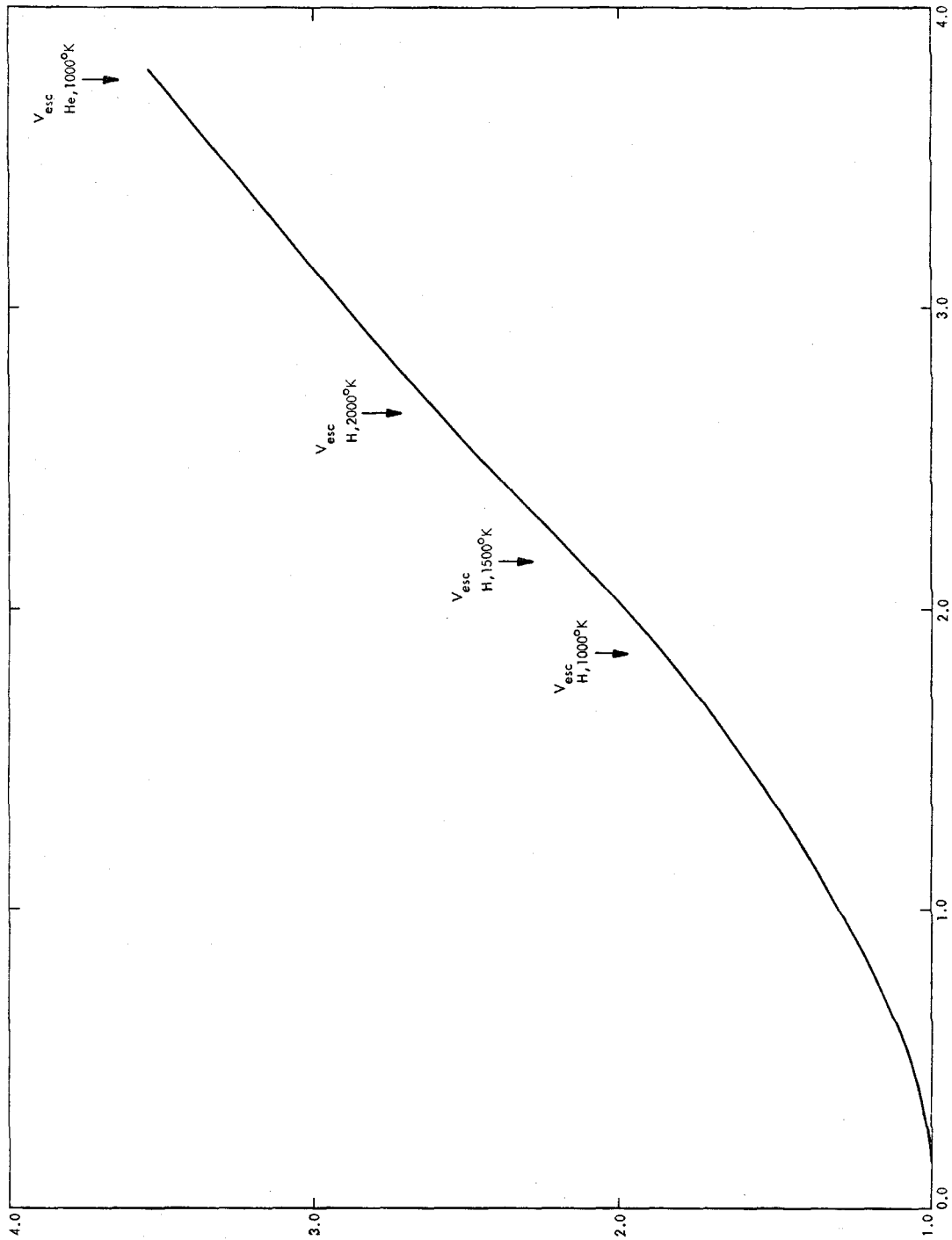
V_{esc} He, 1000°K
V_{esc} H, 2000°K
V_{esc} H, 1500°K
V_{esc} H, 1000°K
4.0
3.0
2.0
1.0
0.0
1.0
2.0
3.0
4.0
$\sqrt{\frac{m}{2kT}} \cdot v$

Figure 8

6 X 10^4
5 X 10^5
1.1 X 10^6
3.7
7.2
1.5 X 10^6
2.5 X 10^6
4.0 X 10^6
3.7 X 10^5
1.5 X 10^6
0
-10
-20
-30
-40
0
20
40
60
80
100
120
140
1
0
-1
0
20
40
60
80
100
ℓ

Figure 9

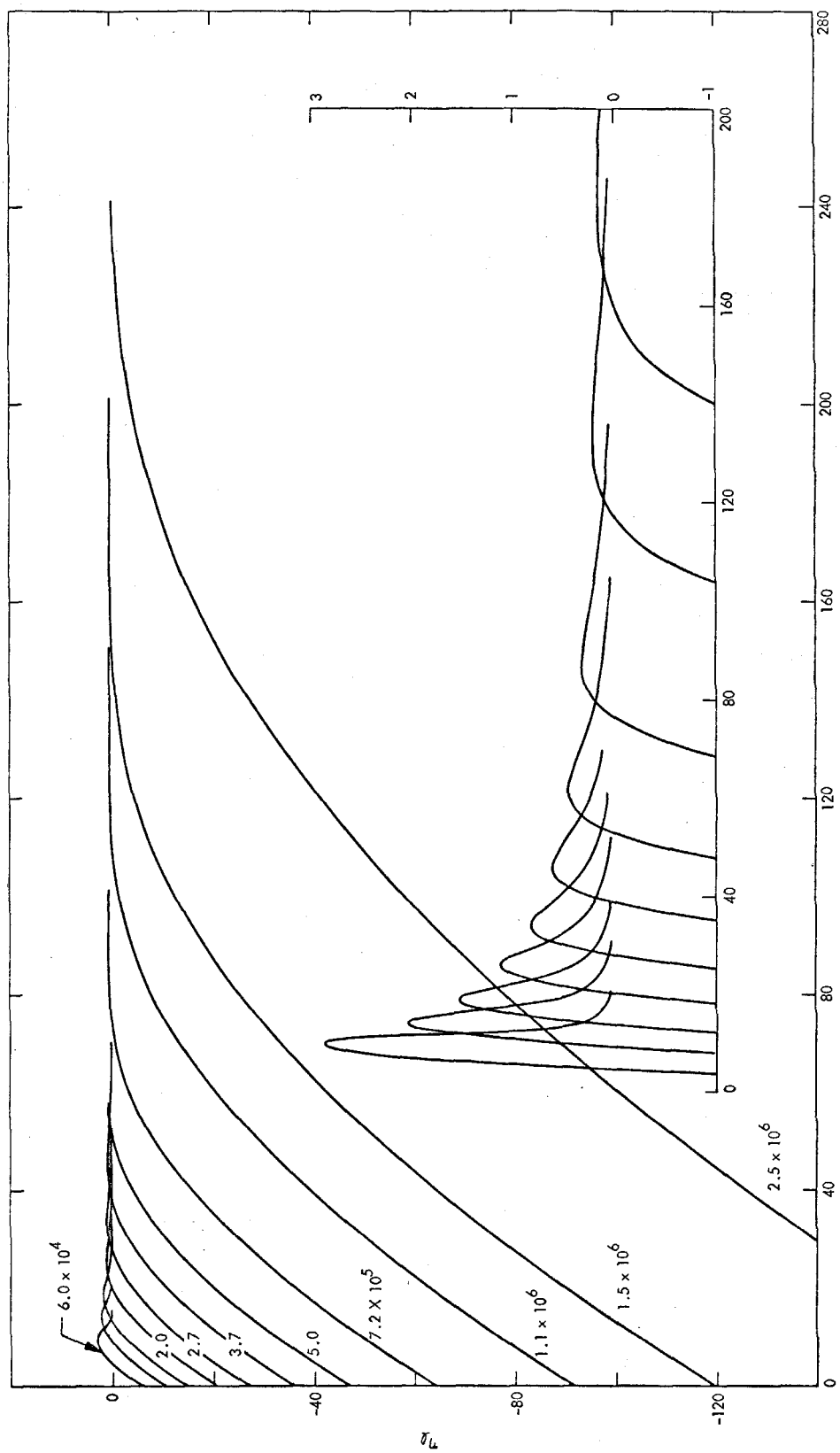
η_2
ℓ
0
-40
-80
-120
0
40
80
120
160
200
240
280
6.0×10^4
2.0
2.7
3.7
5.0
7.2×10^5
1.1×10^6
1.5×10^6
2.5×10^6
3
2
1
0
-1
0
40
80
120
160
200

Figure 10

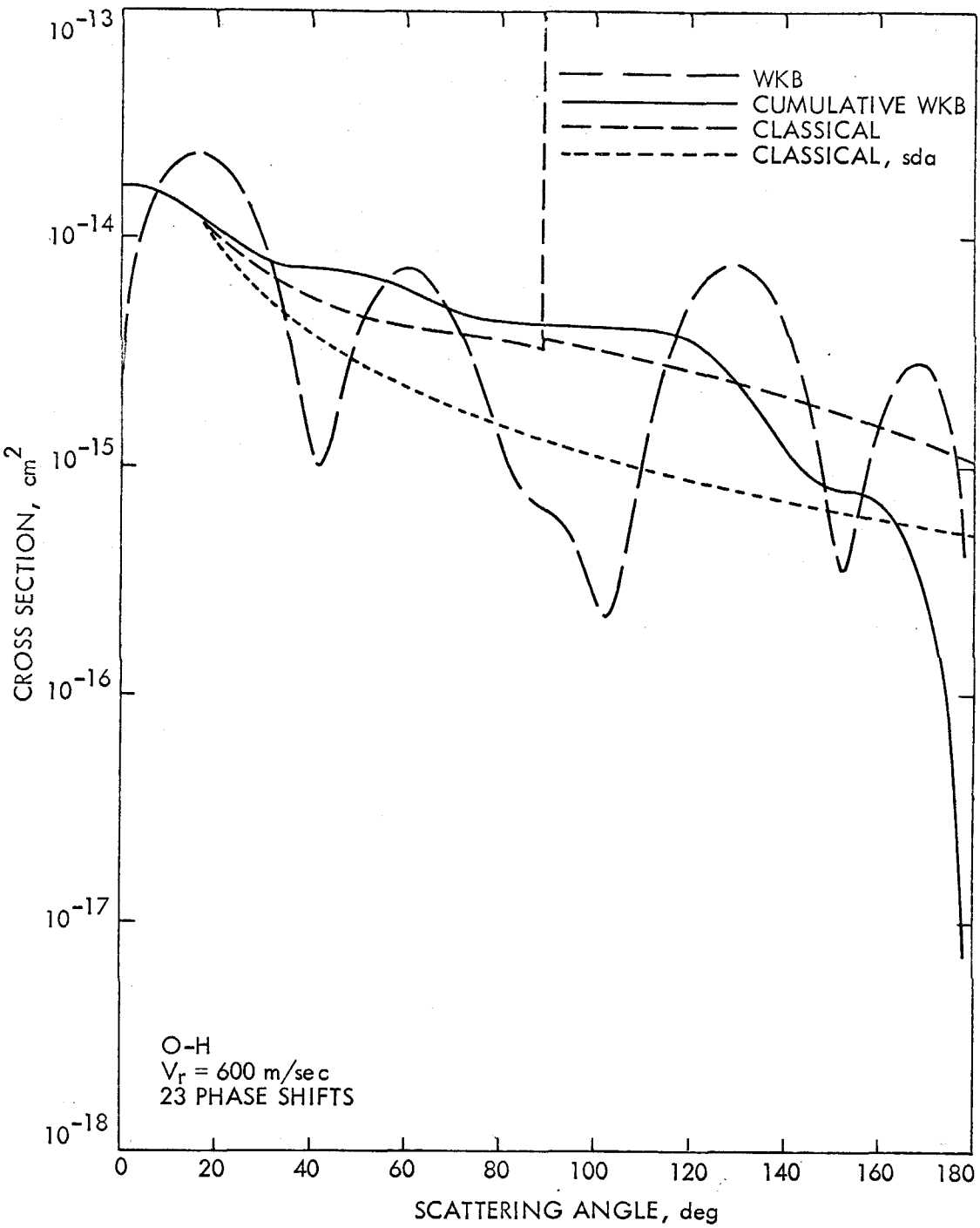
WKB
CUMULATIVE WKB
CLASSICAL
CLASSICAL, sda
CROSS SECTION, cm²
10⁻¹³
10⁻¹⁴
10⁻¹⁵
10⁻¹⁶
10⁻¹⁷
10⁻¹⁸
O-H
Vr = 600 m/sec
23 PHASE SHIFTS
0
20
40
60
80
100
120
140
160
180
SCATTERING ANGLE, deg

Figure 11

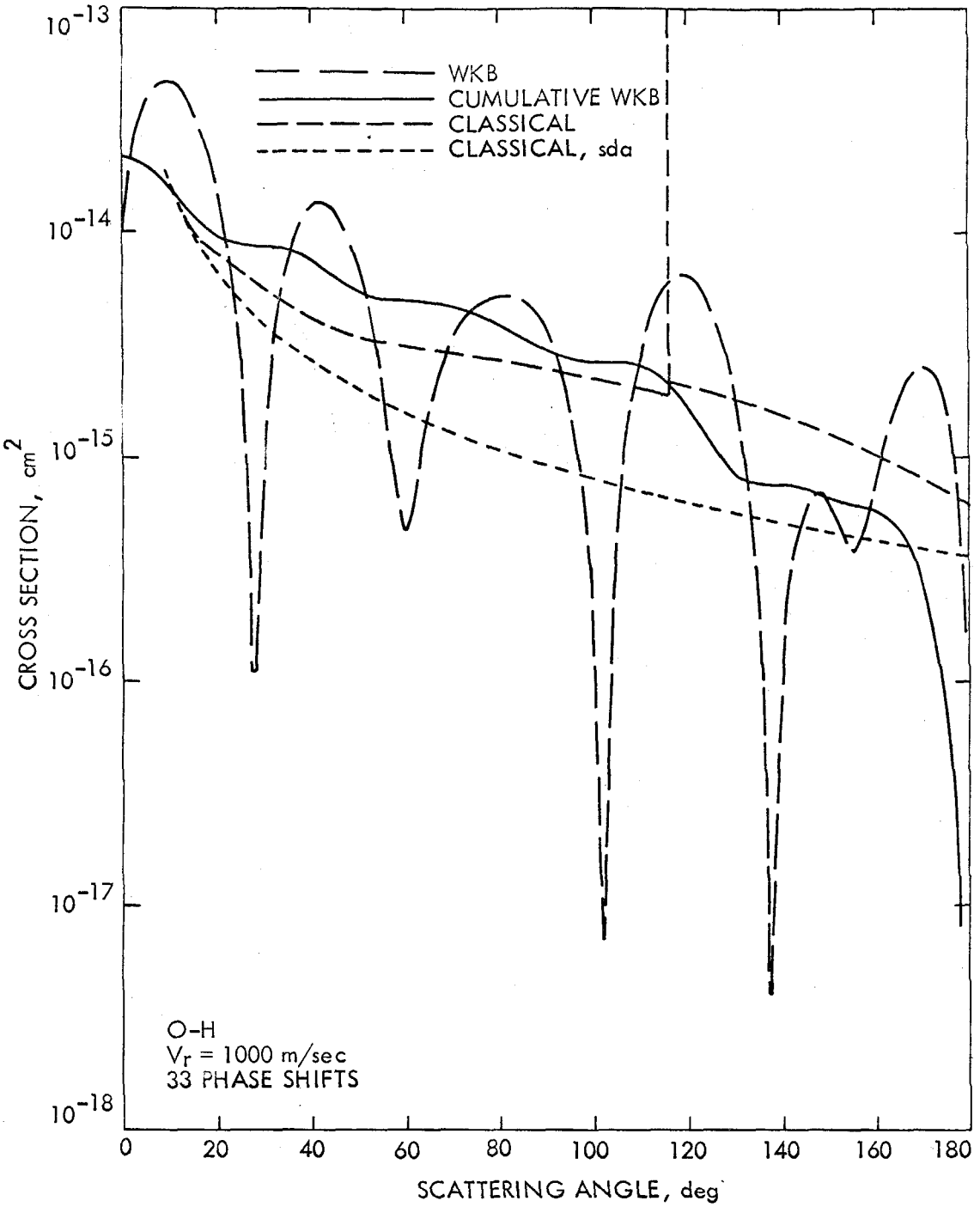
WKB
CUMULATIVE WKB
CLASSICAL
CLASSICAL, sda
O-H
V_r = 1000 m/sec
33 PHASE SHIFTS
CROSS SECTION, cm^2
SCATTERING ANGLE, deg
10^{-13}
10^{-14}
10^{-15}
10^{-16}
10^{-17}
10^{-18}
0
20
40
60
80
100
120
140
160
180

Figure 12

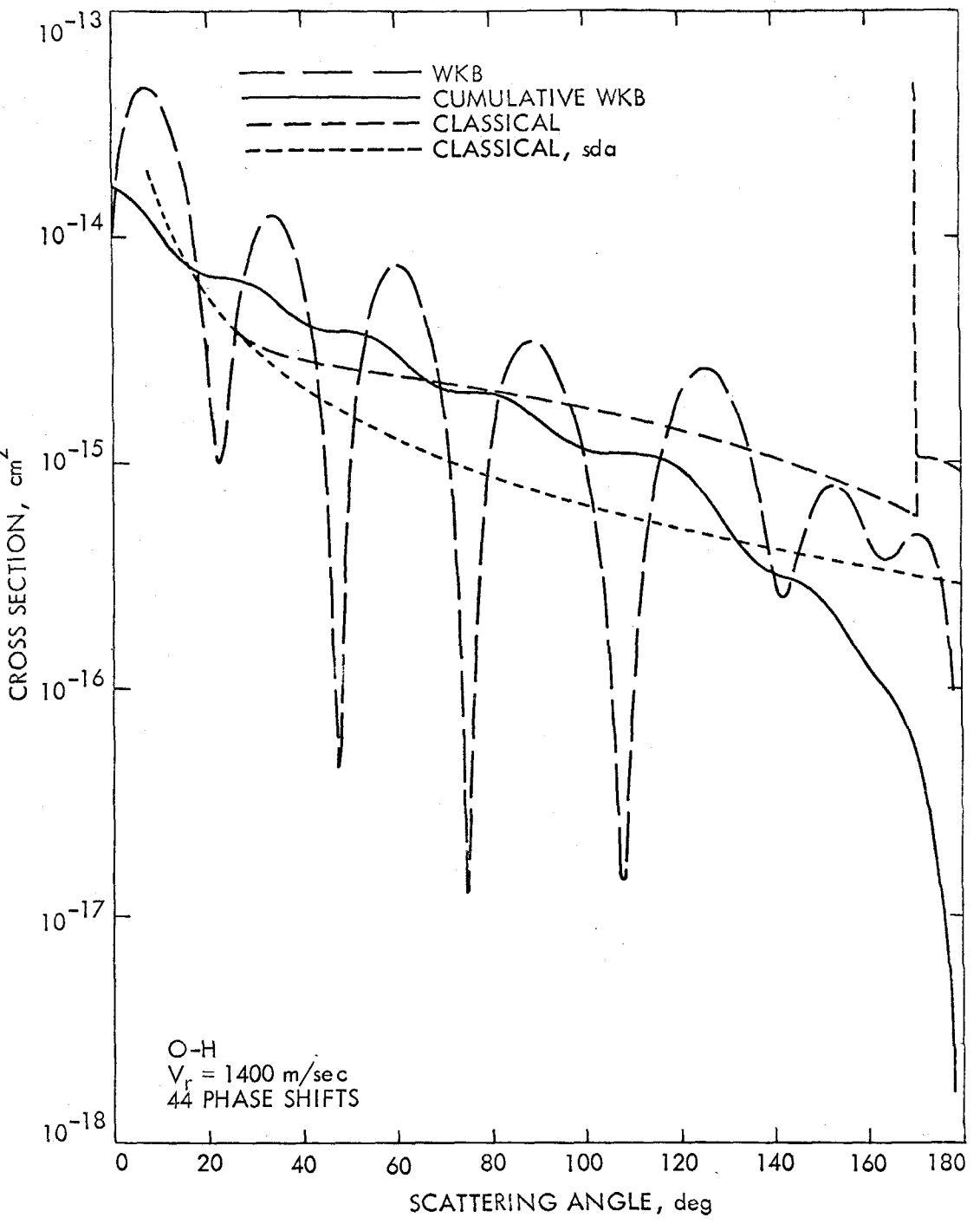
WKB
CUMULATIVE WKB
CLASSICAL
CLASSICAL, sda
O-H
V_r = 1400 m/sec
44 PHASE SHIFTS
CROSS SECTION, cm^2
SCATTERING ANGLE, deg
10^{-13}
10^{-14}
10^{-15}
10^{-16}
10^{-17}
10^{-18}
0
20
40
60
80
100
120
140
160
180

Figure 13

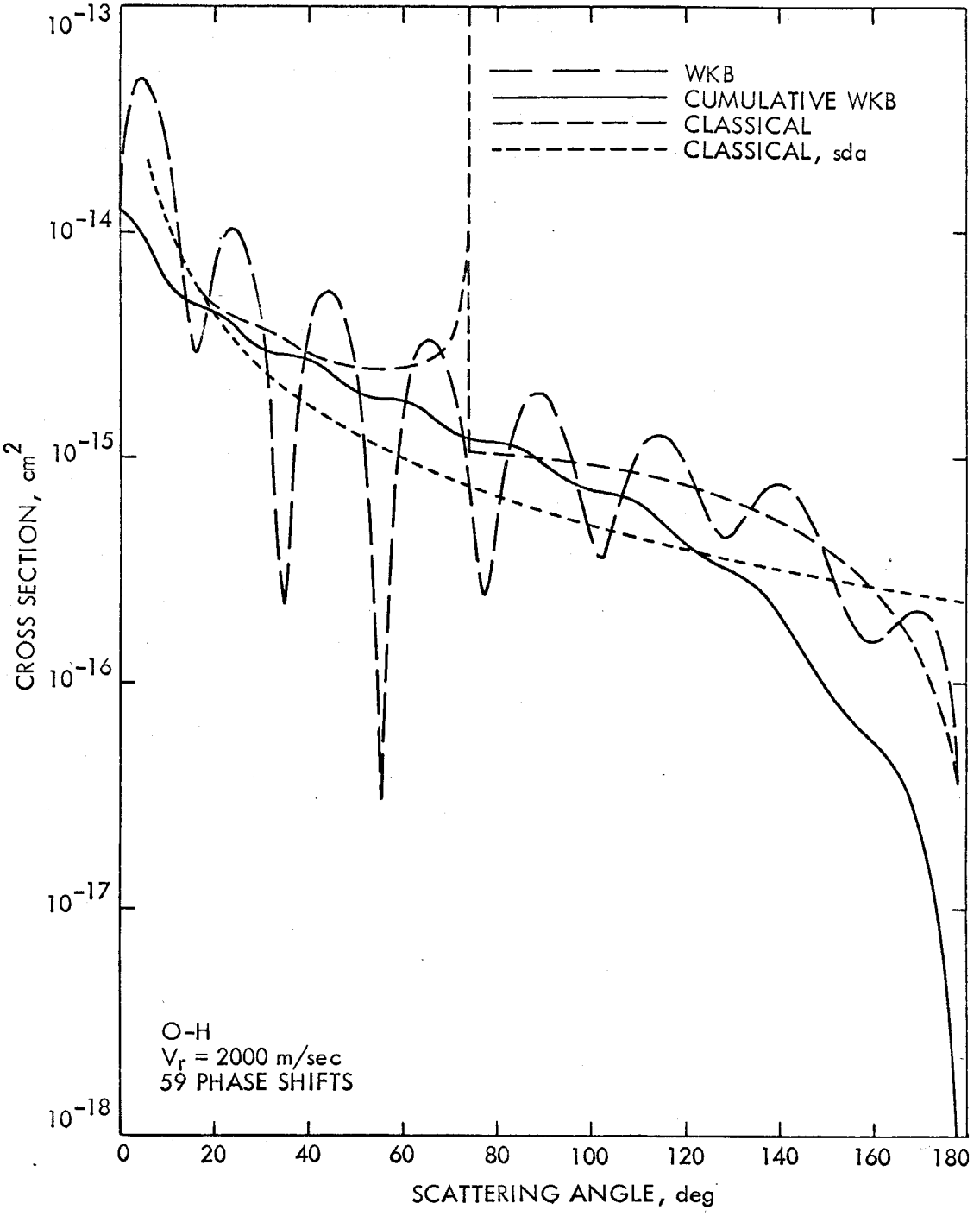
WKB
CUMULATIVE WKB
CLASSICAL
CLASSICAL, sda
O-H
V_r = 2000 m/sec
59 PHASE SHIFTS
CROSS SECTION, cm^2
SCATTERING ANGLE, deg
10^{-13}
10^{-14}
10^{-15}
10^{-16}
10^{-17}
10^{-18}
0
20
40
60
80
100
120
140
160
180

Figure 14

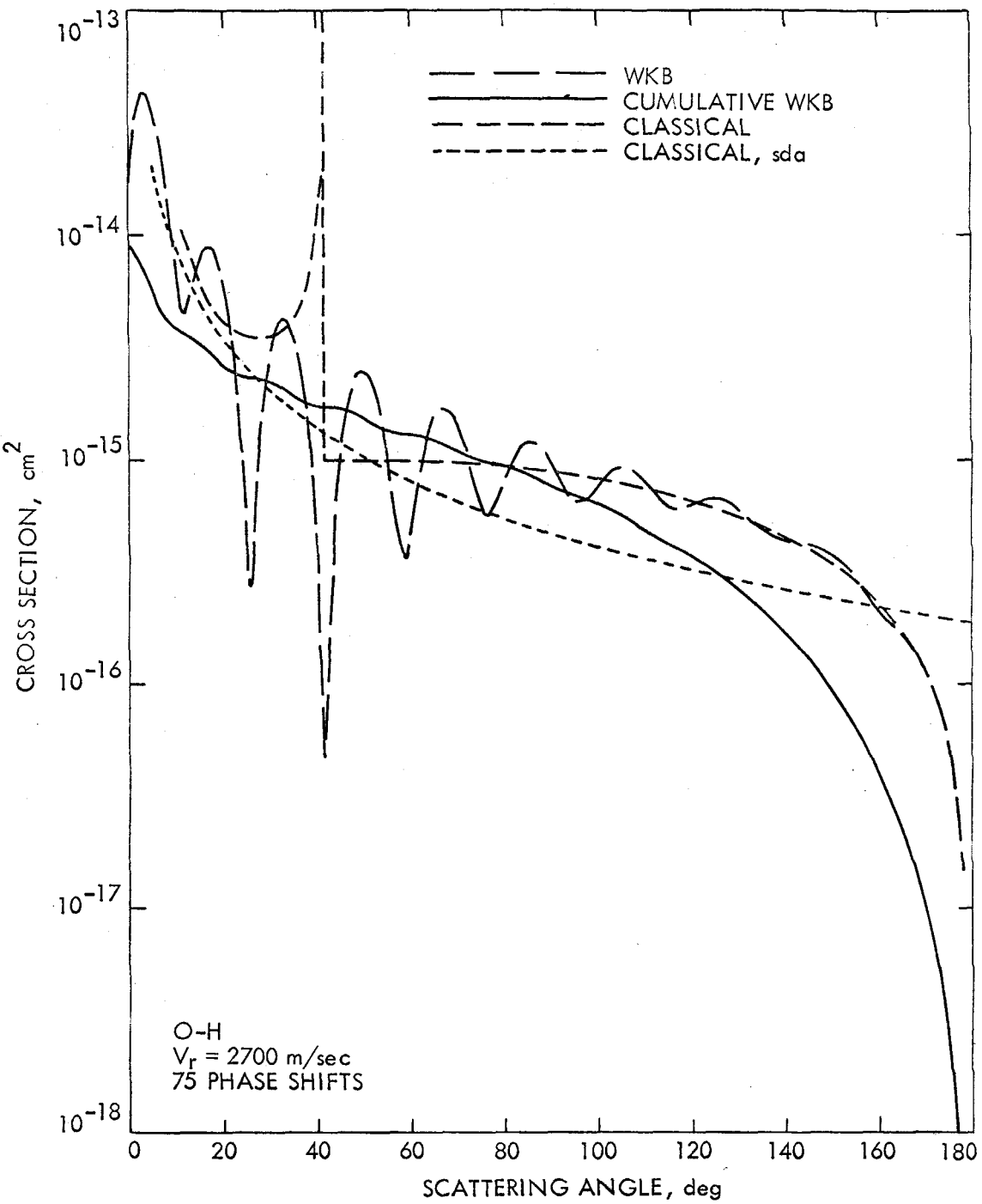
WKB
CUMULATIVE WKB
CLASSICAL
CLASSICAL, sda
CROSS SECTION, cm²
10⁻¹³
10⁻¹⁴
10⁻¹⁵
10⁻¹⁶
10⁻¹⁷
10⁻¹⁸
O-H
V_r = 2700 m/sec
75 PHASE SHIFTS
0
20
40
60
80
100
120
140
160
180
SCATTERING ANGLE, deg

Figure 15

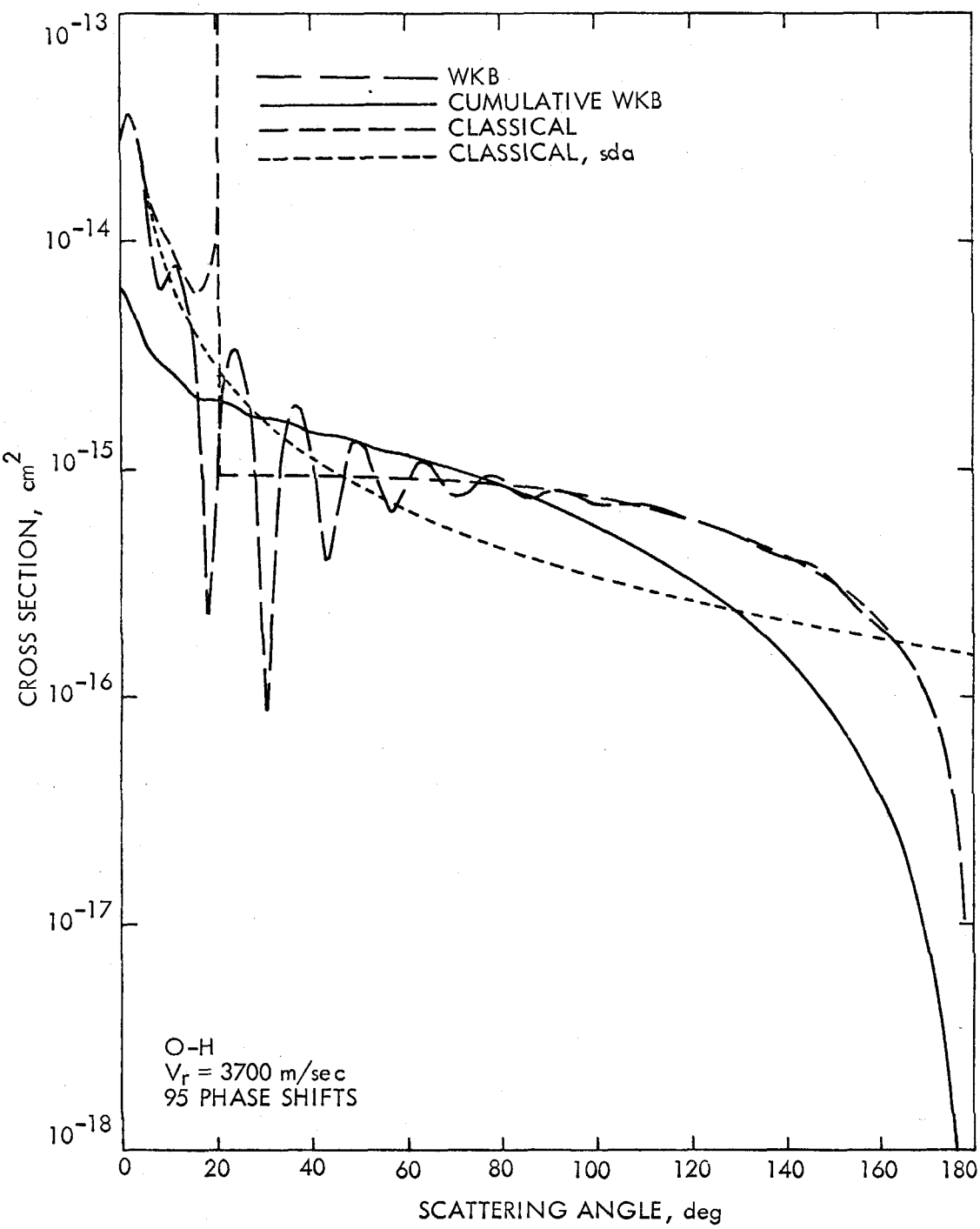
WKB
CUMULATIVE WKB
CLASSICAL
CLASSICAL, sda
O-H
V_r = 3700 m/sec
95 PHASE SHIFTS
CROSS SECTION, cm^2
SCATTERING ANGLE, deg
10^{-13}
10^{-14}
10^{-15}
10^{-16}
10^{-17}
10^{-18}
0
20
40
60
80
100
120
140
160
180

Figure 16

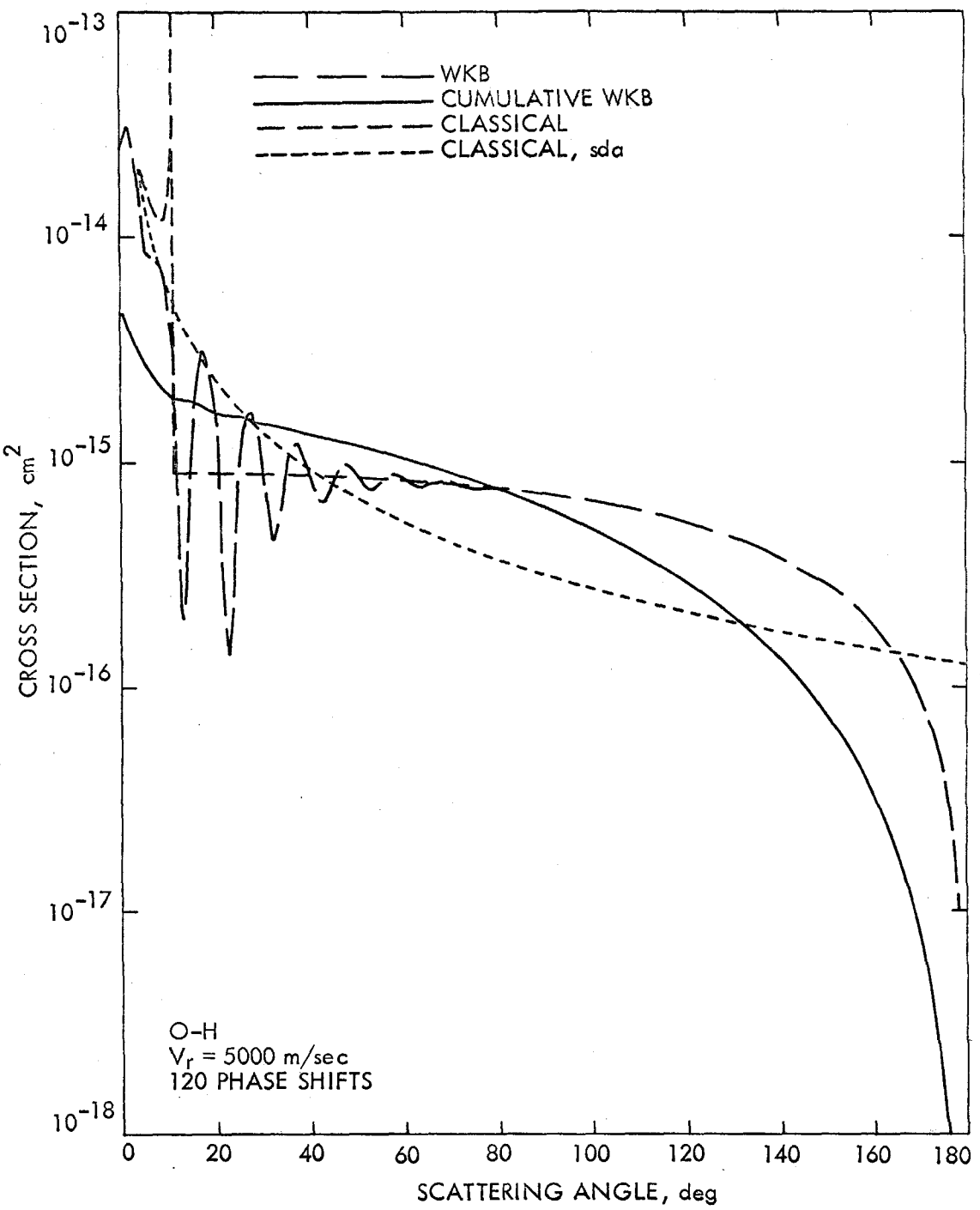
WKB
CUMULATIVE WKB
CLASSICAL
CLASSICAL, sda
CROSS SECTION, cm²
10⁻¹³
10⁻¹⁴
10⁻¹⁵
10⁻¹⁶
10⁻¹⁷
10⁻¹⁸
O-H
V_r = 5000 m/sec
120 PHASE SHIFTS
0
20
40
60
80
100
120
140
160
180
SCATTERING ANGLE, deg

Figure 17

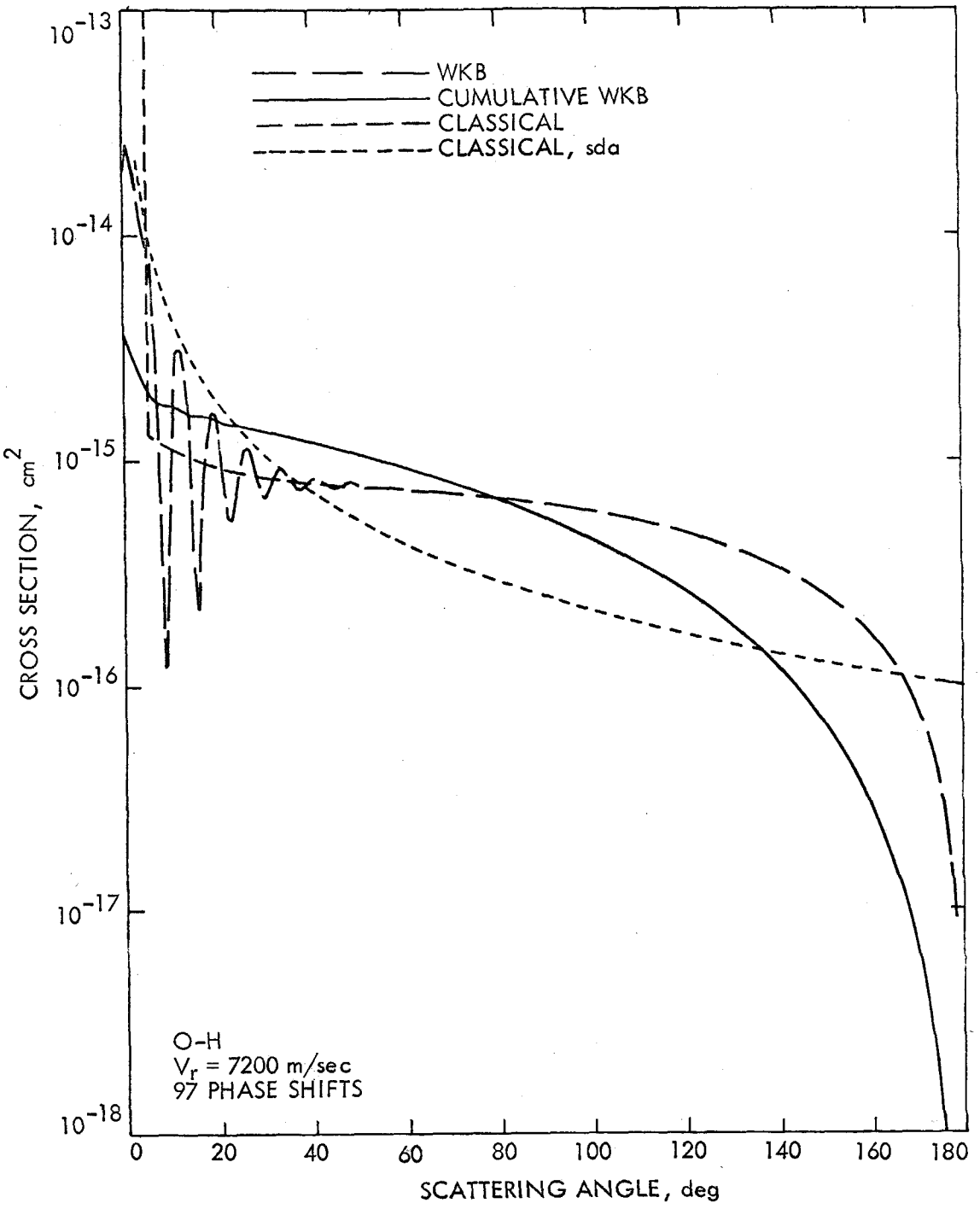
WKB
CUMULATIVE WKB
CLASSICAL
CLASSICAL, sda
CROSS SECTION, cm^2
10^{-13}
10^{-14}
10^{-15}
10^{-16}
10^{-17}
10^{-18}
O-H
V_r = 7200 m/sec
97 PHASE SHIFTS
0
20
40
60
80
100
120
140
160
180
SCATTERING ANGLE, deg

Figure 18

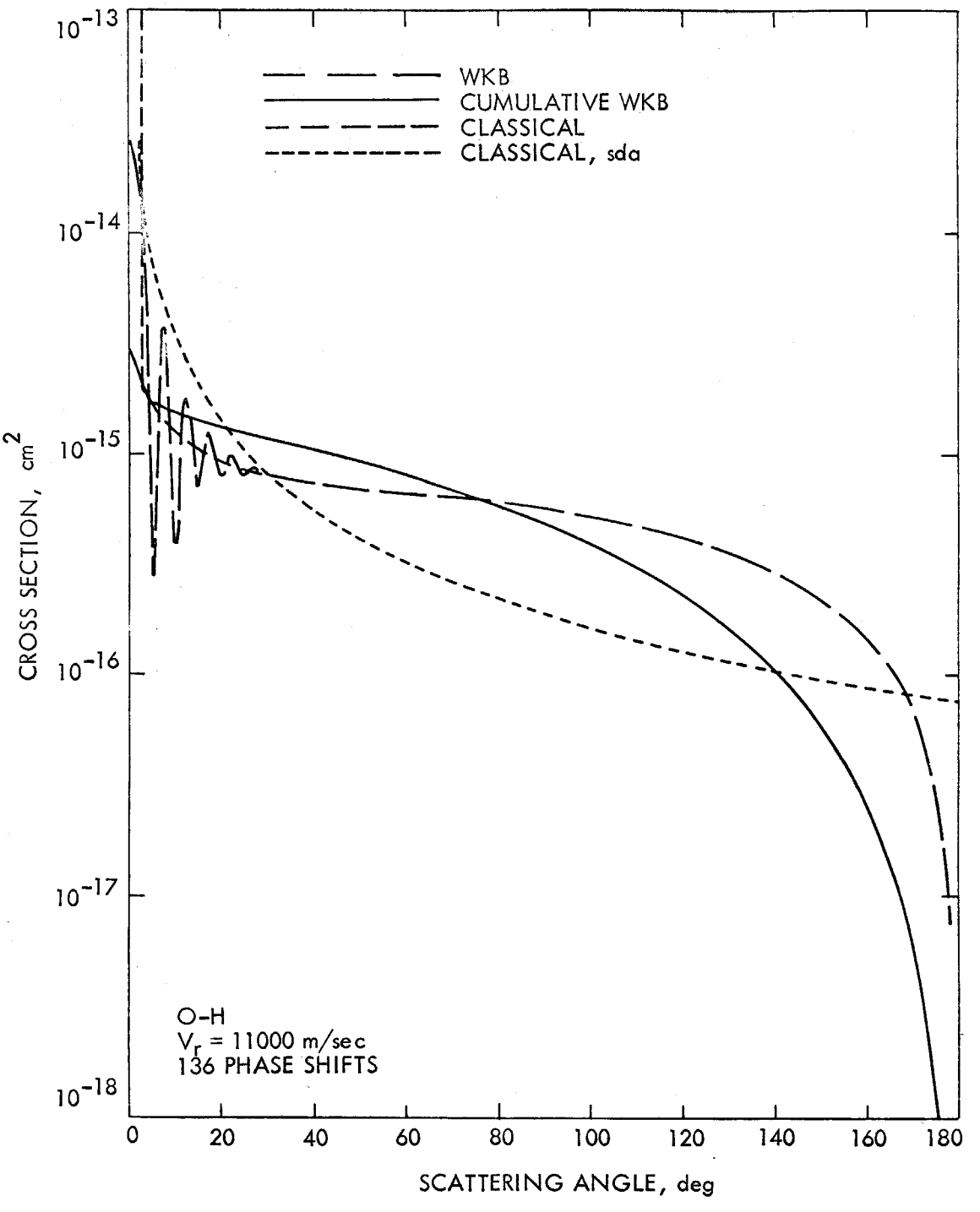
WKB
CUMULATIVE WKB
CLASSICAL
CLASSICAL, sda
O-H
V_r = 11000 m/sec
136 PHASE SHIFTS
CROSS SECTION, cm^2
SCATTERING ANGLE, deg
10^{-13}
10^{-14}
10^{-15}
10^{-16}
10^{-17}
10^{-18}
0
20
40
60
80
100
120
140
160
180

Figure 19

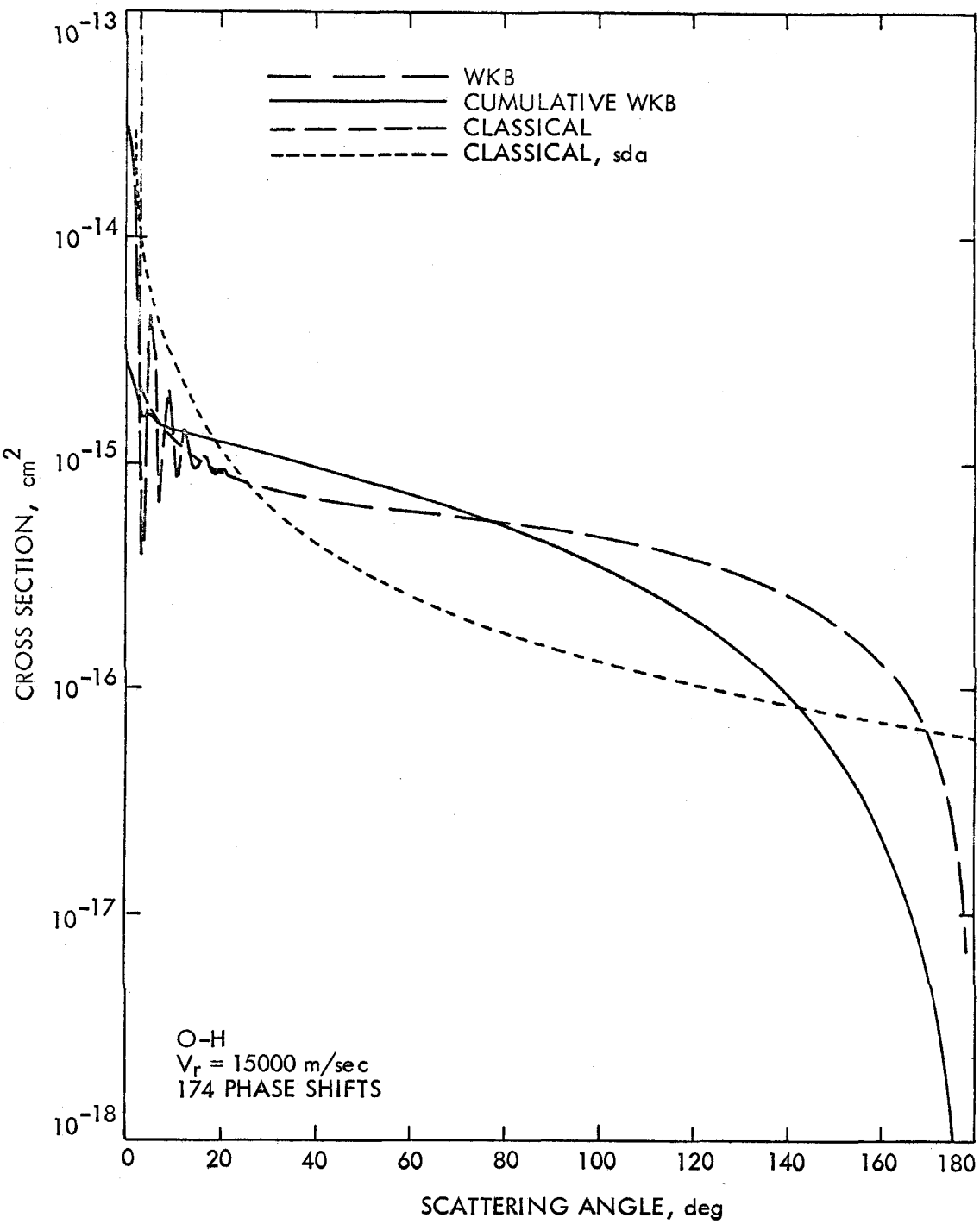
WKB
CUMULATIVE WKB
CLASSICAL
CLASSICAL, sda
10^{-13}
10^{-14}
10^{-15}
10^{-16}
10^{-17}
10^{-18}
CROSS SECTION, cm^2
O-H
V_r = 15000 m/sec
174 PHASE SHIFTS
0
20
40
60
80
100
120
140
160
180
SCATTERING ANGLE, deg

Figure 20

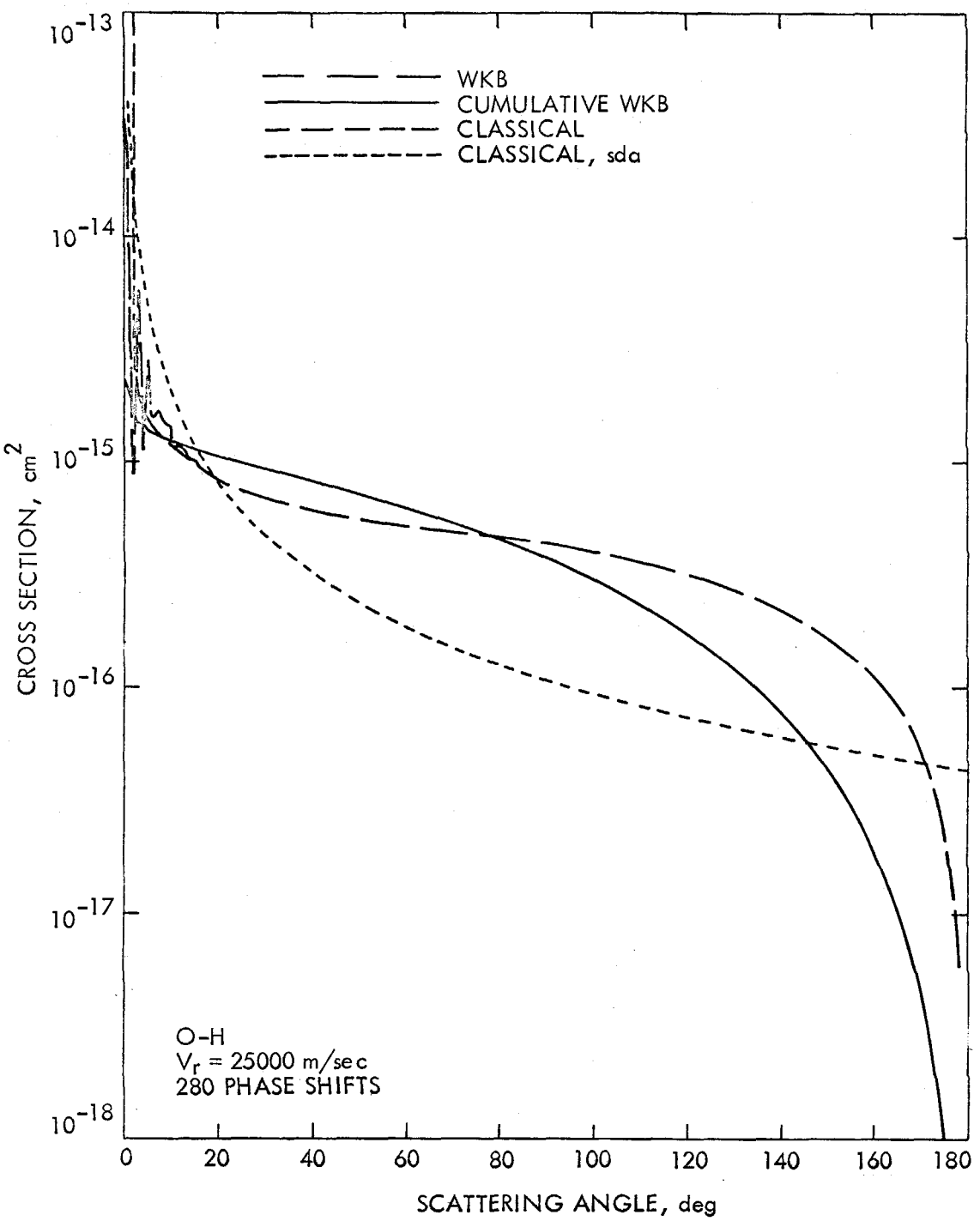
WKB
CUMULATIVE WKB
CLASSICAL
CLASSICAL, sda
CROSS SECTION, cm^2
10^{-13}
10^{-14}
10^{-15}
10^{-16}
10^{-17}
10^{-18}
O-H
V_r = 25000 m/sec
280 PHASE SHIFTS
0
20
40
60
80
100
120
140
160
180
SCATTERING ANGLE, deg

Figure 21

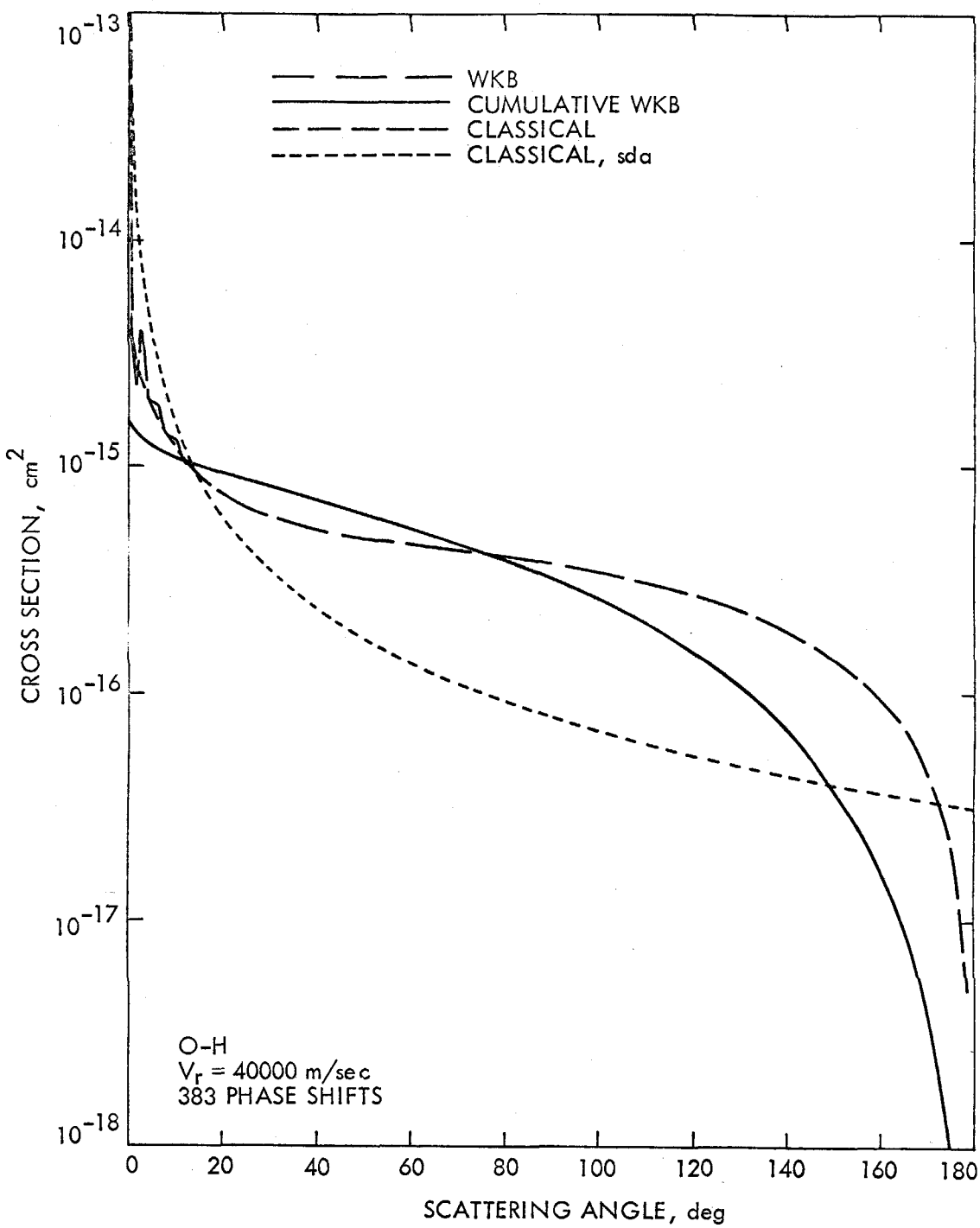
WKB
CUMULATIVE WKB
CLASSICAL
CLASSICAL, sda
O-H
V_r = 40000 m/sec
383 PHASE SHIFTS
CROSS SECTION, cm^2
SCATTERING ANGLE, deg
10^{-13}
10^{-14}
10^{-15}
10^{-16}
10^{-17}
10^{-18}
0
20
40
60
80
100
120
140
160
180

Figure 22

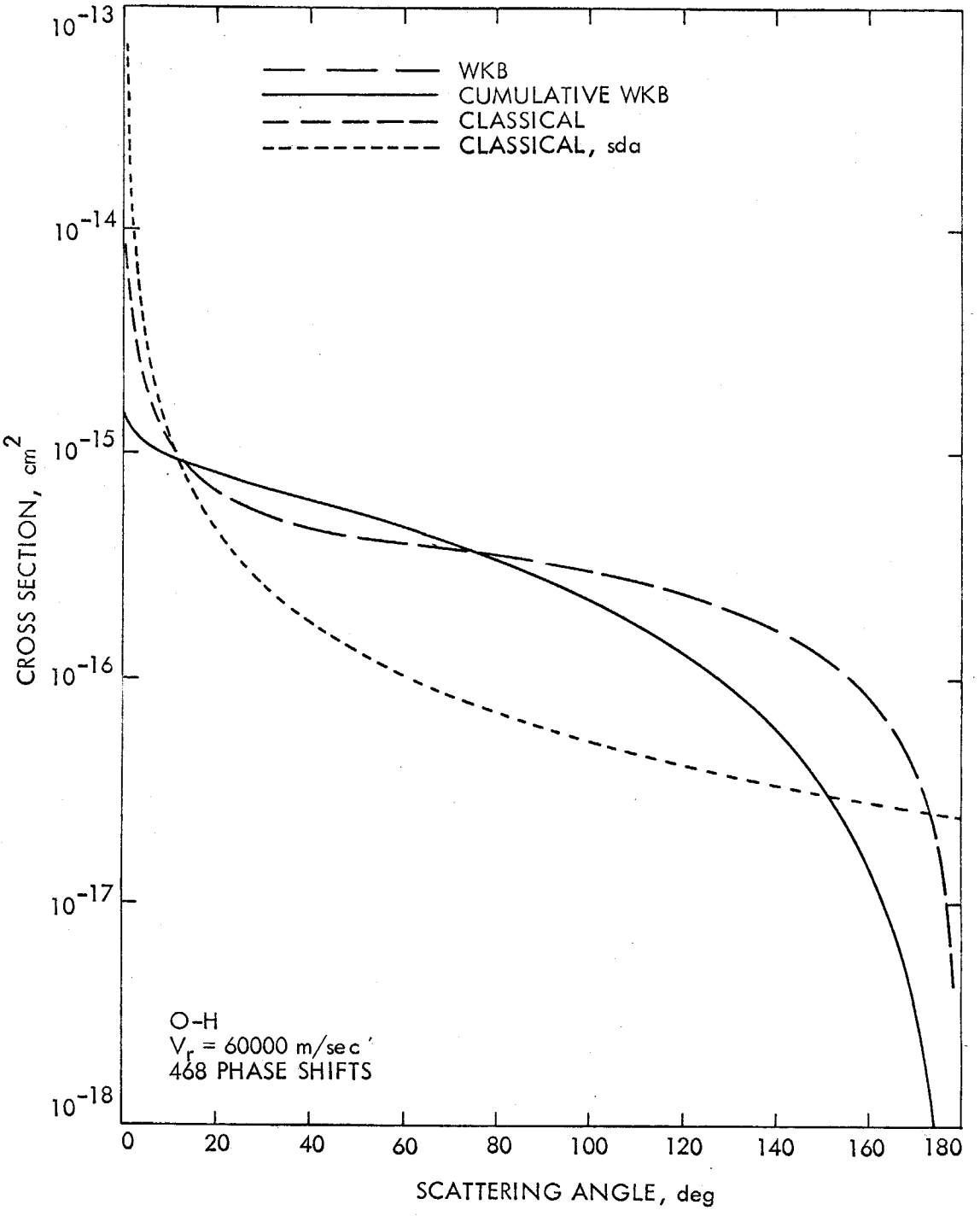
WKB
CUMULATIVE WKB
CLASSICAL
CLASSICAL, sda
10^{-13}
10^{-14}
10^{-15}
10^{-16}
10^{-17}
10^{-18}
CROSS SECTION, cm^2
O-H
V_r = 60000 m/sec
468 PHASE SHIFTS
0
20
40
60
80
100
120
140
160
180
SCATTERING ANGLE, deg

Figure 23

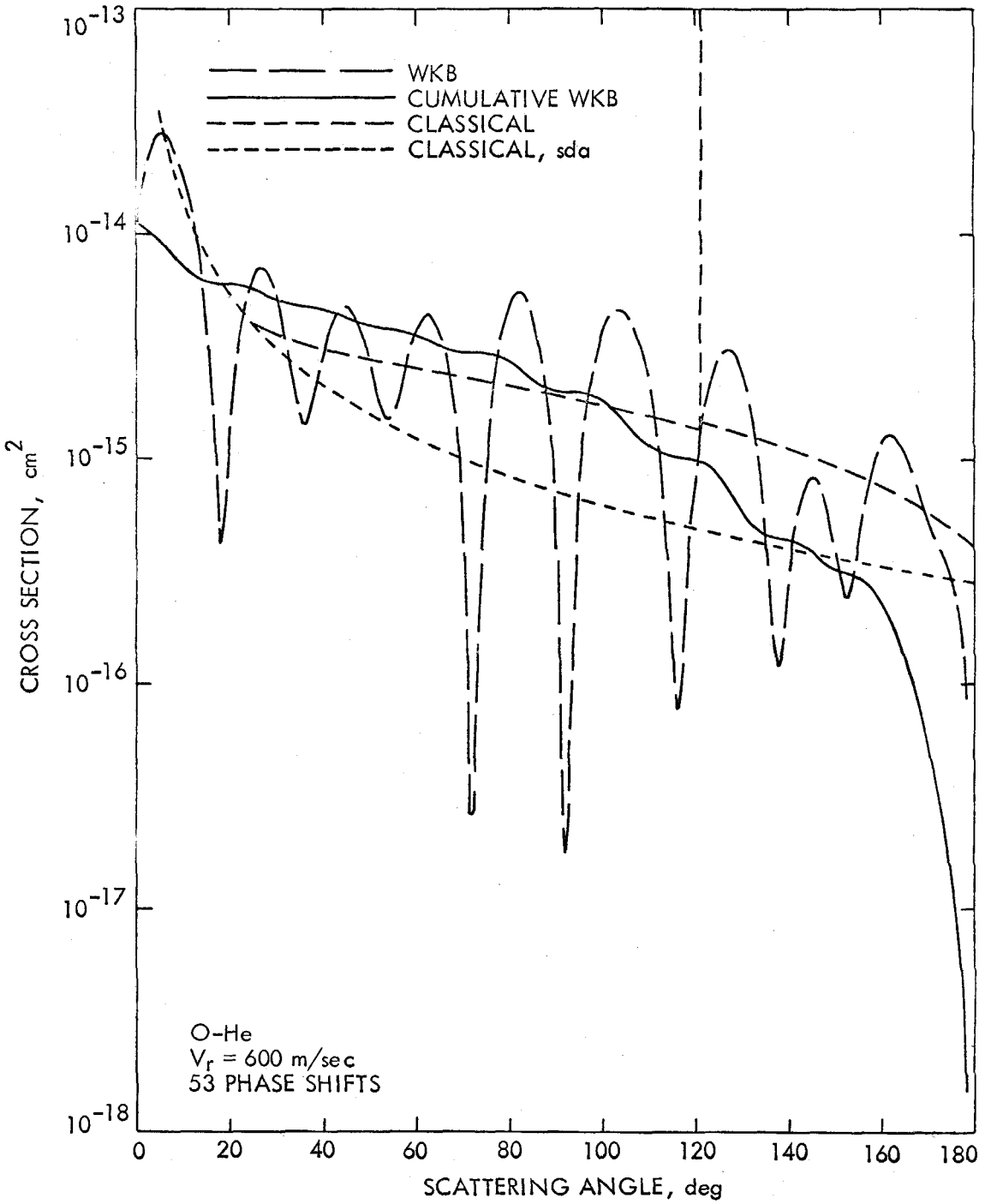
WKB
CUMULATIVE WKB
CLASSICAL
CLASSICAL, sda
O-He
V_r = 600 m/sec
53 PHASE SHIFTS
CROSS SECTION, cm^2
SCATTERING ANGLE, deg
10^{-13}
10^{-14}
10^{-15}
10^{-16}
10^{-17}
10^{-18}
0
20
40
60
80
100
120
140
160
180

Figure 24

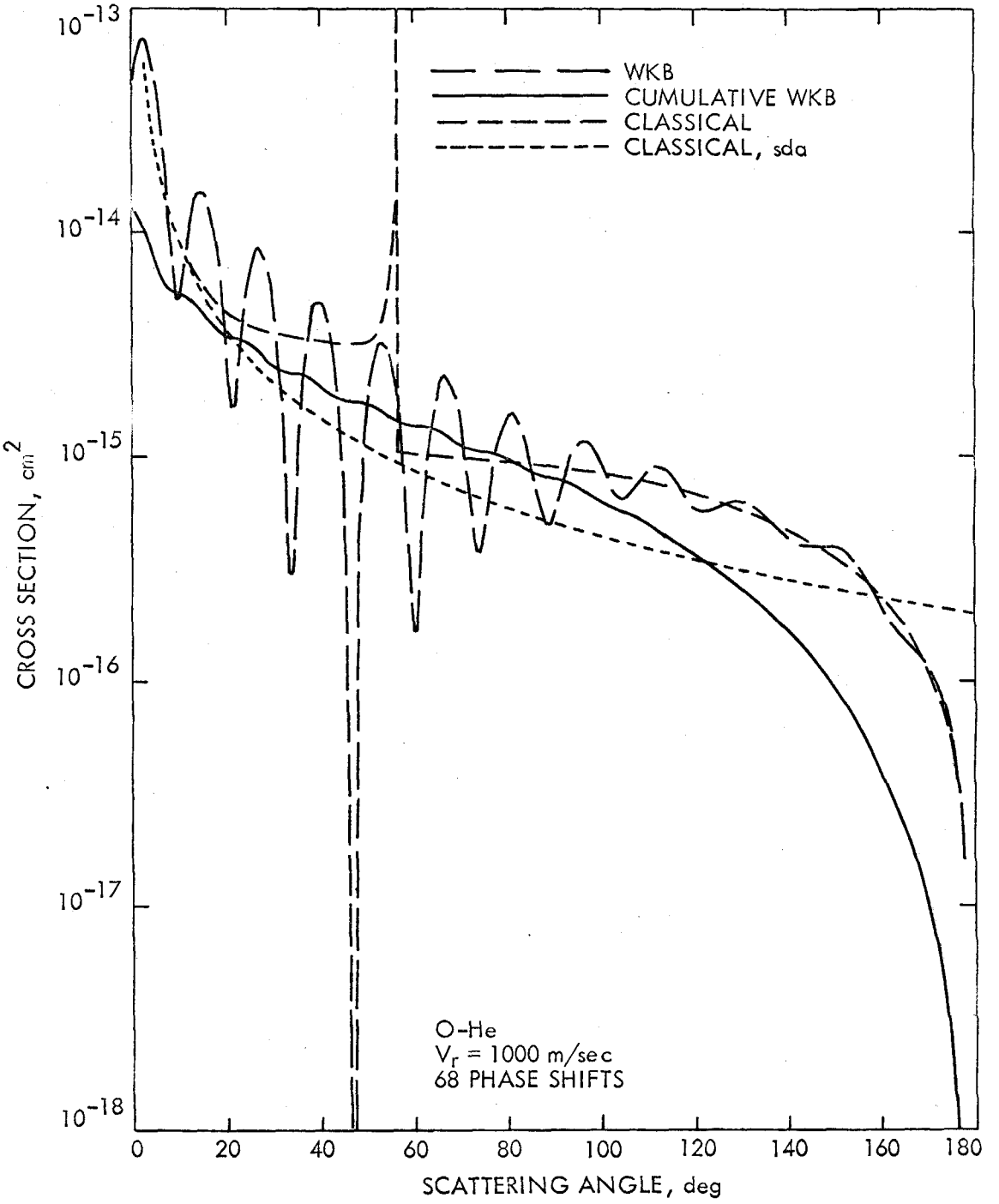
WKB
CUMULATIVE WKB
CLASSICAL
CLASSICAL, sda
O-He
V_r = 1000 m/sec
68 PHASE SHIFTS
CROSS SECTION, cm^2
SCATTERING ANGLE, deg
10^{-13}
10^{-14}
10^{-15}
10^{-16}
10^{-17}
10^{-18}
0
20
40
60
80
100
120
140
160
180

Figure 25

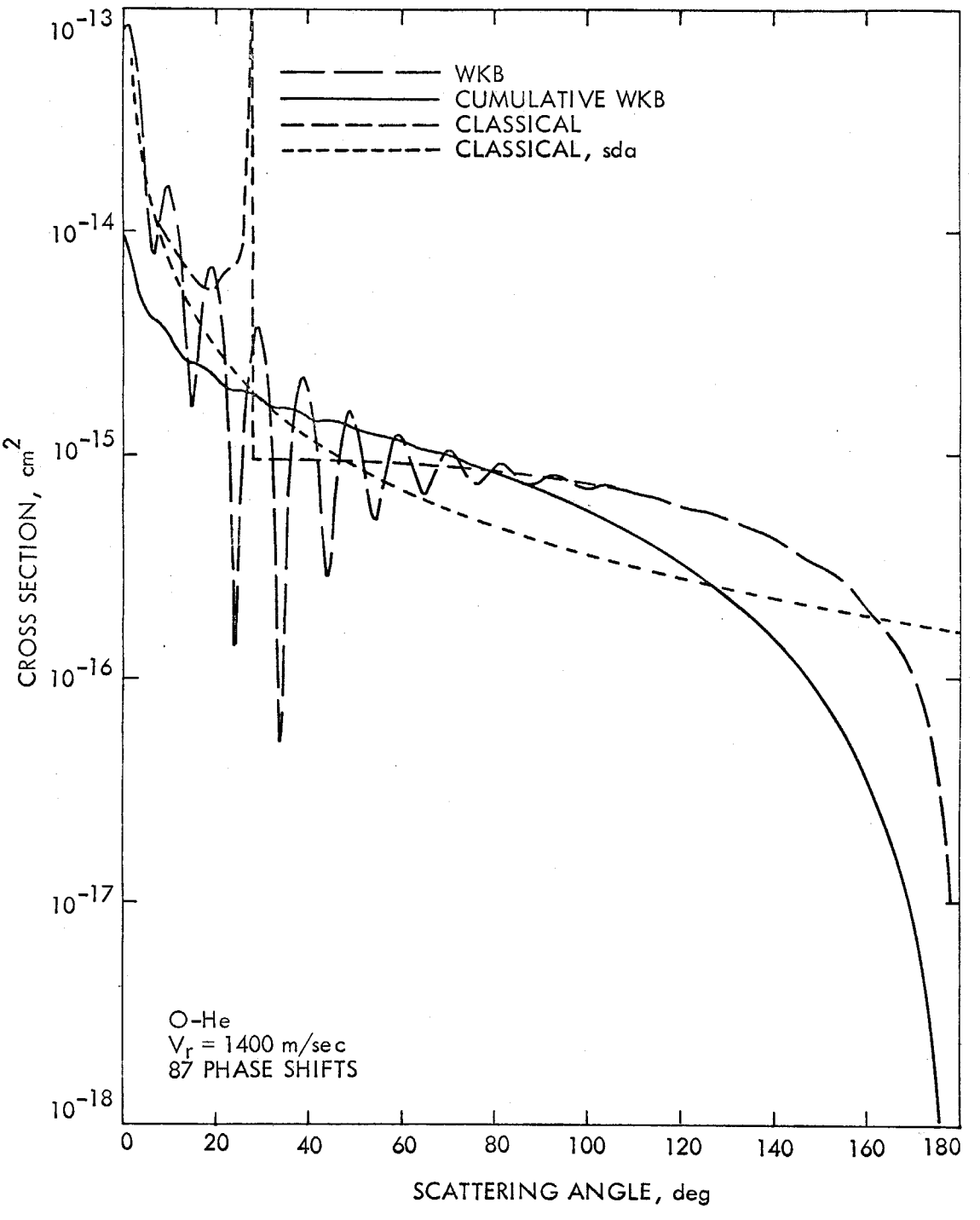
WKB
CUMULATIVE WKB
CLASSICAL
CLASSICAL, sda
O-He
V_r = 1400 m/sec
87 PHASE SHIFTS
CROSS SECTION, cm^2
SCATTERING ANGLE, deg
10^{-13}
10^{-14}
10^{-15}
10^{-16}
10^{-17}
10^{-18}
0
20
40
60
80
100
120
140
160
180

Figure 26

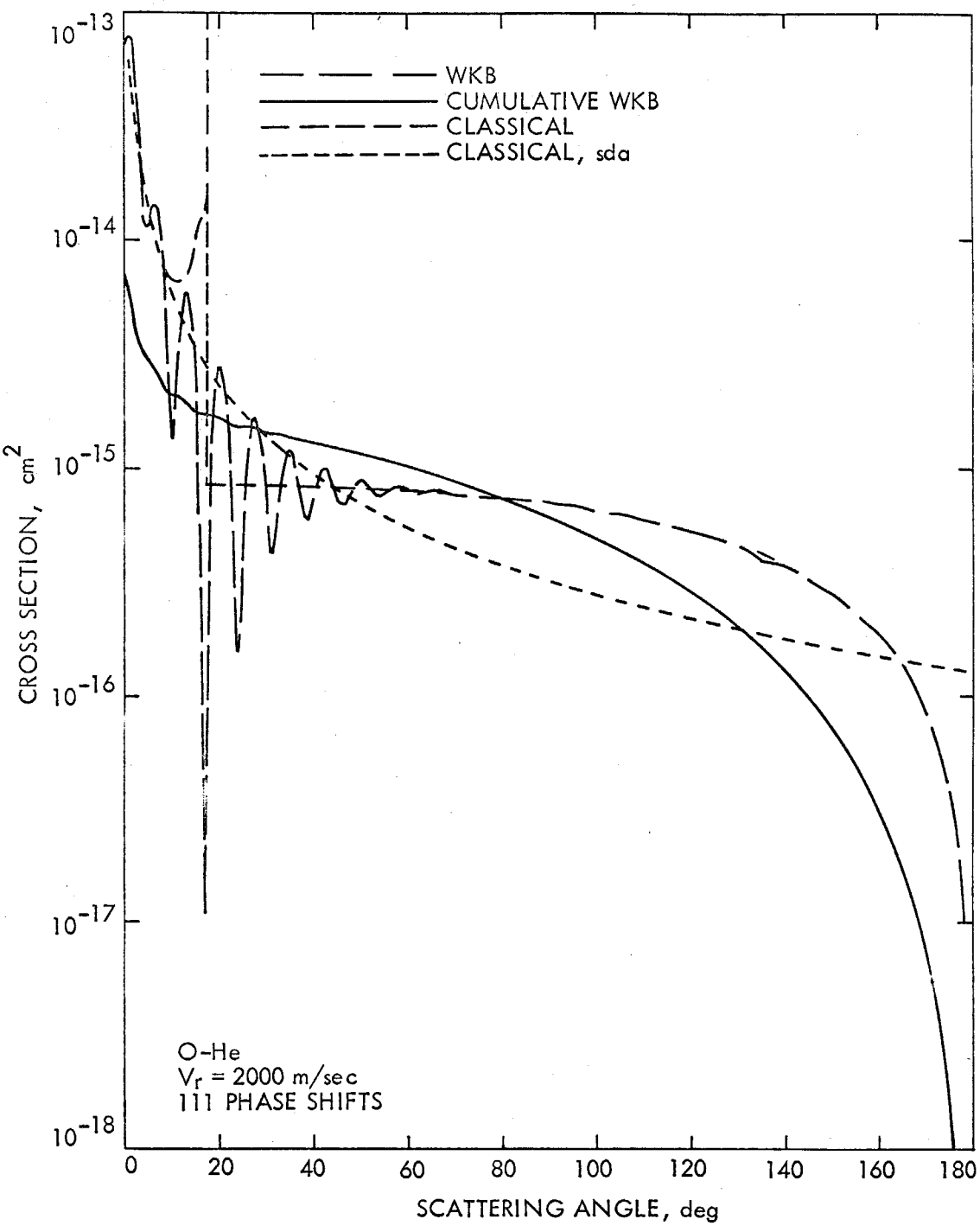
WKB
CUMULATIVE WKB
CLASSICAL
CLASSICAL, sda
CROSS SECTION, cm²
10⁻¹³
10⁻¹⁴
10⁻¹⁵
10⁻¹⁶
10⁻¹⁷
10⁻¹⁸
O-He
Vr = 2000 m/sec
111 PHASE SHIFTS
0
20
40
60
80
100
120
140
160
180
SCATTERING ANGLE, deg

Figure 27

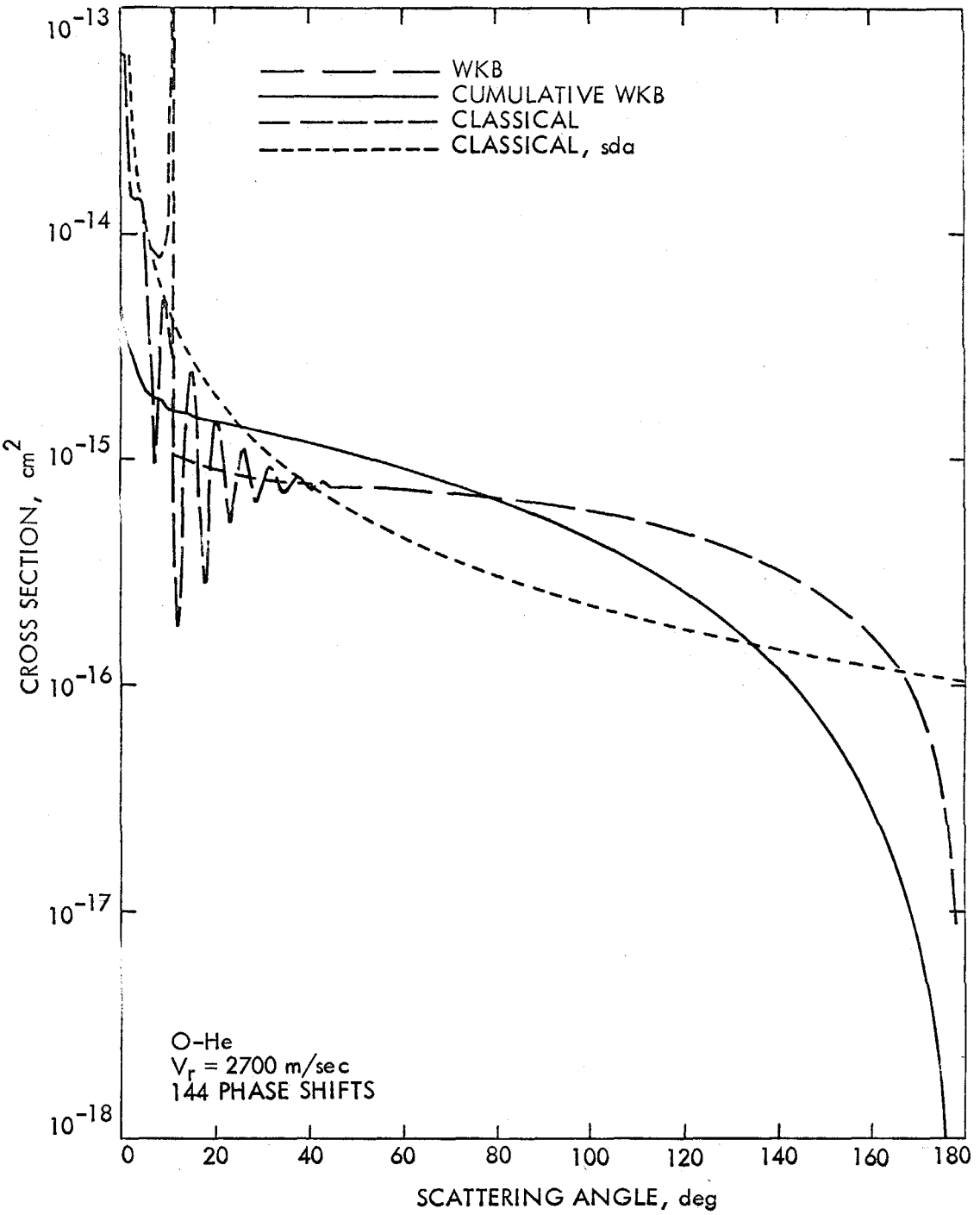
WKB
CUMULATIVE WKB
CLASSICAL
CLASSICAL, sda
O-He
V_r = 2700 m/sec
144 PHASE SHIFTS
CROSS SECTION, cm^2
SCATTERING ANGLE, deg
10^{-13}
10^{-14}
10^{-15}
10^{-16}
10^{-17}
10^{-18}
0
20
40
60
80
100
120
140
160
180

Figure 28

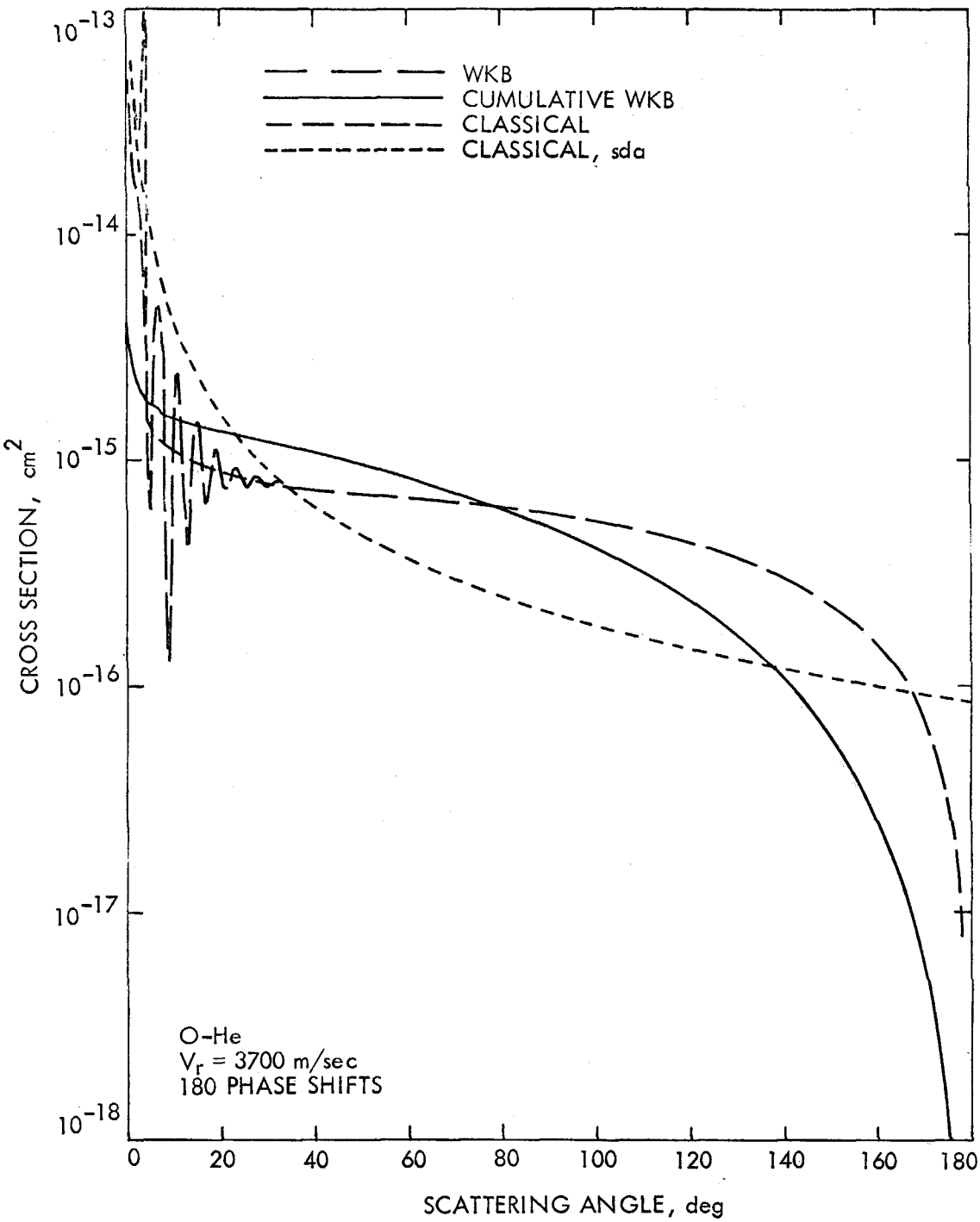
WKB
CUMULATIVE WKB
CLASSICAL
CLASSICAL, sda
O-He
V_r = 3700 m/sec
180 PHASE SHIFTS
CROSS SECTION, cm^2
SCATTERING ANGLE, deg
10^{-13}
10^{-14}
10^{-15}
10^{-16}
10^{-17}
10^{-18}
0
20
40
60
80
100
120
140
160
180

Figure 29

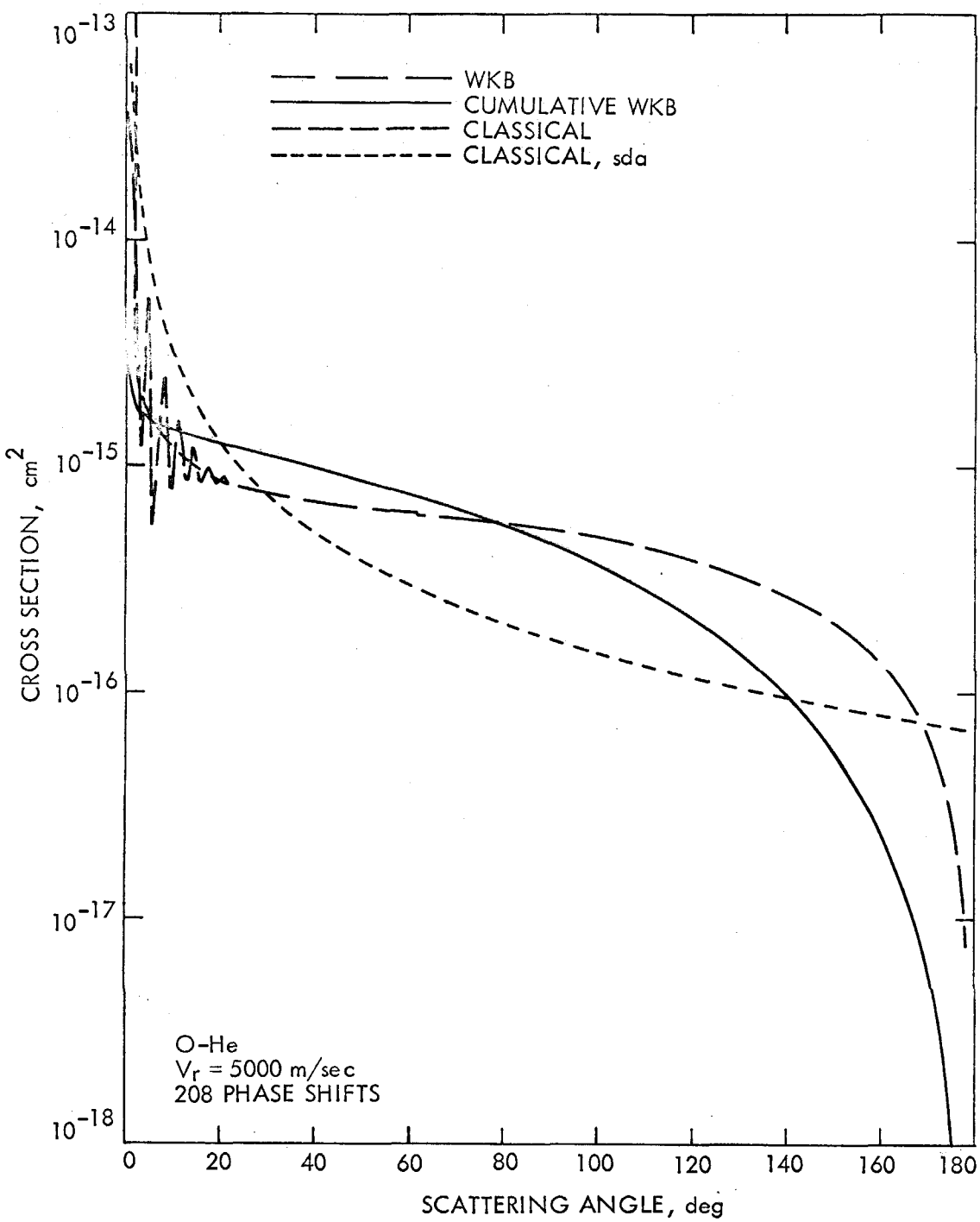
WKB
CUMULATIVE WKB
CLASSICAL
CLASSICAL, sda
10^{-13}
10^{-14}
10^{-15}
10^{-16}
10^{-17}
10^{-18}
CROSS SECTION, cm^2
O-He
V_r = 5000 m/sec
208 PHASE SHIFTS
0
20
40
60
80
100
120
140
160
180
SCATTERING ANGLE, deg

Figure 30

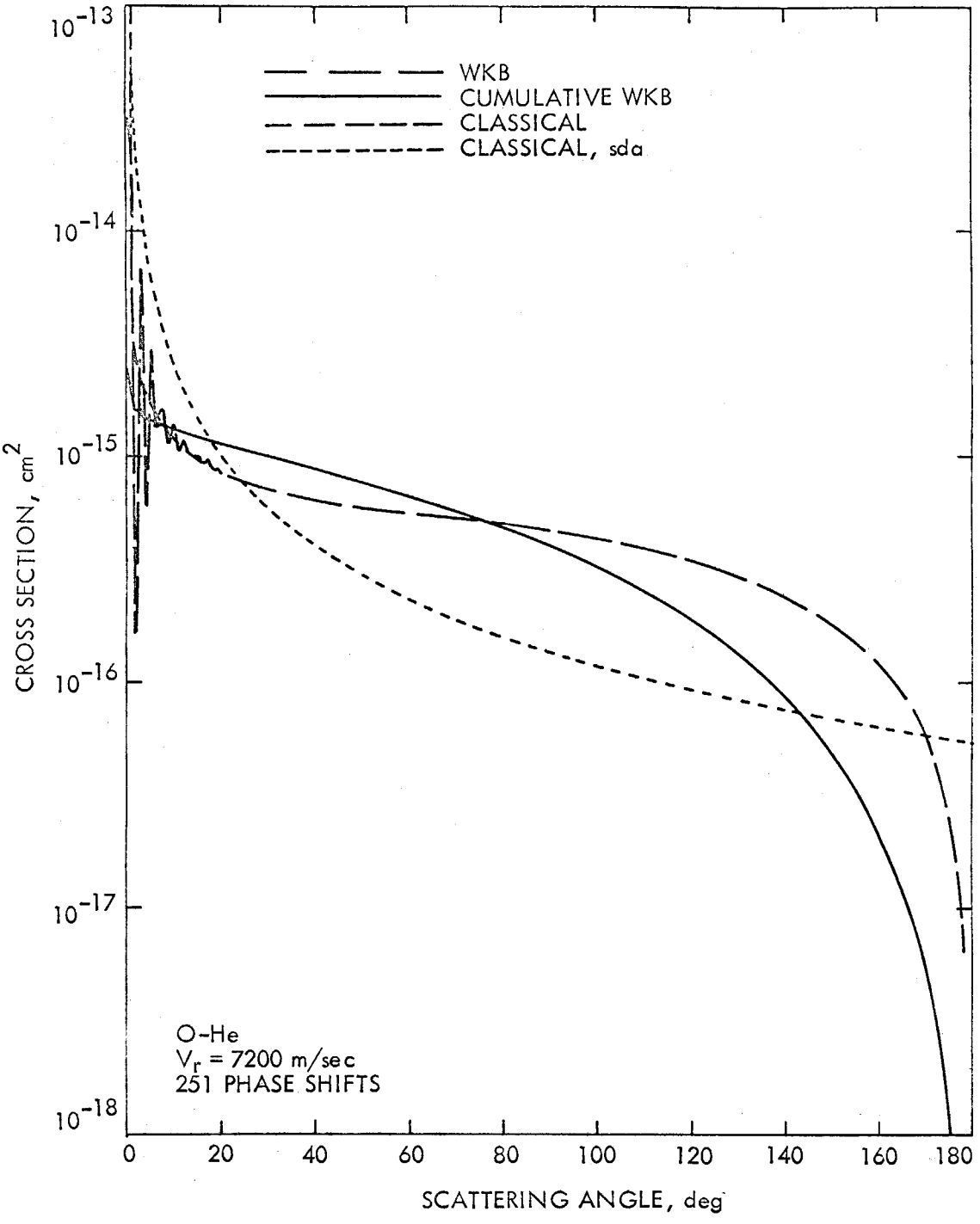
WKB
CUMULATIVE WKB
CLASSICAL
CLASSICAL, sda
10^{-13}
10^{-14}
10^{-15}
10^{-16}
10^{-17}
10^{-18}
CROSS SECTION, cm^2
O-He
V_r = 7200 m/sec
251 PHASE SHIFTS
0
20
40
60
80
100
120
140
160
180
SCATTERING ANGLE, deg

Figure 31

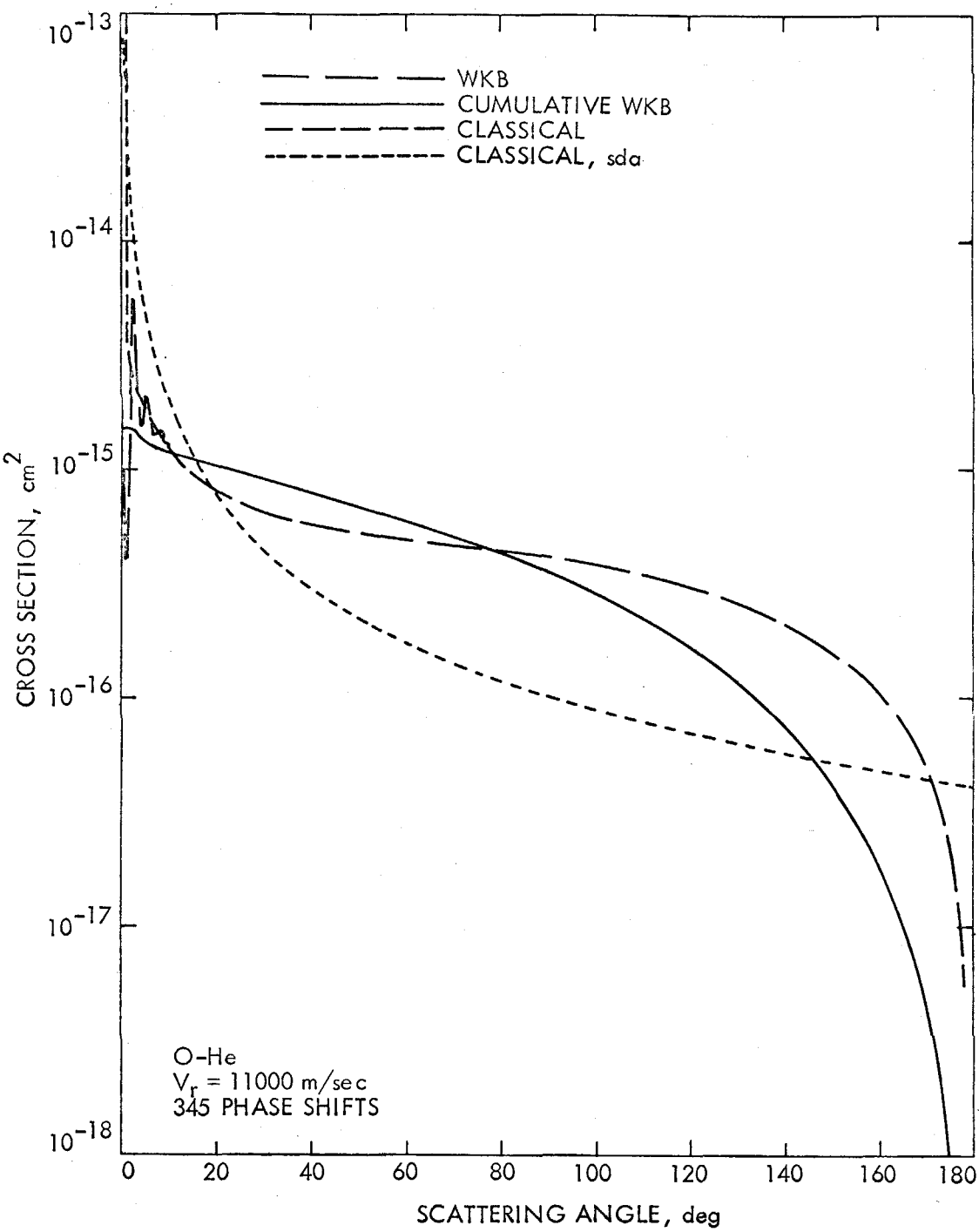
WKB
CUMULATIVE WKB
CLASSICAL
CLASSICAL, sda
O-He
V_r = 11000 m/sec
345 PHASE SHIFTS
CROSS SECTION, cm^2
SCATTERING ANGLE, deg
10^{-13}
10^{-14}
10^{-15}
10^{-16}
10^{-17}
10^{-18}
0
20
40
60
80
100
120
140
160
180

Figure 32

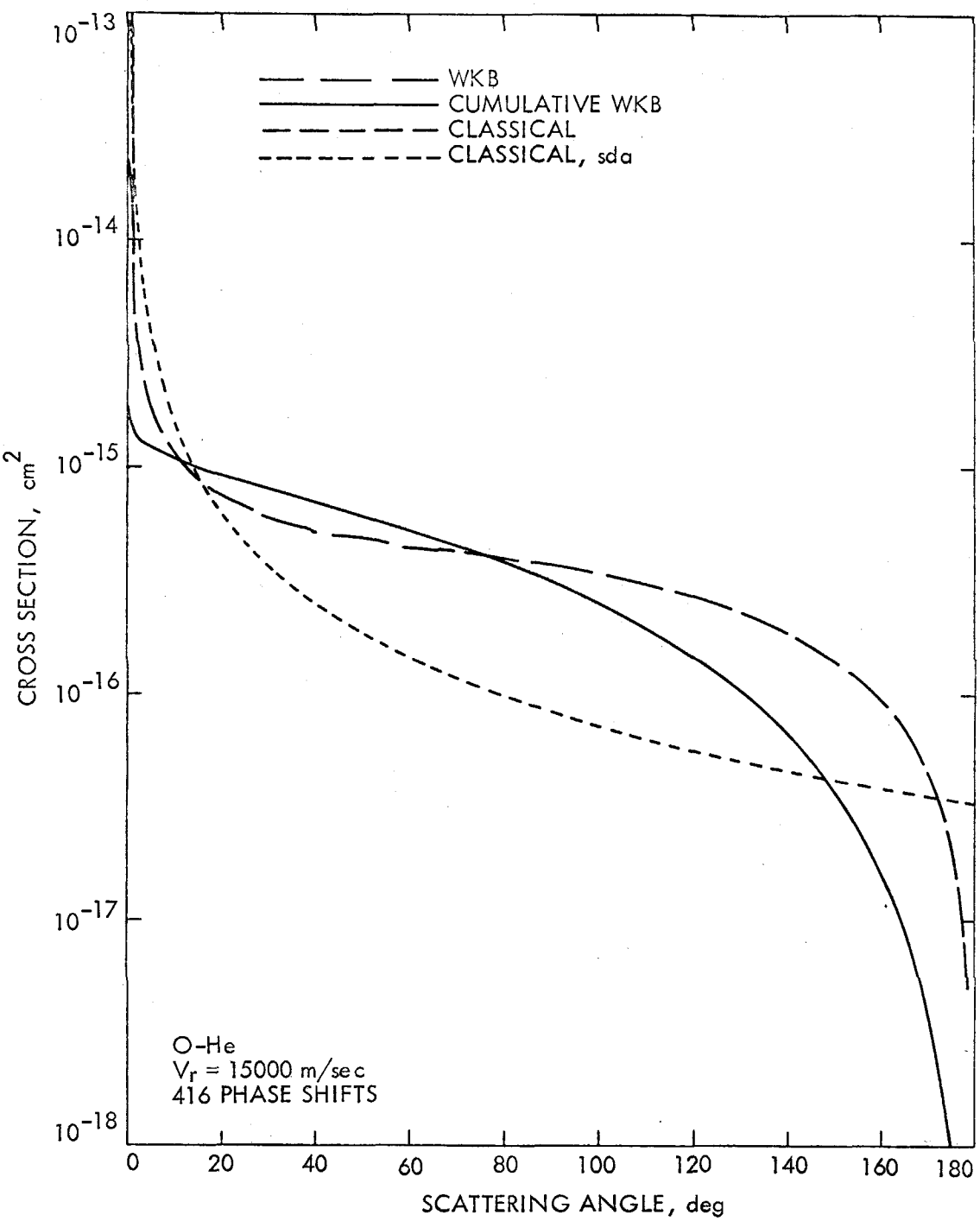
WKB
CUMULATIVE WKB
CLASSICAL
CLASSICAL, sda
O-He
V_r = 15000 m/sec
416 PHASE SHIFTS
CROSS SECTION, cm^2
SCATTERING ANGLE, deg
10^{-13}
10^{-14}
10^{-15}
10^{-16}
10^{-17}
10^{-18}
0
20
40
60
80
100
120
140
160
180

Figure 33

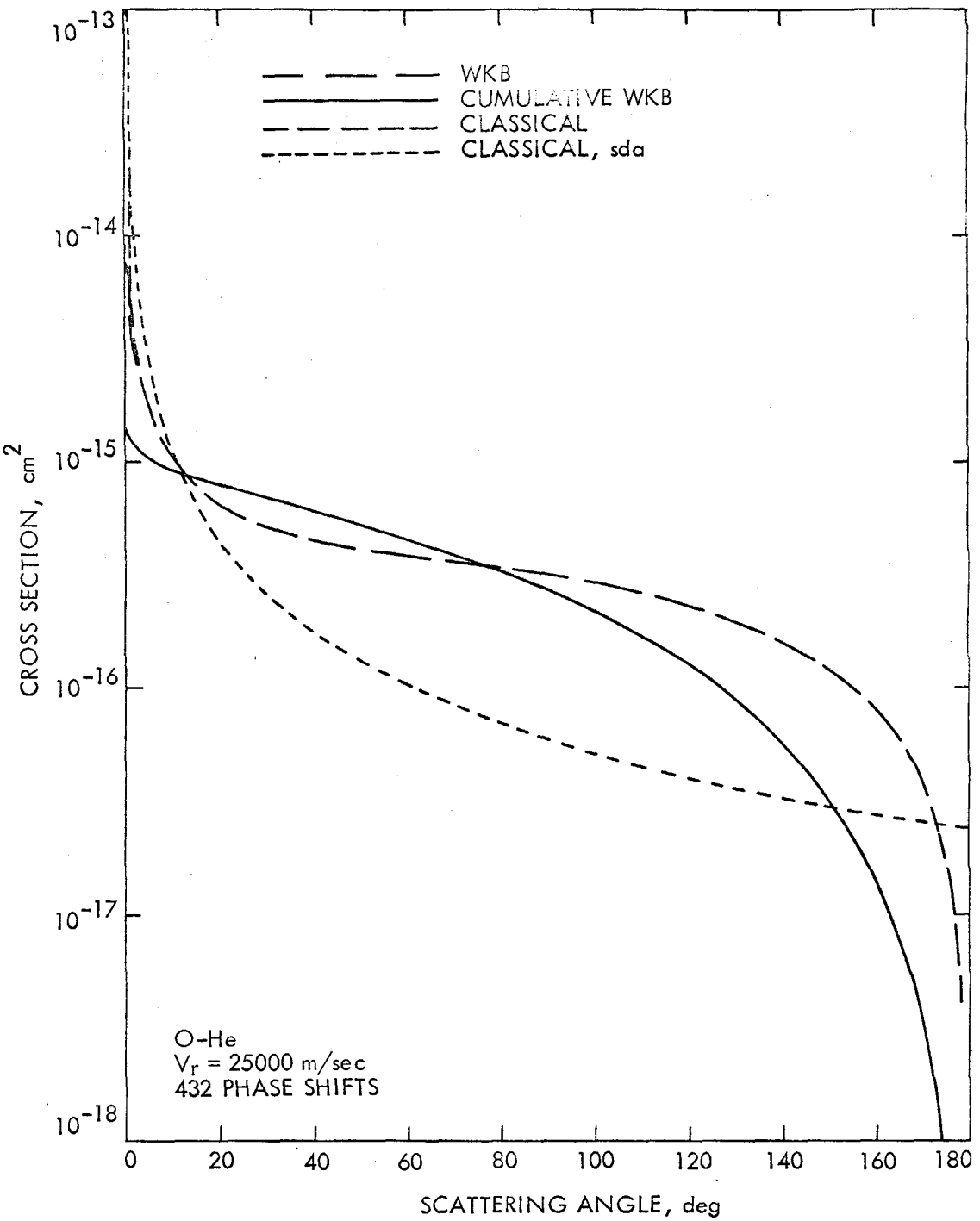
WKB
CUMULATIVE WKB
CLASSICAL
CLASSICAL, sda
10^{-13}
10^{-14}
10^{-15}
10^{-16}
10^{-17}
10^{-18}
CROSS SECTION, cm^2
O-He
V_r = 25000 m/sec
432 PHASE SHIFTS
0
20
40
60
80
100
120
140
160
180
SCATTERING ANGLE, deg

Figure 34

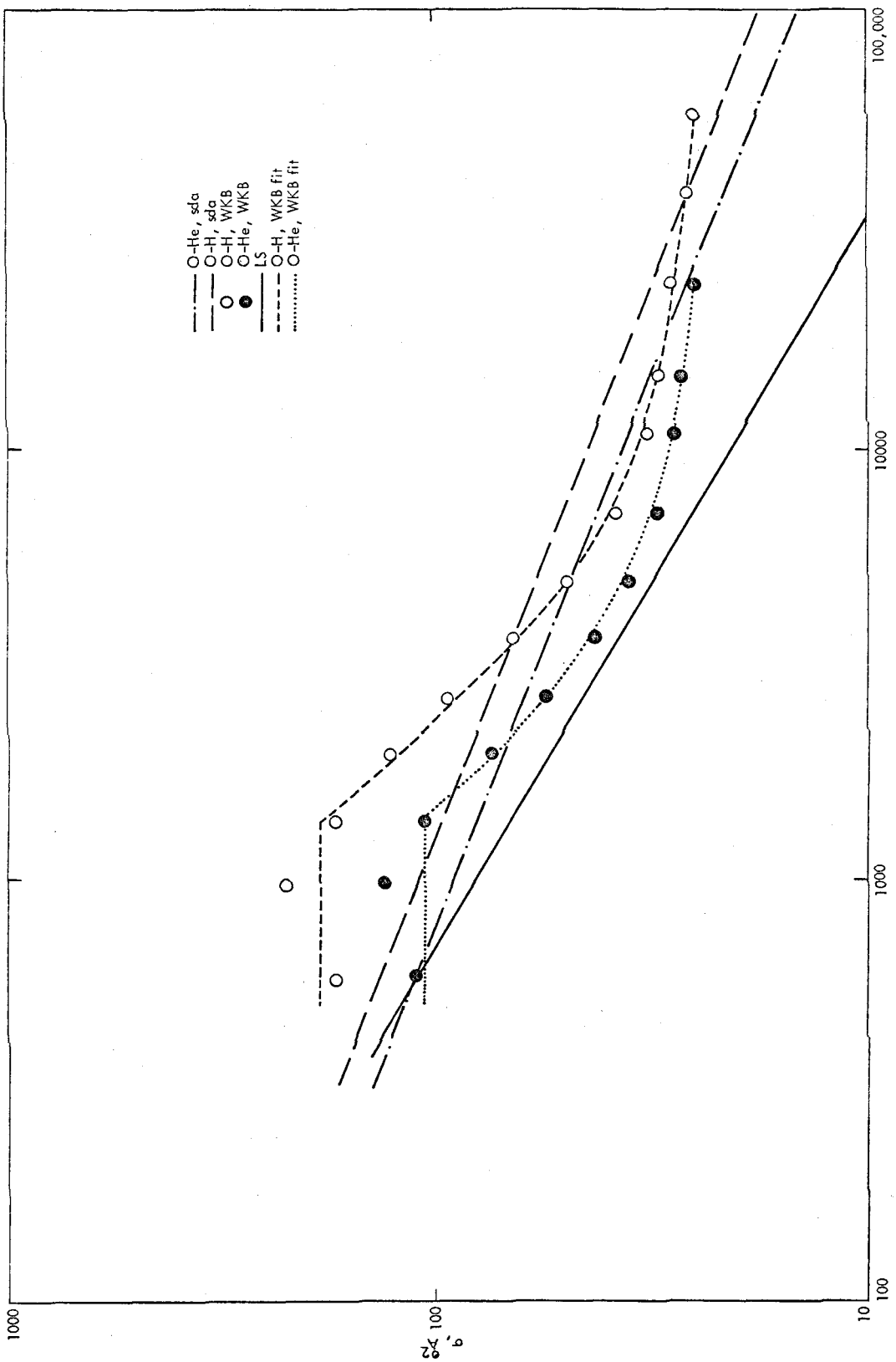
O-He, sda
O-H, sda
O-H, WKB
O-He, WKB
LS
O-H, WKB fit
O-He, WKB fit
$q, \AA^2$
1000
100
10
100
1000
10000
100,000
VELOCITY, m/sec

Figure 35

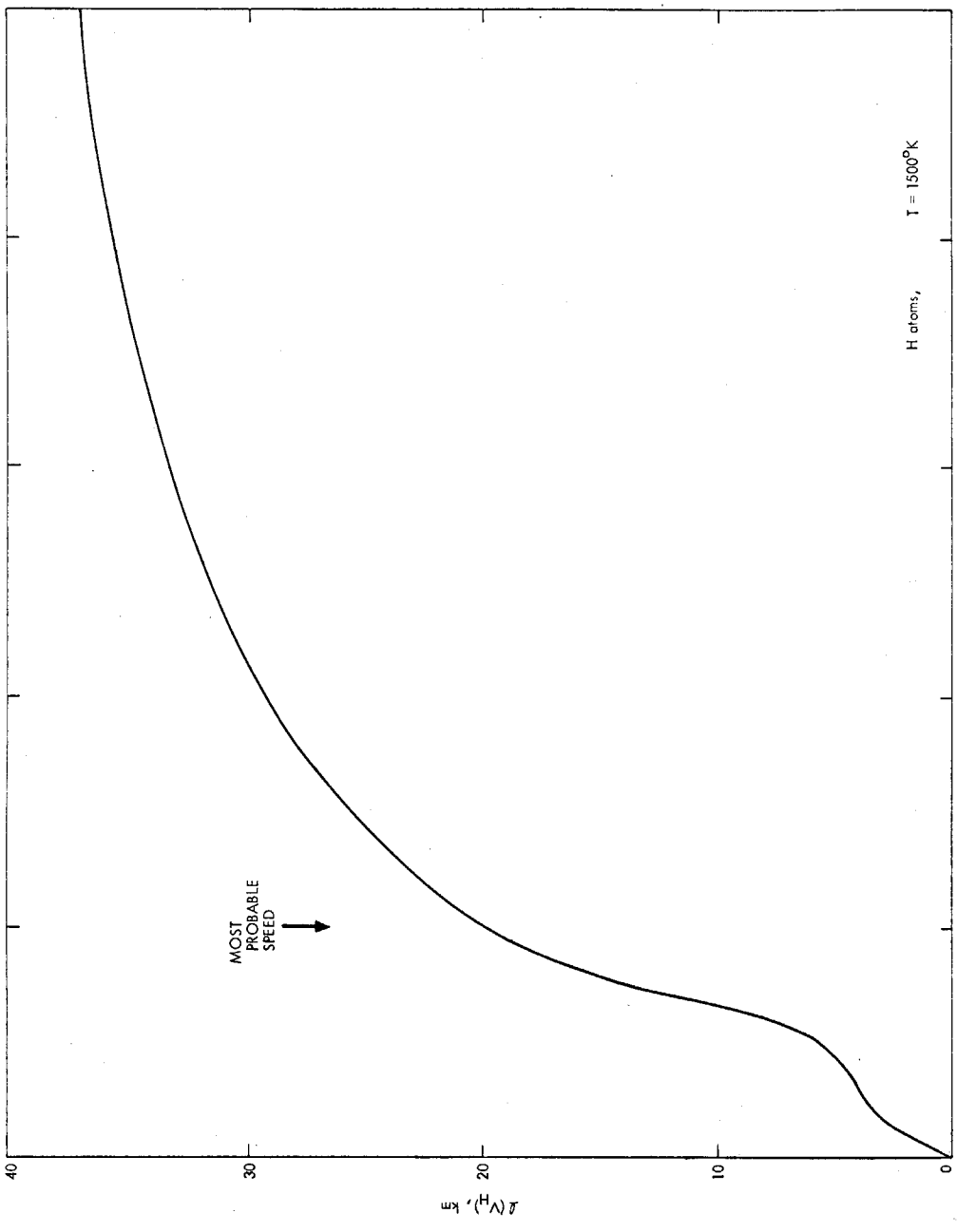
MOST PROBABLE SPEED
H atoms, T = 1500°K
$\sqrt{\frac{m}{2kT}} \cdot v_H$
$\phi(v_H)$, k

Figure 36

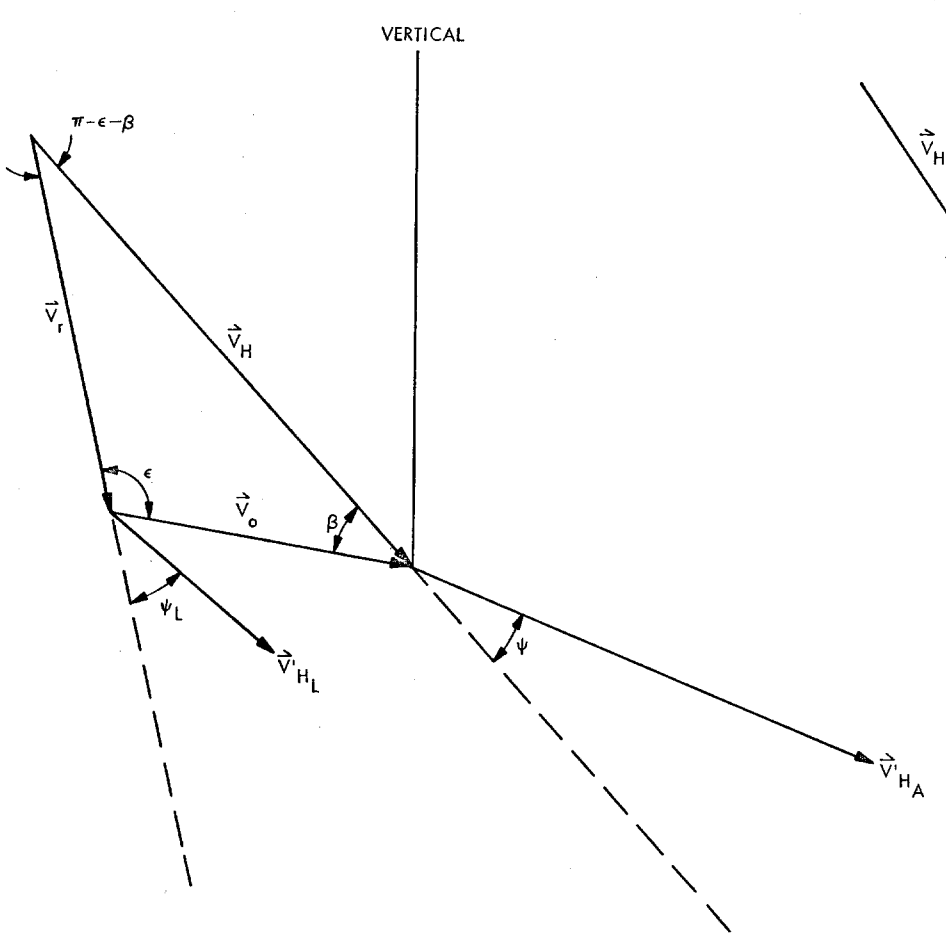
VERTICAL
$\pi-\epsilon-\beta$
$\vec{V}_r$
$\vec{V}_H$
ϵ
$\vec{V}_o$
β
ψ_L
$\vec{V}'_{H_L}$
ψ
$\vec{V}'_{H_A}$

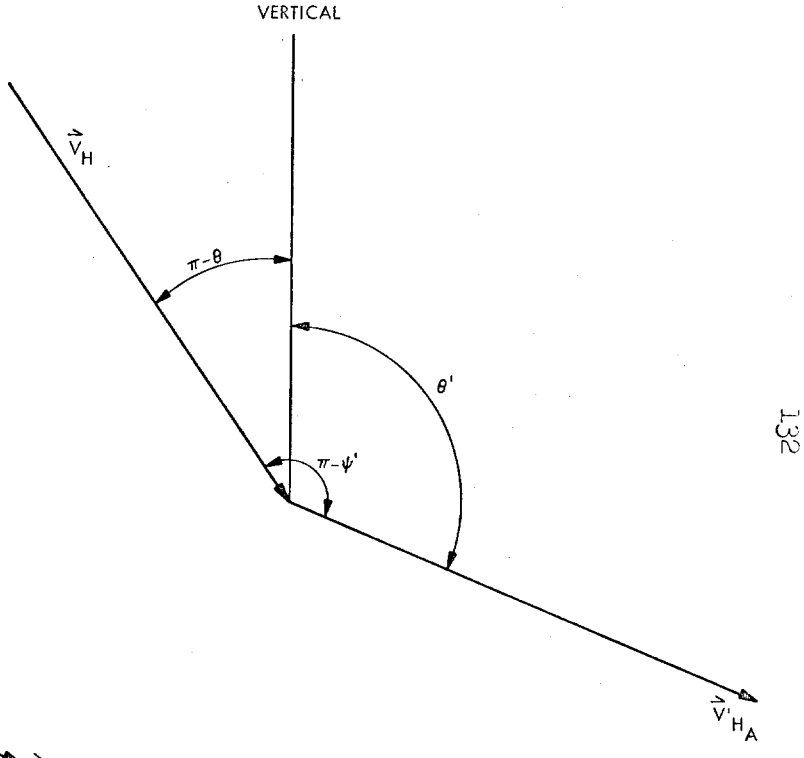
VERTICAL
$\vec{V}_H$
$\pi-\theta$
θ'
$\pi-\psi'$
$\vec{V}'_{H_A}$

Figure 37

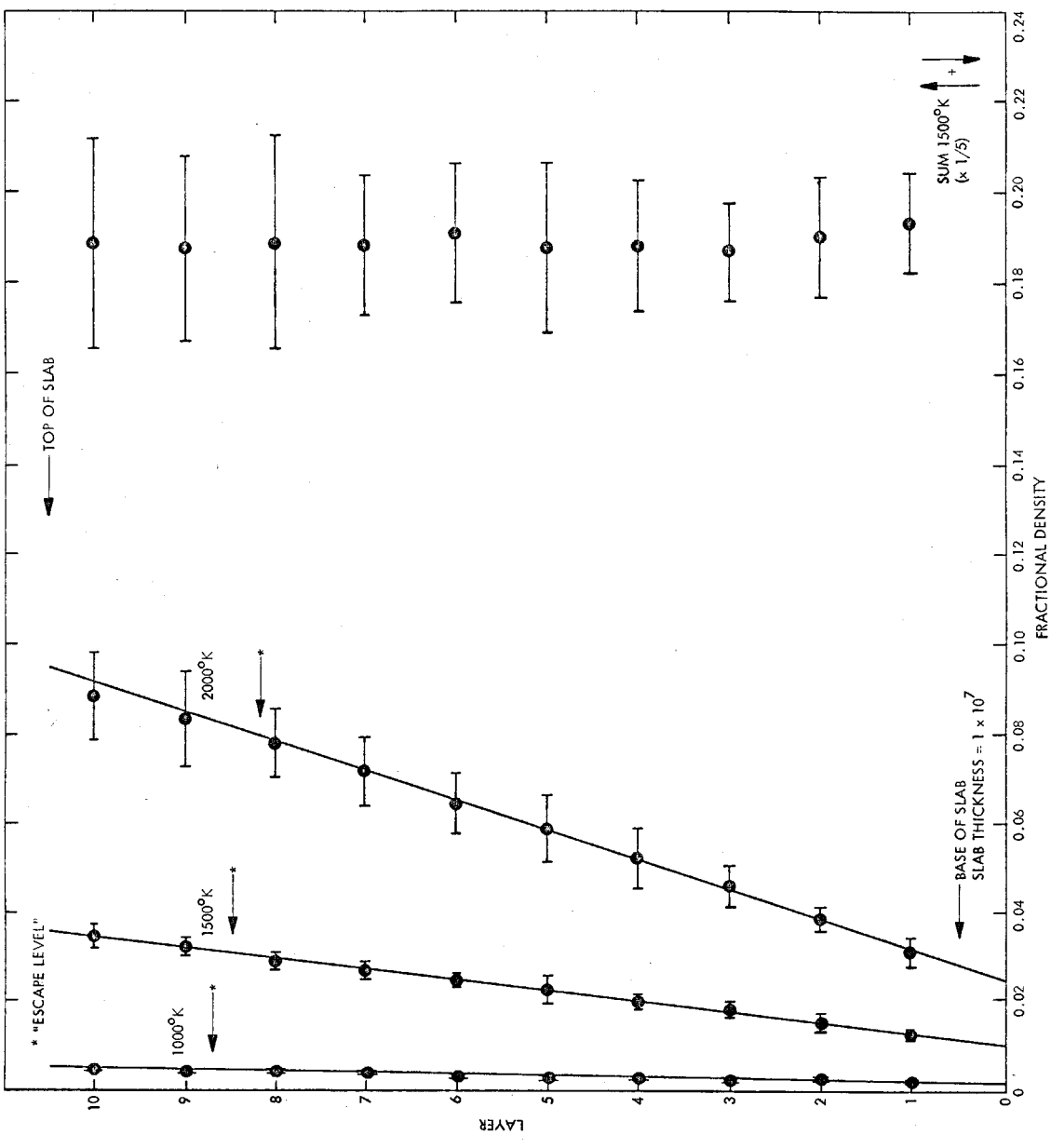
TOP OF SLAB
BASE OF SLAB
SLAB THICKNESS = 1 × 10^7
* "ESCAPE LEVEL"
1000°K
1500°K
2000°K
SUM 1500°K (× 1/5)
LAYER
FRACTIONAL DENSITY
0
0.02
0.04
0.06
0.08
0.10
0.12
0.14
0.16
0.18
0.20
0.22
0.24
1
2
3
4
5
6
7
8
9
10

Figure 38

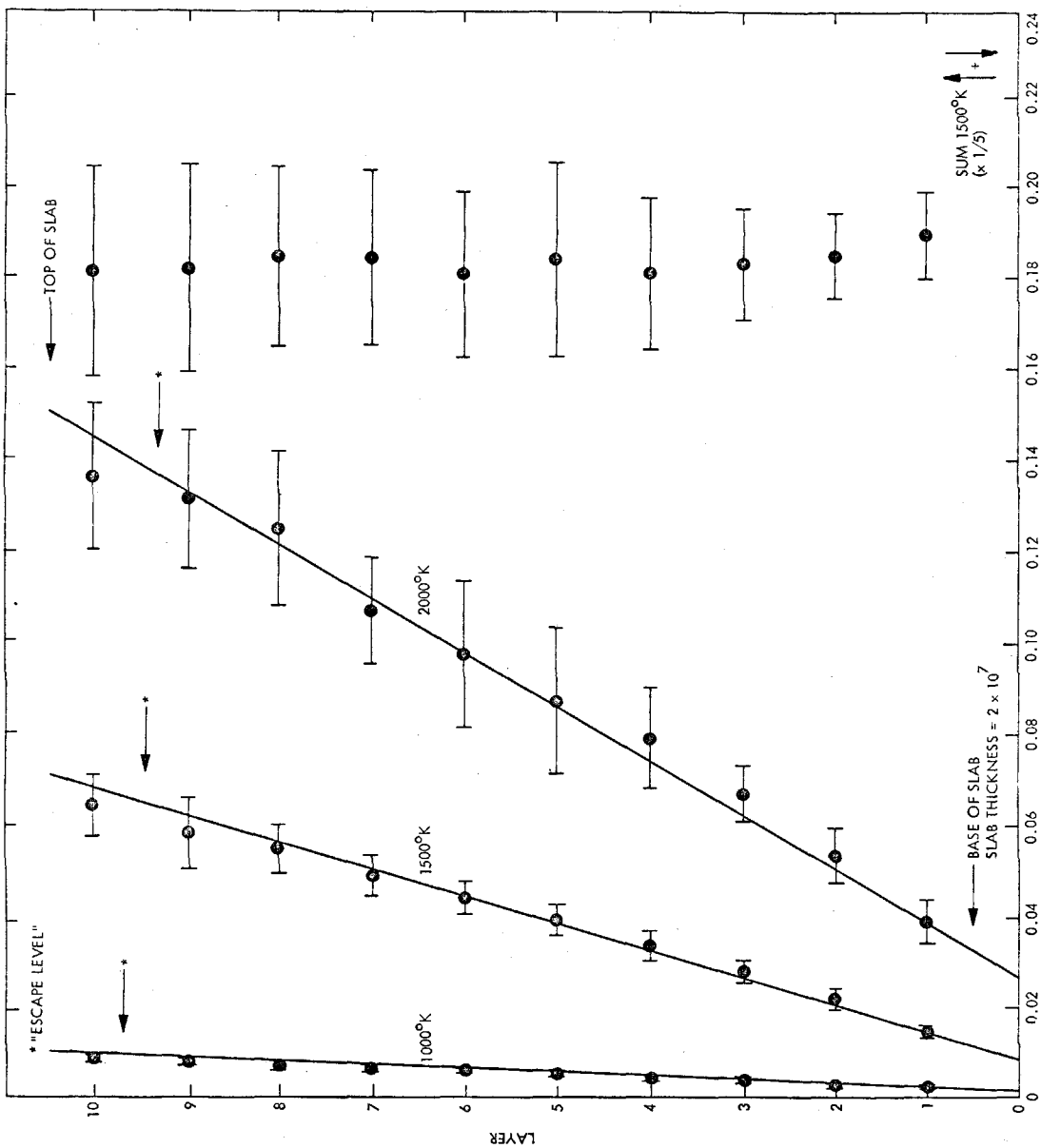
TOP OF SLAB
* "ESCAPE LEVEL"
2000°K
1500°K
1000°K
BASE OF SLAB
SLAB THICKNESS = 2 × 10^7
SUM 1500°K (× 1/5)
LAYER
FRACTIONAL DENSITY
0
0.02
0.04
0.06
0.08
0.10
0.12
0.14
0.16
0.18
0.20
0.22
0.24
1
2
3
4
5
6
7
8
9
10

Figure 39

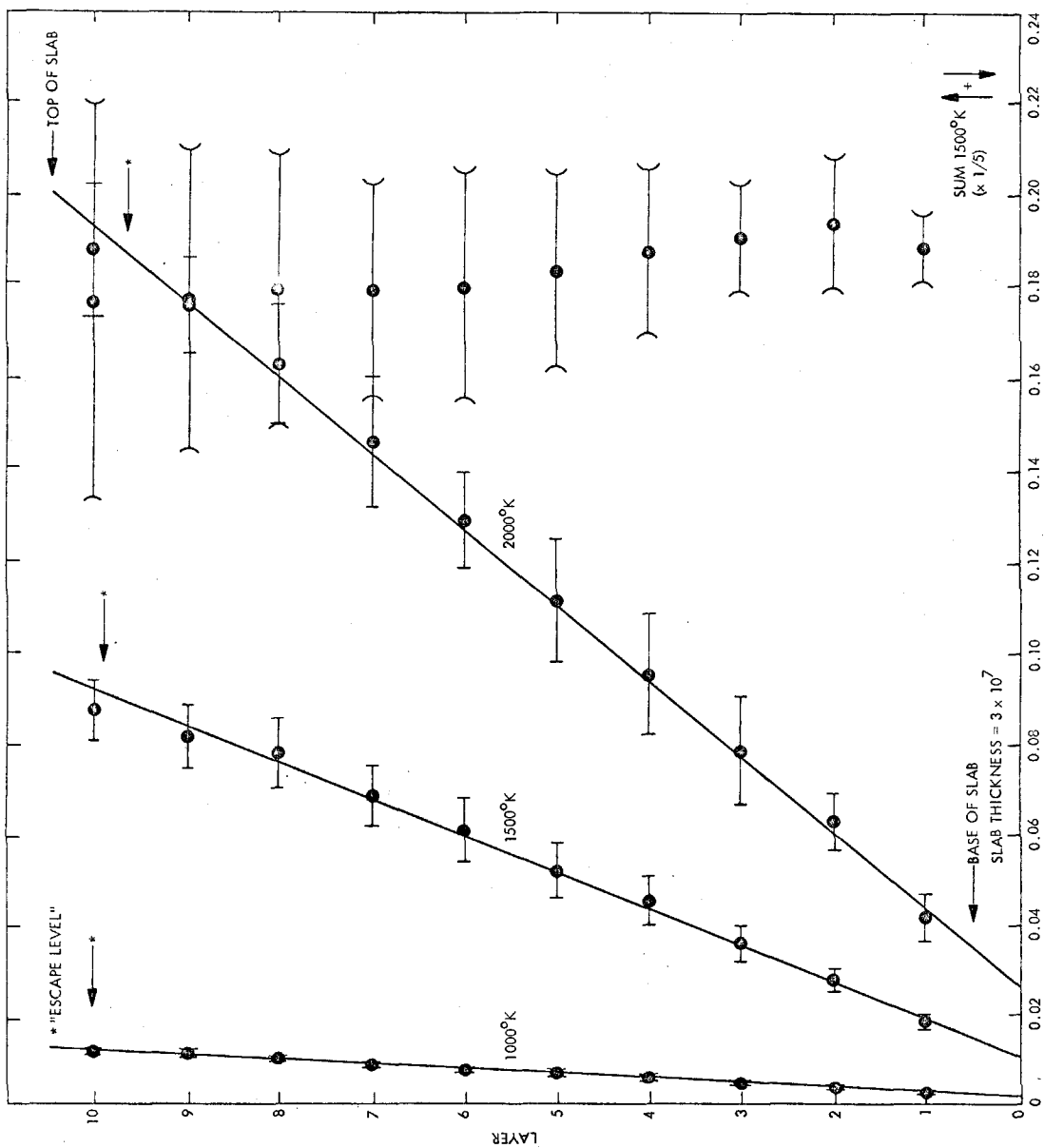
TOP OF SLAB
* "ESCAPE LEVEL"
2000°K
1500°K
1000°K
BASE OF SLAB
SLAB THICKNESS = 3 x 10^7
SUM 1500°K (x 1/5)
LAYER
FRACTIONAL DENSITY
0
1
2
3
4
5
6
7
8
9
10
0.02
0.04
0.06
0.08
0.10
0.12
0.14
0.16
0.18
0.20
0.22
0.24

Figure 40

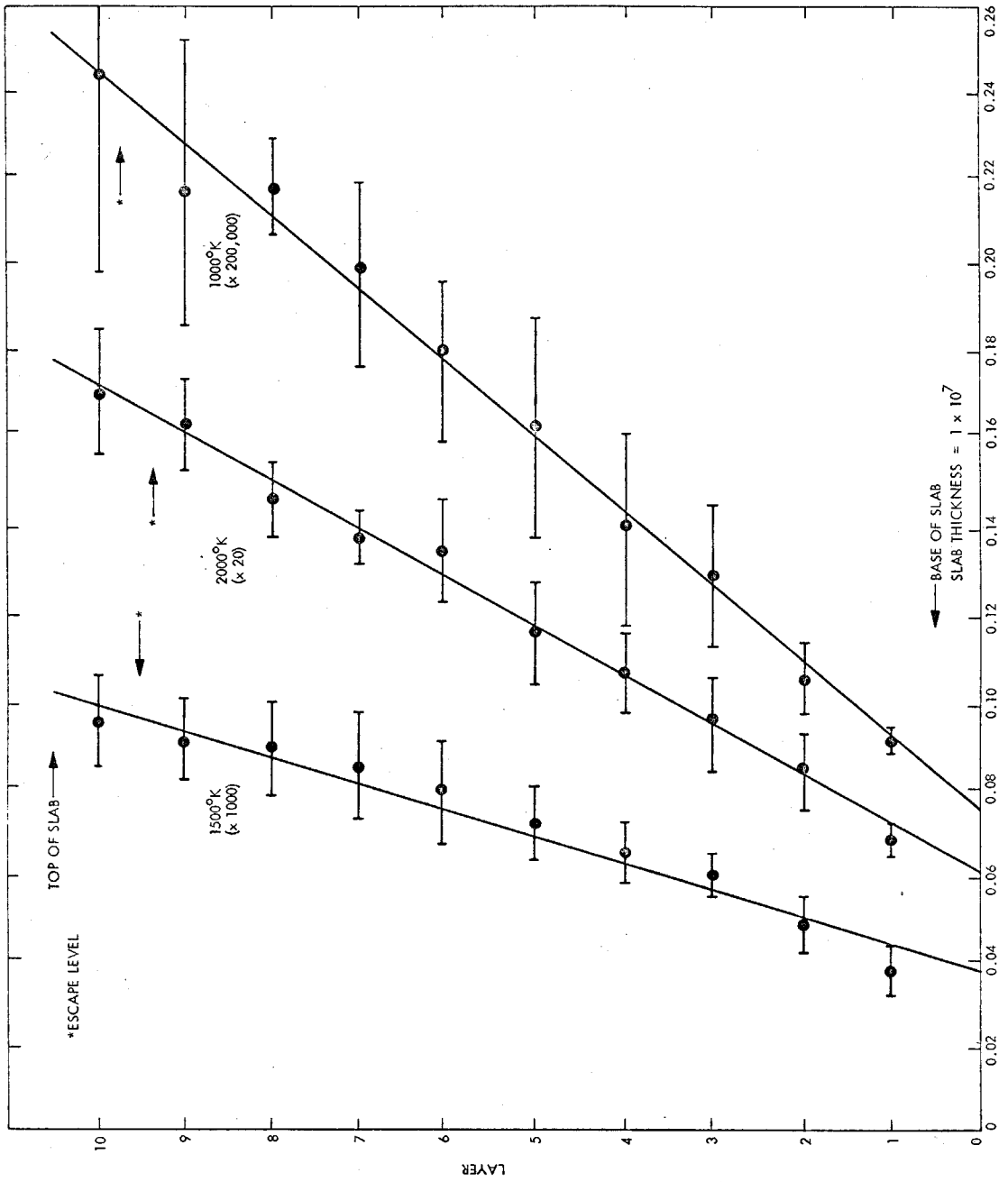
TOP OF SLAB
*ESCAPE LEVEL
1500°K (x 1000)
2000°K (x 20)
1000°K (x 200,000)
BASE OF SLAB
SLAB THICKNESS = 1 x 10^7
LAYER
FRACTIONAL DENSITY
0
1
2
3
4
5
6
7
8
9
10
0.02
0.04
0.06
0.08
0.10
0.12
0.14
0.16
0.18
0.20
0.22
0.24
0.26

Figure 41

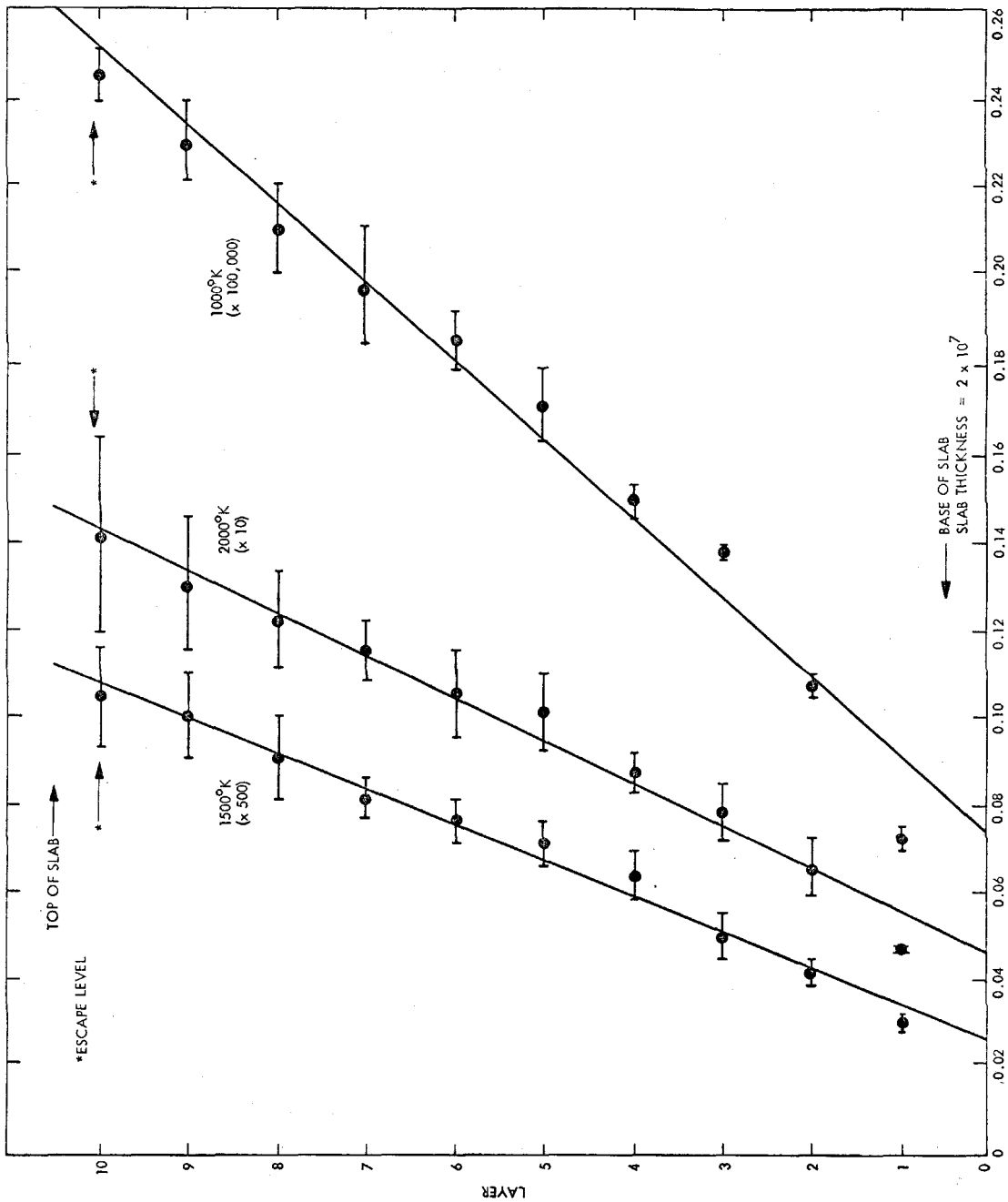
1000°K
(x 100,000)
2000°K
(x 10)
1500°K
(x 500)
TOP OF SLAB
*ESCAPE LEVEL
BASE OF SLAB
SLAB THICKNESS = 2 x 10^7
LAYER
FRACTIONAL DENSITY
0
1
2
3
4
5
6
7
8
9
10
.02
0.04
0.06
0.08
0.10
0.12
0.14
0.16
0.18
0.20
0.22
0.24
0.26

Figure 42

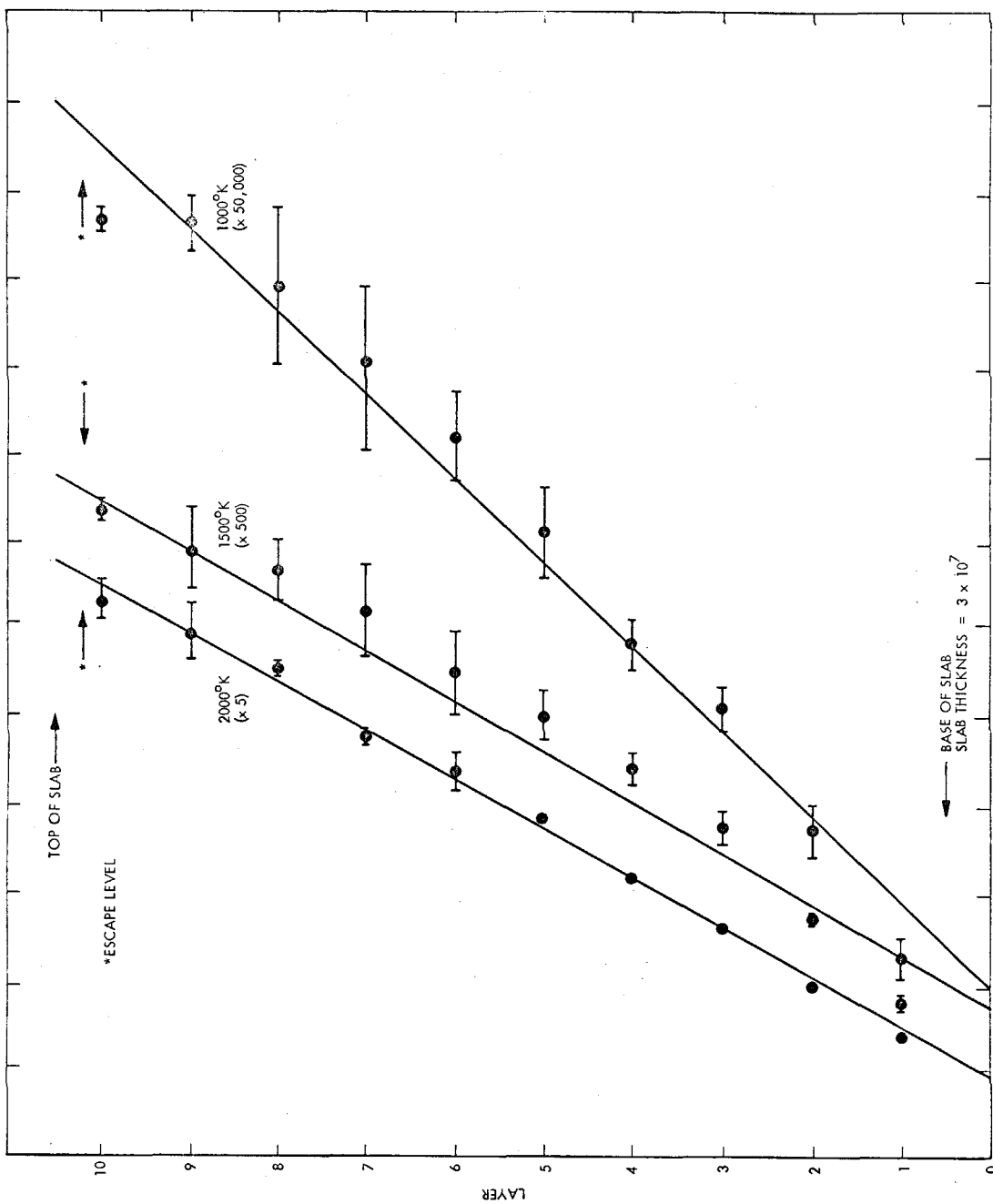
TOP OF SLAB
*ESCAPE LEVEL
2000°K (x 5)
1500°K (x 500)
1000°K (x 50,000)
BASE OF SLAB
SLAB THICKNESS = 3 x 10^7
LAYER
FRACTIONAL DENSITY
0
1
2
3
4
5
6
7
8
9
10
0.02
0.04
0.06
0.08
0.10
0.12
0.14
0.16
0.18
0.20
0.22
0.24
0.26

Figure 43

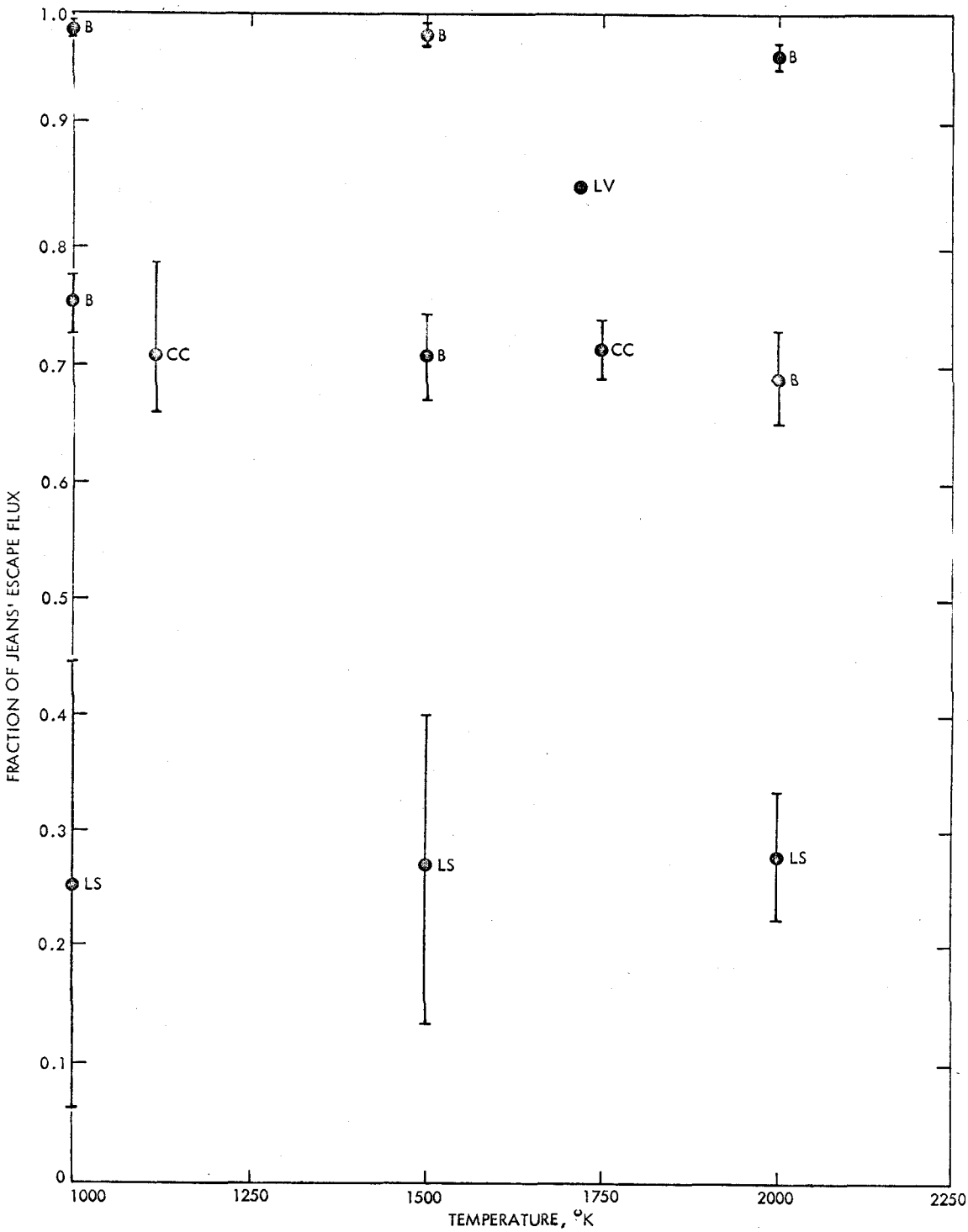
1.0
0.9
0.8
0.7
0.6
0.5
0.4
0.3
0.2
0.1
0
B
B
B
LV
B
CC
B
CC
B
LS
LS
LS
1000
1250
1500
1750
2000
2250
FRACTION OF JEANS' ESCAPE FLUX
TEMPERATURE, °K

Figure 44

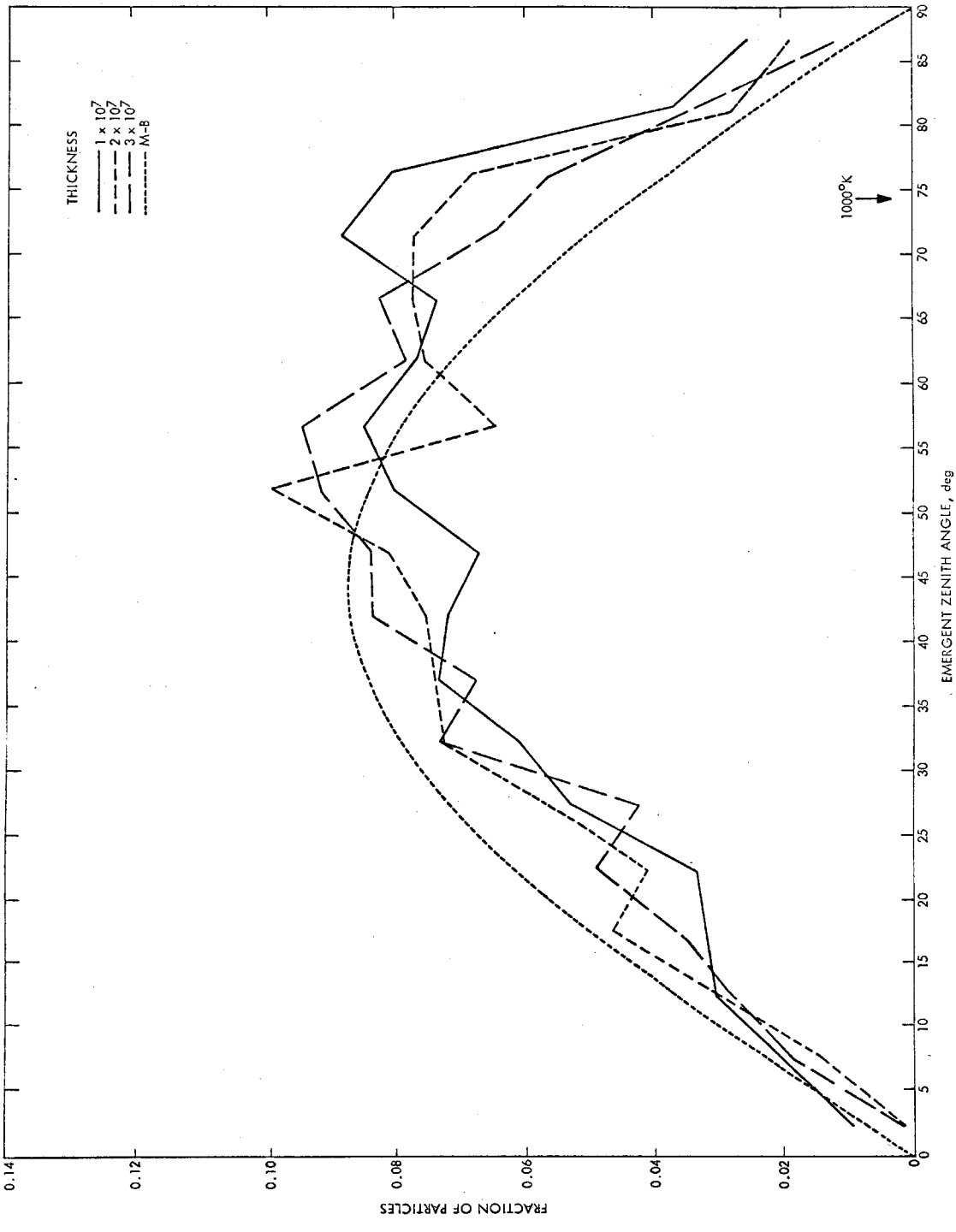
THICKNESS
1 × 10⁷
2 × 10⁷
3 × 10⁷
M-B
1000°K
FRACTION OF PARTICLES
EMERGENT ZENITH ANGLE, deg
0.14
0.12
0.10
0.08
0.06
0.04
0.02
0
0
5
10
15
20
25
30
35
40
45
50
55
60
65
70
75
80
85
90

Figure 45

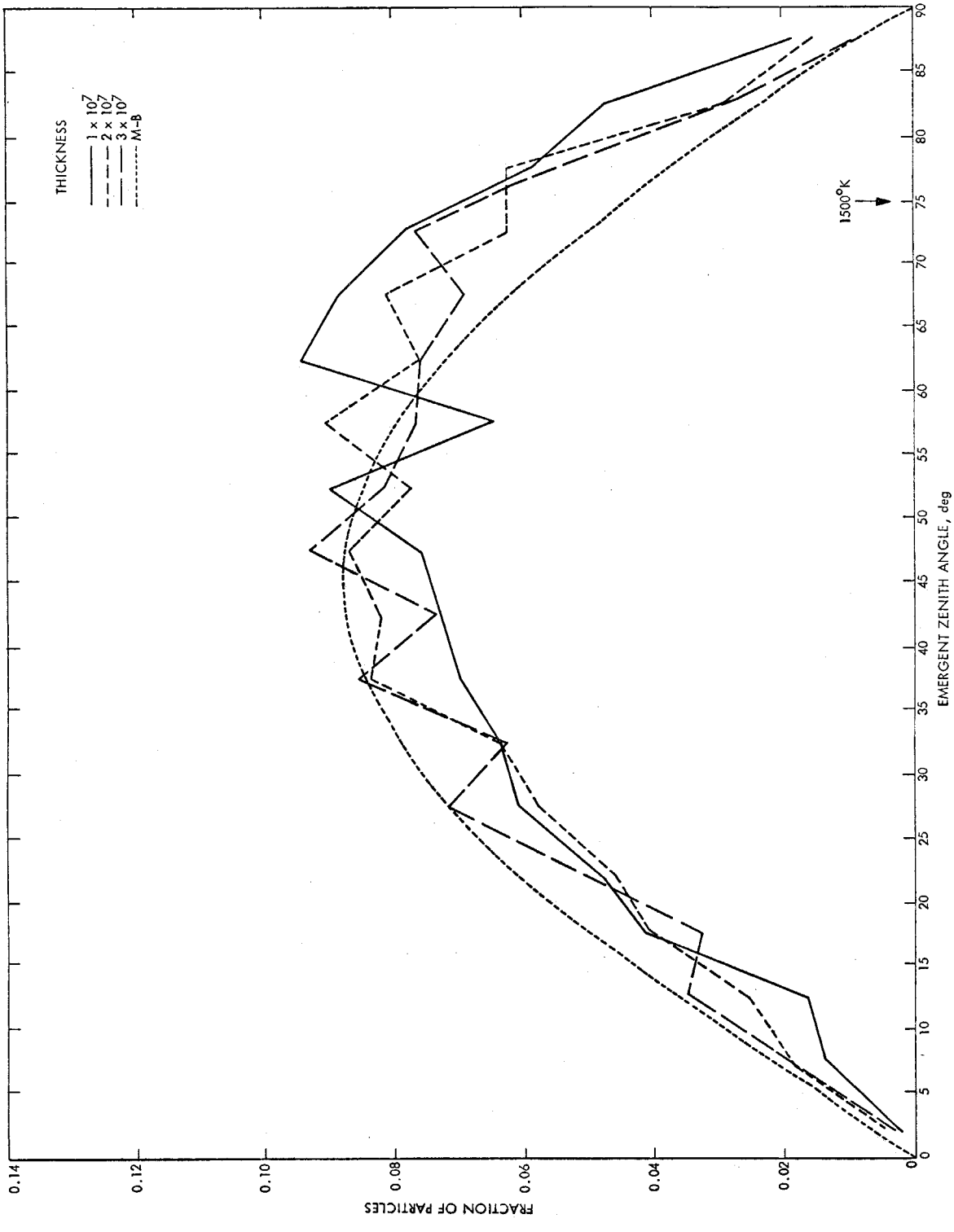
THICKNESS
1 × 10^7
2 × 10^7
3 × 10^7
M-B
1500°K
FRACTION OF PARTICLES
EMERGENT ZENITH ANGLE, deg
0.14
0.12
0.10
0.08
0.06
0.04
0.02
0
5
10
15
20
25
30
35
40
45
50
55
60
65
70
75
80
85
90

Figure 46

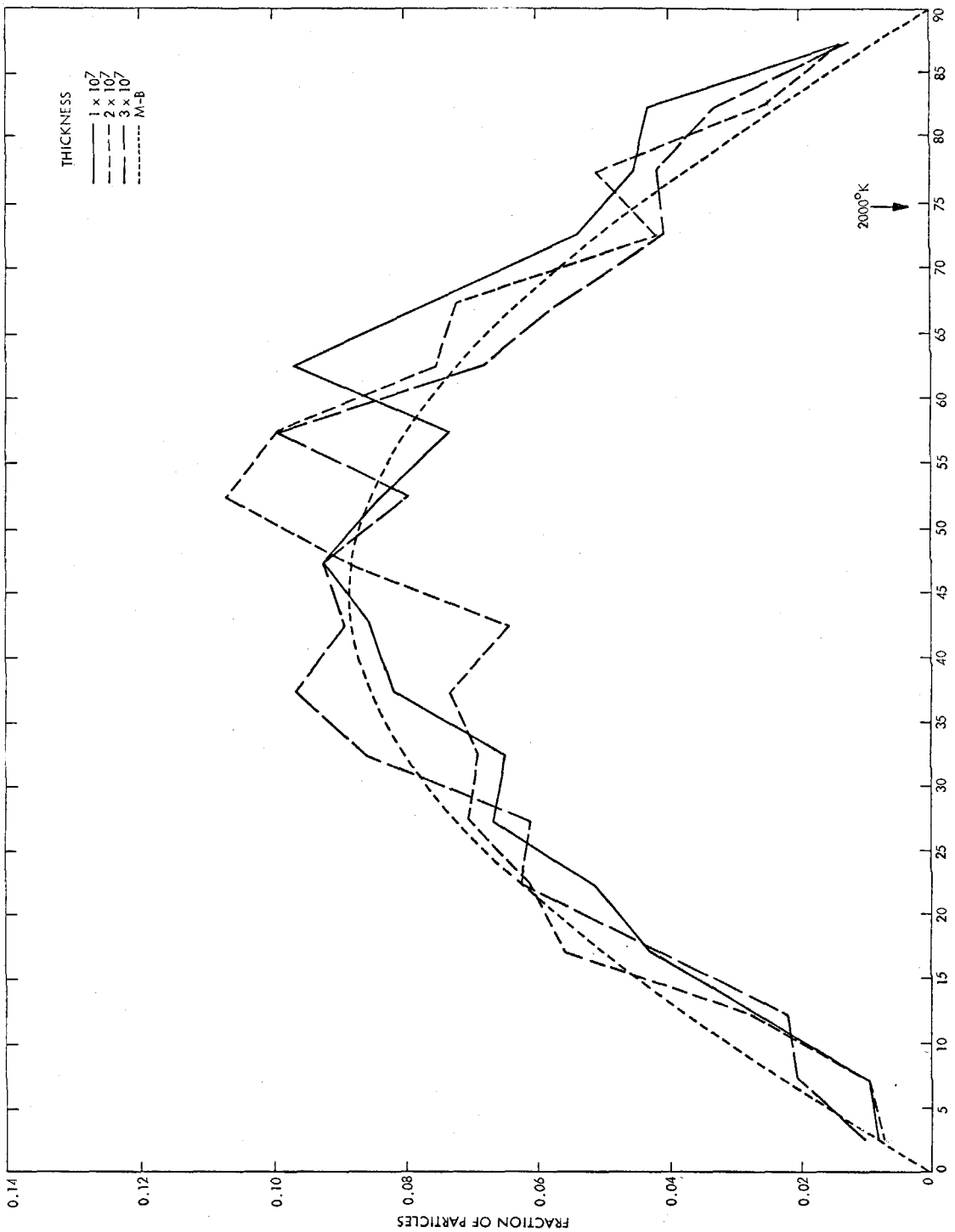
THICKNESS
1 × 10^7
2 × 10^7
3 × 10^7
M-B
2000°K
FRACTION OF PARTICLES
0.14
0.12
0.10
0.08
0.06
0.04
0.02
0
0
5
10
15
20
25
30
35
40
45
50
55
60
65
70
75
80
85
90
EMERGENT ZENITH ANGLE, deg

Figure 47

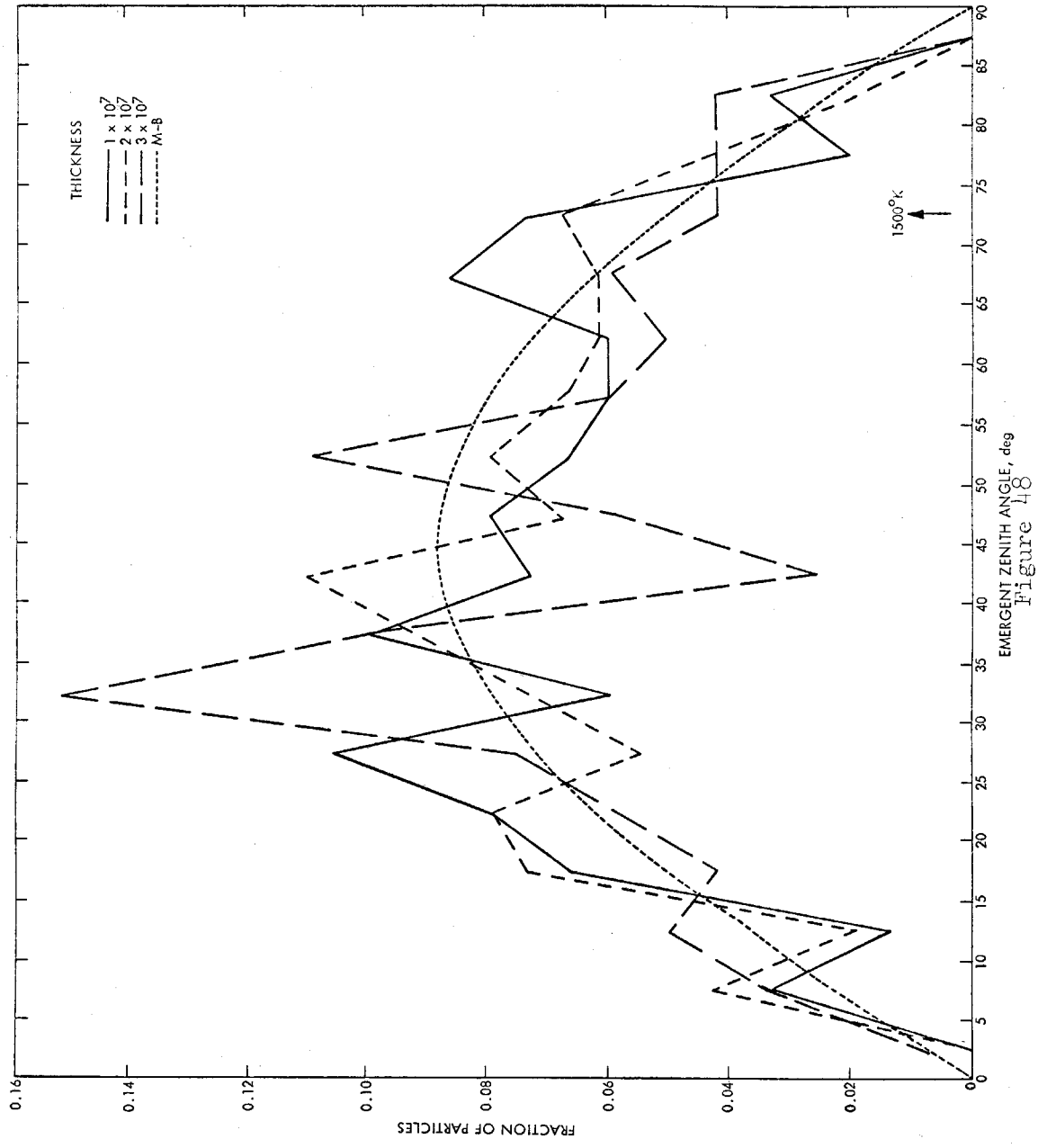
THICKNESS
1 × 10⁷
2 × 10⁷
3 × 10⁷
M-B
1500°K
FRACTION OF PARTICLES
EMERGENT ZENITH ANGLE, deg
0.16
0.14
0.12
0.10
0.08
0.06
0.04
0.02
0
5
10
15
20
25
30
35
40
45
50
55
60
65
70
75
80
85
90

Figure 18

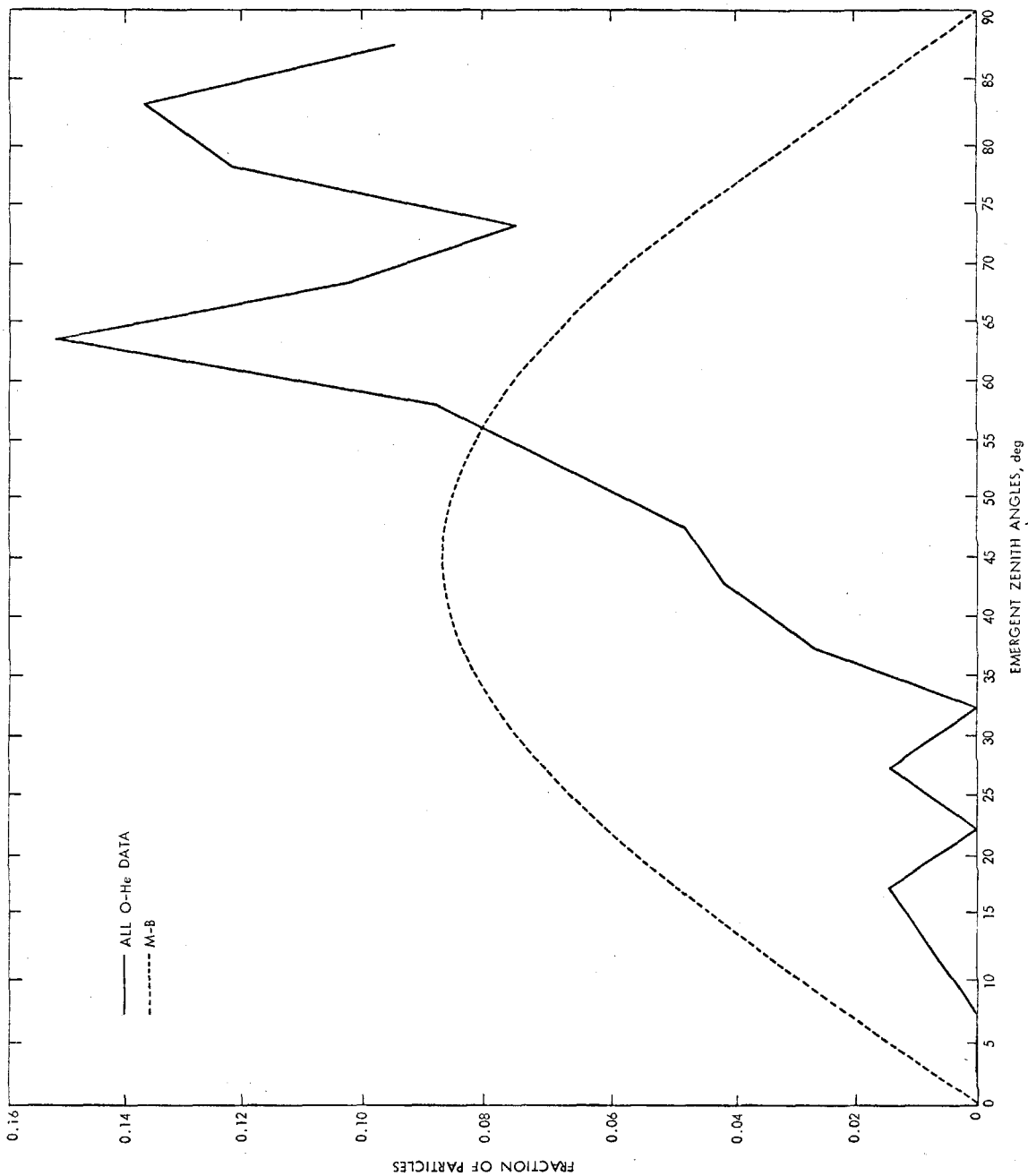
ALL O-He DATA
M-B
FRACTION OF PARTICLES
0.16
0.14
0.12
0.10
0.08
0.06
0.04
0.02
0
5
10
15
20
25
30
35
40
45
50
55
60
65
70
75
80
85
90
EMERGENT ZENITH ANGLES, deg

Figure 49

```
      DIMENSION IAESC(18),DENS(10),T1(101),T3(51,51),T4(13,101),DV(12),T
     15(51)
      READ (5,17) IR1
      IR2=23
      IR3=10**8-1
      READ (5,17) NUMB
      READ (5,85) ((T4(I,J),J=1,101),I=1,NUMB)
    8 READ (5,85) ((T3(I,J),J=1,51),I=1,51),(T5(I),I=1,51)
   85 FORMAT (F12.2)
      READ (5,10) A,IA,B,IB,C,IC,D,ID
   10 FORMAT (4(F10.2,I10))
      A=A*10.**IA
      B=B*10.**IB
      C=C*10.**IC
      D=D*10.**ID
      READ (5,17) MH,MO
   17 FORMAT (2I10)
      AMH=MH
      AMH=AMH*1.66*10.**(-24)
      AMHR=AMH*10.**30
      AMO=MO
      AMO=AMO*1.66*10.**(-24)
    6 READ (5,85) DSTOP
      DO 22 I=1,10
   22 DENS(I)=0.
      DO 30 I=1,18
   30 IAESC(I)=0
      READ (5,85) T
      IF (T) 8,8,9
    9 READ (5,17) M
      READ (5,17) IZ,IY
      IF (IZ) 520,520,521
  520 READ (5,85) (T1(I),I=1,101)
```

```
521 NESC=0
    NDMN=0
    PI=3.14159265
    AK=1.38044*10.**(-16)
    CON1=2.*AK*T/AMH
    CON2=5.*10.**(-7)
    CON3=10.**(-8)
    CON4=10.**(-6)
    CON5=2.*PI*10.**(-8)
    D1=140000.**3
    D2=140000.**2
    D3=D/3.
    D4=A/2.
    D5=C/3.
    D6=3./D
    D7=3./C
    D8=D4*D2+B*140000.+D5*D1
    D9=10./SQRT(CON1)
    D10=2./27.
    D11=1./27.
    D12=AMH/AMO
    D13=D4*D7
    D14=B*D7
    D15=D7*.000001
    D16=-2.*AMHR*AMH
    D17=AMHR*(AMH-AMO)
    D18=2.*AMO
    D19=-2.*AMHR
    CUB2=D4*D7*.01
    CUB3=B*D7*.0001
    DS10=10./DSTOP
    DS01=DSTOP/10.
    VESC=10.785*10.**5
```

```
      PIP=PI/180.
      PIPER=.2*180./PI
      DV(1)=40000.
      DV(2)=40000.
      DV(3)=60000.
      DV(4)=70000.
      DV(5)=100000.
      DV(6)=130000.
      DV(7)=220000.
      DV(8)=330000.
      DV(9)=400000.
      DV(10)=1000000.
      DV(11)=1500000.
      DV(12)=2000000.
      C1=(AMH+AMO)*AMHR
      C4=4.*C1
      C5=2.*C1
        IF (IY) 522,523,523
  522 DHOLD=0.
      CHOLD=1.
        GO TO 524
  523 DHOLD=OSTUP
      CHOLD=-1.
  524 DO 11 I=1,N
        IR1=IR1*IR2
      ARNDM=RND(IR1,IR3)
      ARNDM=ARNDM*CON4
      IRNDM=ARNDM
      AHOLD=IRNDM
      AHOLD=ARNDM-AHOLD
      AHOLD=T1(IRNDM+1)+AHOLD*(T1(IRNDM+2)-T1(IRNDM+1))
      VH=SQRT(AHOLD*CON1)
      IR1=IR1*IR2
```

```
      ARNDM=MOD(IR1,IR3)
      ARNDM=ARNDM*COM3
      CALP=SIGN(SQRT(ARNDM),CHOLD)
      SALP=SQRT(1.-CALP**2)
      DEPTH=DHOLD
   83 VHT=VH*D9+1.
      IF (VHT-51.) 200,200,201
  201 FRPTH=T5(51)
      GO TO 202
  200 IHOLD=VHT
      AHOLD=IHOLD
      FRPTH=T5(IHOLD)+(VHT-AHOLD)*(T5(IHOLD+1)-T5(IHOLD))
  202 IR1=IR1*IR2
      ARNDM=MOD(IR1,IR3)
      ARNDM=ARNDM*COM3
      DIST=-ALOG(ARNDM)*FRPTH
      TEST=DEPTH+DIST*CALP
      VALP=VH*CALP
      IF (TEST-DSTOP) 20,21,21
   21 IHOLD=DEPTH*DS10+1.
      AHOLD=DS01/ABS(VALP)
      AHOLD2=IHOLD
      DENS(IHOLD)=DENS(IHOLD)+AHOLD*(AHOLD2*DS01-DEPTH)*DS10
      IHOLD2=IHOLD+1
      IF (IHOLD2-11) 25,24,23
   23 WRITE (6,26)
   26 FORMAT (14H ERROR STEP 26)
      GO TO 11
   25 DO 27 J=IHOLD2,10
   27 DENS(J)=DENS(J)+AHOLD
   24 IF (VESC-VH) 28,28,29
   28 NESC=NESC+1
      IHOLD=ARCOS(CALP)*PIPER+1.
```

```
    IAESC(IHOLD)=IAESC(IHOLD)+1
    GO TO 11
29  CALP=-CALP
    TEST=DSTOP-TEST+DSTOP
    IHOLD=TEST*DS10+1.
    IF (IHOLD-10) 33,32,31
31  WRITE (6,34)
34  FORMAT (14H ERROR STEP 31)
    GO TO 11
33  IF (IHOLD-1) 5,7,7
 5  DO 4 J=1,10
 4  DENS(J)=DENS(J)+AHOLD
    NDWN=NDWN+1
    GO TO 11
 7  IHOLD2=IHOLD+1
    DO 35 J=IHOLD2,10
35  DENS(J)=DENS(J)+AHOLD
32  AHOLD2=IHOLD
    DENS(IHOLD)=DENS(IHOLD)+AHOLD*(AHOLD2*DS01-TEST)*DS10
    GO TO 36
20  AHOLD=DS01/ABS(VALP)
    IF (TEST) 37,37,38
37  IHOLD=DEPTH*DS10
    AHOLD2=IHOLD
    DENS(IHOLD+1)=DENS(IHOLD+1)+AHOLD*(DEPTH-AHOLD2*DS01)*DS10
    IF (IHOLD) 1,2,3
 1  WRITE (6,12)
12  FORMAT (14H ERROR STEP 12)
    GO TO 11
 3  DO 39 J=1,IHOLD
39  DENS(J)=DENS(J)+AHOLD
 2  NDWN=NDWN+1
    GO TO 11
```

```
 38 IHOLD3=DEPTH*DS10
    IHOLD2=TEST*DS10
    IF (DEPTH-TEST) 204,205,206
205 WRITE (6,207) I
207 FORMAT (15H ERROR STEP 207,I10)
    GO TO 36
204 AHOLD2=IHOLD2
    AHOLD3=IHOLD3+1
    IF (AHOLD2-AHOLD3) 208,209,210
208 DENS(IHOLD2+1)=DENS(IHOLD2+1)+AHOLD*(TEST-DEPTH)*DS10
    GO TO 36
209 AHOLD4=AHOLD2*DS01
    DENS(IHOLD2)=DENS(IHOLD2)+AHOLD*(AHOLD4-DEPTH)*DS10
    DENS(IHOLD2+1)=DENS(IHOLD2+1)+AHOLD*(TEST-AHOLD4)*DS10
    GO TO 36
210 DENS(IHOLD2+1)=DENS(IHOLD2+1)+AHOLD*(TEST-AHOLD2*DS01)*DS10
    DENS(IHOLD3+1)=DENS(IHOLD3+1)+AHOLD*(AHOLD3*DS01-DEPTH)*DS10
    IHOLD4=IHOLD3+2
    DO 211 J=IHOLD4,IHOLD2
211 DENS(J)=DENS(J)+AHOLD
    GO TO 36
206 AHOLD2=IHOLD3
    AHOLD3=IHOLD2+1
    IF (AHOLD2-AHOLD3) 212,213,214
212 DENS(IHOLD3+1)=DENS(IHOLD3+1)+AHOLD*(DEPTH-TEST)*DS10
    GO TO 36
213 AHOLD4=AHOLD2*DS01
    DENS(IHOLD3)=DENS(IHOLD3)+AHOLD*(AHOLD4-TEST)*DS10
    DENS(IHOLD3+1)=DENS(IHOLD3+1)+AHOLD*(DEPTH-AHOLD4)*DS10
    GO TO 36
214 DENS(IHOLD3+1)=DENS(IHOLD3+1)+AHOLD*(DEPTH-AHOLD2*DS01)*DS10
    DENS(IHOLD2+1)=DENS(IHOLD2+1)+AHOLD*(AHOLD3*DS01-TEST)*DS10
    IHOLD4=IHOLD2+2
```

```
      DO 215 J=IHOLD4,IHOLD3
  215 DENS(J)=DENS(J)+AHOLD
   36 DEPTH=TEST
      IR1=IR1*IR2
      ARNDM=MOD(IR1,IR3)
      ARNDM=ARNDM*CON2
      AHOLD2=ARNDM+1.
      AHOLD=VMT
      IF (AHOLD-51.) 216,217,217
  217 AHOLD=51.
  216 IHOLD=AHOLD
      IHOLD2=AHOLD2
      AHOLD3=IHOLD
      AHOLD4=IHOLD2
      VO1=T3(IHOLD,IHOLD2)+(AHOLD2-AHOLD4)*(T3(IHOLD,IHOLD2+1)-T3(IHOLD,
     1IHOLD2))
      VO2=T3(IHOLD+1,IHOLD2)+(AHOLD2-AHOLD4)*(T3(IHOLD+1,IHOLD2+1)-T3(IH
     1OLD+1,IHOLD2))
      VO=VO1+(AHOLD-AHOLD3)*(VO2-VO1)
      V1=VH+VO
      V2=ABS(VH-VO)
      IR1=IR1*IR2
      ARNDM=MOD(IR1,IR3)
      ARNDM=ARNDM*CON3
      IF (V2-140000.) 13,14,14
   13 IF (V1-140000.) 218,219,219
  218 VR=(ARNDM*V1**3+(1.-ARNDM)*V2**3)**.33333333
      GO TO 220
  219 V23=V2**3
      V12=V1**2
      V13=V1**3
      AHOLD=D3*(D1-V23)
      DENOM=(AHOLD+D4*(V12-D2)+B*(V1-140000.)+D5*(V13-D1))*ARNDM
```

```
      IF (AHOLD-DENOM) 221,222,222
  222 VR=(D6*DENOM+V23)**.33333333
      GO TO 220
  221 CUB4=(AHOLD-DENOM-D8)*D15
      P=CUB3-.33333333*CUB2**2
      Q=CUB4-CUB2*CUB3*.33333333+D10*CUB2**3
      R=D11*P**3+.25*Q**2
      AHOLD=-.5*Q
      AHOLD2=SQRT(R)
      AA=AHOLD+AHOLD2
      BB=AHOLD-AHOLD2
      VR=SIGN(ABS(AA)**.33333333,AA)+SIGN(ABS(BB)**.33333333,BB)-.333333
     133*CUB2
      VR=VR*100.
      GO TO 220
   14 CUB4=-ARNDM*(D4*V1**2+B*V1+D5*V1**3)-(1.-ARNDM)*(D4*V2**2+B*V2+D5*
     1V2**3)
      CUB4=CUB4*D15
      P=CUB3-.33333333*CUB2**2
      Q=CUB4-.33333333*CUB2*CUB3+D10*CUB2**3
      R=D11*P**3+.25*Q**2
      AHOLD=-.5*Q
      AHOLD2=SQRT(R)
      AA=AHOLD+AHOLD2
      BB=AHOLD-AHOLD2
      VR=SIGN(ABS(AA)**.33333333,AA)+SIGN(ABS(BB)**.33333333,BB)-.333333
     133*CUB2
      VR=VR*100.
  220 COSBT=(VH**2+VO**2-VR**2)/(2.*VH*VO)
      AHOLD=1.-COSBT**2
      IF (AHOLD) 900,901,901
  900 WRITE (6,902) I,COSBT
  902 FORMAT (19H ERROR STEP 902,I10,E15.6)
```

```
      COSBT=1.
      AHOLD=0.
  901 SINBT=SQRT(AHOLD)
   45 IR1=IR1*IR2
      ARNDM=MOD(IR1,IR3)
      GAMMA=ARNDM*CON5
      IF (VR-500000.) 62,63,63
   62 IF (VR-370000.) 64,65,65
   65 J=6
      AHOLD=VR-370000.
      GO TO 66
   64 IF (VR-270000.) 67,68,68
   68 J=5
      AHOLD=VR-270000.
      GO TO 66
   67 IF (VR-200000.) 69,70,70
   70 J=4
      AHOLD=VR-200000.
      GO TO 66
   69 IF (VR-140000.) 71,72,72
   72 J=3
      AHOLD=VR-140000.
      GO TO 66
   71 IF (VR-100000.) 73,74,74
   74 J=2
      AHOLD=VR-100000.
      GO TO 66
   73 IF (VR-60000.) 75,75,76
   76 J=1
      AHOLD=VR-60000.
      GO TO 66
   75 J=1
      AHOLD=0.
```

```
      GO TO 66
   63 IF (VR-720000.) 77,77,78
   77 J=7
      AHOLD=VR-500000.
      GO TO 66
   78 IF (VR-1100000.) 79,79,80
   79 J=8
      AHOLD=VR-720000.
      GO TO 66
   80 IF (VR-1500000.) 81,81,82
   81 J=9
      AHOLD=VR-1100000.
      GO TO 66
   82 IF (NUMB-12) 40,41,42
   41 WRITE (6,43)
   43 FORMAT (14H ERROR STEP 43)
      GO TO 11
   40 IF (VR-2500000.) 44,44,46
   44 J=10
      AHOLD=VR-1500000.
      GO TO 66
   46 J=10
      AHOLD=1000000.
      GO TO 66
   42 IF (VR-2500000.) 51,51,52
   51 J=10
      AHOLD=VR-1500000.
      GO TO 66
   52 IF (VR-4000000.) 223,223,224
  223 J=11
      AHOLD=VR-2500000.
      GO TO 66
  224 IF (VR-6000000.) 225,225,226
```

```
225 J=12
    AHOLD=VR-4000000.
    GO TO 66
226 J=12
    AHOLD=2000000.
 66 AHOLD2=DV(J)
    IR1=IR1*IR2
    ARNDM=MOD(IR1,IR3)
    ARNDM=ARNDM*CON4
    IRNDM=ARNDM+1.
    AHOLD3=IRNDM-1
    SCAT1=T4(J,IRNDM)+(ARNDM-AHOLD3)*(T4(J,IRNDM+1)-T4(J,IRNDM))
    J=J+1
    SCAT2=T4(J,IRNDM)+(ARNDM-AHOLD3)*(T4(J,IRNDM+1)-T4(J,IRNDM))
    SCAT=SCAT1+(AHOLD/AHOLD2)*(SCAT2-SCAT1)
    SCATR=SCAT*PIP
    CSCAT=COS(SCATR)
    SSCAT=SQRT(1.-CSCAT**2)
    AHOLD=SSCAT/(CSCAT+D12)
    CSCAT=SIGN(SQRT(1./(AHOLD**2+1.)),AHOLD)
    SSCAT=SQRT(1.-CSCAT**2)
    IR1=IR1*IR2
    ARNDM=MOD(IR1,IR3)
    AZMTH=ARNDM*CON5
    CAZ=COS(AZMTH)
    SAZ=SIN(AZMTH)
    C2=D16*VR*CSCAT
    C3=D17*VR**2
    VA=(-C2+SQRT(C2**2-C4*C3))/C5
    CEPS=(VR**2+V0**2-VH**2)/(2.*VR*V0)
    AHOLD=1.-CEPS**2
    IF (AHOLD) 910,911,911
910 WRITE (6,912) I,CEPS
```

```
912 FORMAT (15H ERROR STEP 912,110,E15.6)
    CEPS=1.
    AHOLD=0.
911 SEPS=SQRT(AHOLD)
    XCOMP=VA*SSCAT*CAZ+VO*SEPS
    YROT=VA*SSCAT*SAZ
    ZCOMP=VA*CSCAT-VO*CEPS
    AHOLD=XCOMP**2+YROT**2
    AHOLD2=SQRT(AHOLD+ZCOMP**2)
    AHOLD=SQRT(AHOLD)
    CSCAT=ZCOMP/AHOLD2
    SSCAT=AHOLD/AHOLD2
    CAZ=XCOMP/AHOLD
    SAZ=YROT/AHOLD
    VH=AHOLD2
    CROT=-CEPS*COSBT+SEPS*SINBT
    SROT=SEPS*COSBT+CEPS*SINBT
    XROT=XCOMP*CROT-ZCOMP*SROT
    ZROT=XCOMP*SROT+ZCOMP*CROT
    AHOLD=XROT**2+YROT**2
    AHOLD2=SQRT(AHOLD+ZROT**2)
    AHOLD=SQRT(AHOLD)
    CSCAT=ZROT/AHOLD2
    SSCAT=AHOLD/AHOLD2
    AZMTH=ATAN2(YROT,XROT)
    CGA=COS(GAMMA-AZMTH)
502 CALP=CALP*CSCAT+SALP*SSCAT*CGA
    SALP=SQRT(1.-CALP**2)
    DEPTH=TEST
    GO TO 83
 11 CONTINUE
    WRITE (6,84) MH,MO,T,N,NESC,NDWN,(DENS(I),I=1,10),(IAESC(I),I=1,18
   1),IR1,A,B,C,D,DSTOP,IY
```

```
84 FORMAT (44H MASSES,TEMP,NO OF ATOMS,NO ESCAPING,NO DOWN,2I3,F6.0,3
  1I10//,10E11.5//,1816//,I12,5E12.4,I5////)
   GO TO 6
   END
```